DYNAMIC ANALYSIS AND CONTROL OF A ROLL BENDING PROCESS

by

MICHAEL BRUCE HALE

B.S., Oklahoma State University
(1983)

SUBMITTED TO THE DEPARTMENT OF
MECHANICAL ENGINEERING
IN PARTIAL FULFILLMENT OF THE
REQUIREMENTS OF THE DEGREE OF

MASTER OF SCIENCE IN
MECHANICAL ENGINEERING

at the

MASSACHUSETTS INSTITUTE OF TECHNOLOGY

June 1985

Signature of Author _____
Department of Mechanical Engineering
June 3, 1985

Certified by _____
David E. Hardt
Thesis Supervisor

Accepted by _____
Ain A. Sonin
Chairman, Department Graduate Committee

DYNAMIC ANALYSIS AND CONTROL OF A ROLL BENDING PROCESS

by

MICHAEL BRUCE HALE

Submitted to the Department of Mechanical Engineering
on June 3, 1985 in partial fulfillment of the
requirements for the Degree of Master of Science in
Mechanical Engineering

ABSTRACT

Recent research has shown that the roll bending process can be automated by the addition of a closed-loop control system that continuously measures the springback of the metal workpiece. In the present work the components of a roll bending system, controlled by such a closed-loop scheme, are analyzed to determine important dynamic characteristics of the roll bending process. Dynamic models are developed for the individual components and for the roll bending process as a whole. These models are verified using an experimental roll bending apparatus. A linear control analysis and a nonlinear simulation are performed, using the system model, to determine the limits of the roll bending system response. The analysis shows that very good system response is possible using a simple proportional controller and proportional-plus-derivative feedback. The analysis also indicates that the derivative feedback, which for roll bending is the rate of change of unloaded curvature, can be approximated by the rate of change of the control variable, roll velocity. Experiments were performed which verified the control analysis. The experiments also show that workpiece vibration is a major problem as the roll bending system bandwidth is increased because the control system is unable to distinguish between workpiece vibration and curvature disturbances. Because the workpiece dynamics change as the workpiece moves through the roll bending apparatus, the control system must be designed for the worst case. Workpiece vibration is the major factor which limits the roll bending system response. Nevertheless, the proposed control scheme represents a major improvement in the control of the roll bending system because of the increased bandwidth and stability possible.

Thesis Supervisor: Dr. David E. Hardt
Title: Assistant Professor of Mechanical Engineering

ACKNOWLEDGMENTS

I would like to thank Professor David Hardt for his guidance and support throughout this research. The time spent in discussion with Professor Hardt resulted in many valuable insights.

I would also like to thank the Aluminum Company of America for their financial support and technical assistance.

Thanks also to James Owen who generously consented to examine the first draft of this document. His careful review and helpful suggestions have made the final version a much more readable and incisive manuscript.

Finally, a special thanks to my family for their love and support and prayers. Thanks especially to Patti whose companionship remains a comfort and an inspiration.

TABLE OF CONTENTS

LIST OF FIGURES

Chapter 1

INTRODUCTION

Motivation

In an effort to increase productivity and remain competitive in the world market, many companies are considering production process automation. In the metal forming industry much interest has been generated by the introduction of automation for traditionally manual operations such as brakeforming and roll bending. The first generation of automation for these processes was the addition of a simple position servomechanism and controller. On a brakepress, for example, a position servomechanism (servo) enabled the operator to program a series of movements which could be repeated very quickly and precisely. This did not significantly improve productivity, however, because of the extensive reworking needed to achieve the necessary shape accuracy. Even though the brakepress position could be controlled very closely, final part shape varied because of material property variations. More recent work by Hardt [1], Allison and Gossard [2], and Stelson [3] has shown that a material adaptive control scheme can be developed for the brakeforming process which will significantly improve productivity by explicitly accounting for material properties in-process.

A variation of the brakeforming process, the roll

bending process, is used in many metal forming situations that fit within the particular hardware restraints. The roll bending process, where applicable, is much faster than the brakeforming process because rather than forming the material in discrete steps, as in brakeforming, the workpiece is formed continuously as the material is rolled through the machine. The advantages of the continuous forming provide the motivation for the research presented in this thesis. The roll bending operation has great potential as an efficient and versatile metal forming process. The goal of this research was to develop an automatic control scheme for the roll bending process that would take advantage of the inherent speed of the roll bender while incorporating a closed-loop control scheme.

Previous Research

The three-roll pyramid roll bender shown in Figure 1 is a typical configuration that consists of a pair of fixed outer rolls and a movable center roll. One or more of the rolls is driven, and friction between the rolls and the workpiece permits the material to be rolled through the machine. As the workpiece moves, the center roll is adjusted to produce a variable bend along the length of the workpiece. This process is used to form long flat workpieces such as heavy plate used in boilers and reactor vessels. Roll bending is also used extensively to form long thin workpieces such as

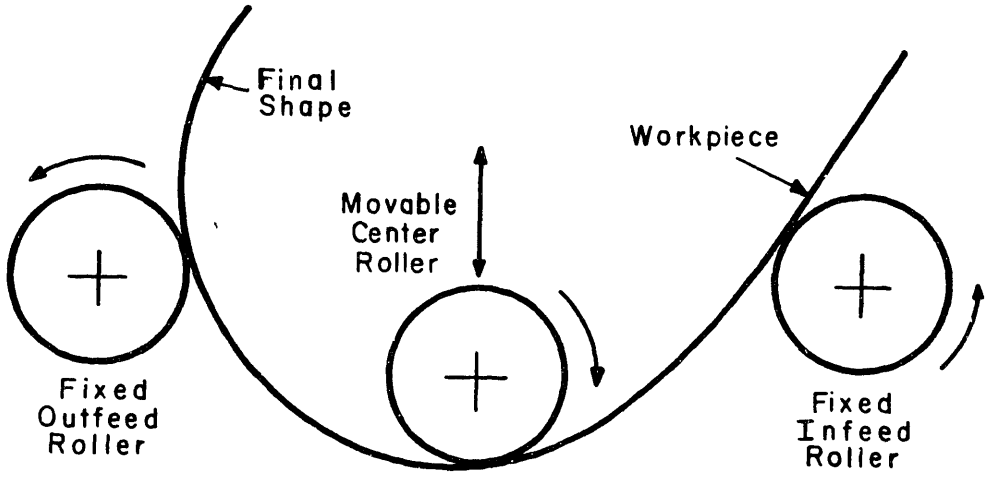

Figure 1. Pyramid 3-Roll Bender Configuration

aluminum extrusions. In the aluminum industry roll bending is also used for final straightening and contour correction of extrusions. This operation is entirely manual and the accuracy of the final product shape is dependent on the skill of the operator.

In recent years some effort has been directed toward automating the roll bending process. The major obstacle confronting researchers has been material springback. In roll bending, the metal workpiece is plastically deformed as the workpiece moves through the machine. As the workpiece exits the bending apparatus the elastic stresses in the metal are relaxed and the metal "springs back". Thus the metal

does not obtain its final shape until the workpiece has exited the machine. Some of the earliest attempts to deal with the material springback problem (Sachs [4] and Shanley [5]) used empirical data to characterize springback for certain materials and workpiece shapes. Other researchers ([6] to [14]) used various analytical methods in an attempt to predict stress and strain conditions as well as springback for various materials. Later, Hansen and Jannerup [15] developed a more complex model for elastic-plastic bending of beams that could be used to obtain a more nearly accurate estimate of the workpiece springback. Cook, Hansen, and Trostmann, [16] used the beam model in [15] to design an open-loop controller for a roll bending machine and demonstrated that good control of the final part shape is possible if the material properties, including springback, are known beforehand. The condition of prior knowledge of material properties is very restrictive, though, and seriously limits the usefulness of the controller. Foster [17] developed a machine which measures the final part shape as the workpiece exits the bending apparatus. This measurement can be incorporated into a closed-loop curvature controller. The advantage of this type of control scheme is that no prior knowledge of material properties is required for controller implementation. The curvature measurement, though, is taken after the workpiece has exited from the bending apparatus. At this point the workpiece already has been formed to its

final shape so the information cannot be used to correct the current error, but only to maintain a relatively constant final curvature. More recent research by Hardt, Roberts, and Stelson [18], in the area of roll bending, and similar research by Gossard and Stelson [19], in the area of brake-forming, has shown that it is possible to measure the important material properties, including springback, during forming and thus design a closed-loop controller for these processes. Hale and Hardt [20], and Lee and Stelson [21] have extended the approach in [18] to include the roll straightening process and have conducted experiments that show that with a closed-loop controller, straightening is nothing more than bending to zero curvature. Although the control scheme presented in [18] works well in theory, the productivity gains possible with this closed-loop curvature controller are limited by the assumption that workpiece feedrate will be very slow. This assumption was necessary to avoid unwanted oscillation and instability. In [18] and [20] the feedrates are kept below 0.7 in/sec. In [21] the workpiece was actually stepped through the bending device and the forming was performed while the workpiece was stationary. This closed-loop control method enhances the versatility of the roll bending process by making one-pass forming of arbitrary shapes possible, but it does not exploit the inherent speed advantages of the roll bending process. Thus much of the possible productivity gains are lost.

Thesis Overview

The work described in this thesis presents a new control method that greatly improves the roll bending system response. In Chapter 2, a complete static analysis of the roll bending process is presented. In addition, three bending cases that merit special attention: straightening, forming unsymmetrical sections, and bidirectional bending, are examined in some detail to determine how the control approach presented in [18] must be modified to apply to these cases. In Chapter 3 the roll bending system is broken down into five primary components. Models of each of these five components are developed to determine their individual influence on system dynamics and response. These models are verified using an experimental bending apparatus that is described briefly in Chapter 3 and in more detail in Appendix 1 and [22]. In Chapter 4 the dynamic models are used to develop a digital controller that satisfies specific control objectives. The relative importance of the control objectives listed in Chapter 4 varies according to the type of bending, so the control analysis is presented first in general terms and then examined using the experimental apparatus for specific types of bending. This analysis indicates that the roll bending system bandwidth can be greatly increased by a simple modification to the control system presented in [18]. Using a proportional-plus-integral controller with a

velocity servo results in a much simplified dynamic system with good stability and improved bandwidth. The new control method presented allows the same system response to be maintained at much greater feedrates, resulting in large productivity gains for very little cost. The experimental procedures and results are presented in Chapter 5. The results verify the models developed in Chapter 3 as well as the new control method proposed in Chapter 4. Chapter 6 contains the conclusions and also some suggestions for future research. The major conclusion is that there is a rather severe limitation imposed on maximum system bandwidth because of workpiece vibration. More research is needed to characterize completely the effect of the workpiece vibration on the final curvature of the workpiece. In addition, a more detailed study of the mechanics of bending could yield some insight into the problems and possibilities of one-pass two-dimensional and three-dimensional bending. The appendices contain more detailed information on the experimental hardware and software as well as an error analysis and hardware concerns and measurement alternatives.

Chapter 2

STATIC ANALYSIS OF BENDING MECHANICS

The closed-loop curvature control scheme for both the roll bending process and the brakeforming process is based on real-time measurement of the material springback. The development of this control scheme is repeated below.

Moment-Curvature Relationship

A workpiece in a three-roll bending machine can be modeled as a beam under three-point loading as shown in Figure 2. As the beam is loaded, the material is initially stressed elastically. If the beam is loaded so that the stress in the beam is always below the yield stress, then when the beam is unloaded, the material will "spring back" and regain its original shape. If, however, the beam is loaded so that some of the fibers are loaded past the elastic limit, then the beam is plastically deformed and will be permanently deformed when unloaded. Figure 2 shows the stress state in a beam that is loaded past the yield point. The final workpiece shape depends on the initial shape, the initial stress state, and the stress distribution, all as a function of position along the workpiece. The relationship between the stress state of a workpiece and the resulting curvature can be seen in the moment-curvature relationship, which can be derived from the stress-strain relationship.

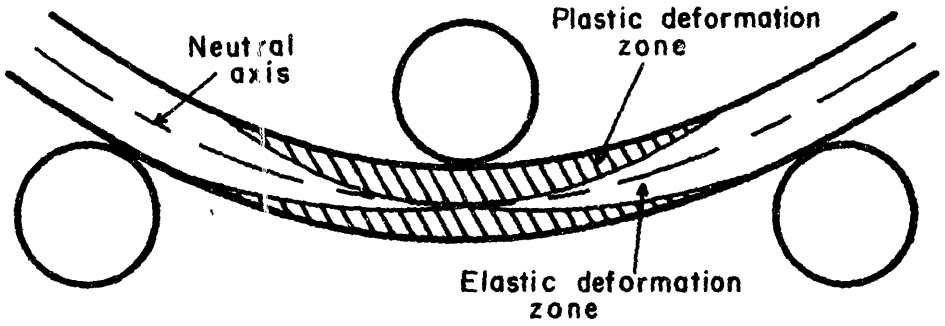

Figure 2. Stress State in a Loaded Beam

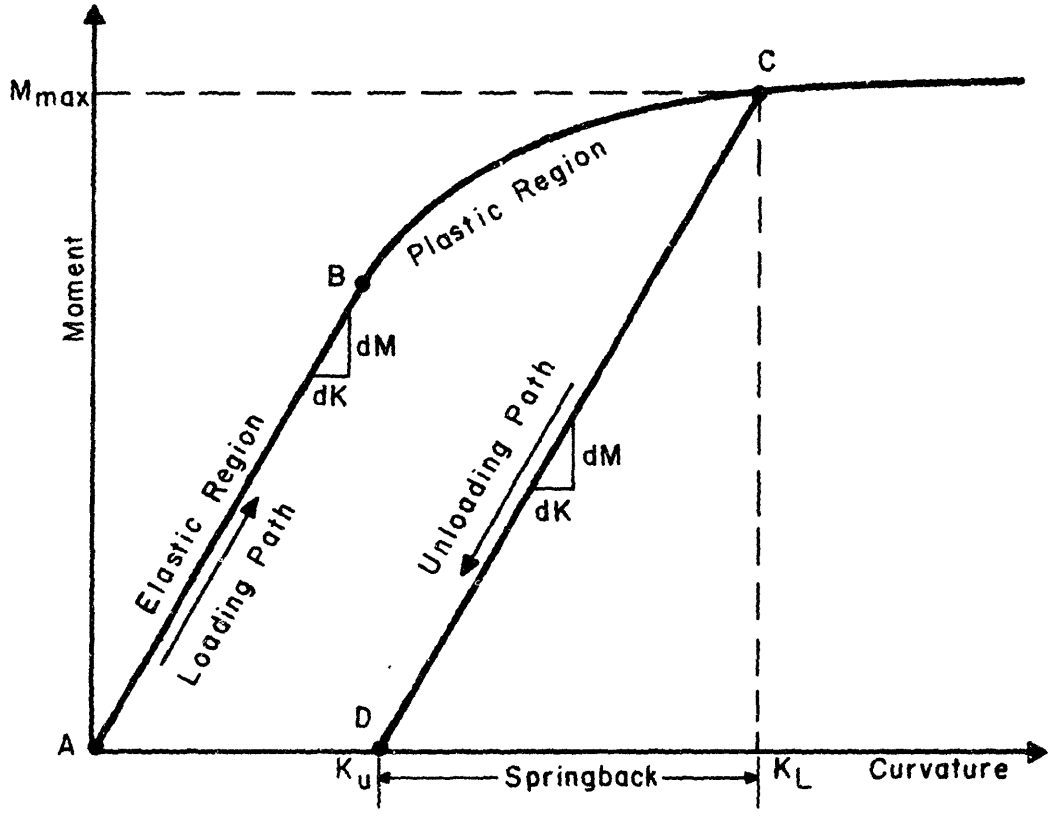

Figure 3. Moment-Curvature Relationship

Figure 3 is a general moment-curvature diagram for an initially flat workpiece. This diagram is drawn for a single point along the length of the workpiece. A similar diagram is needed for every point on the workpiece to characterize completely the workpiece curvature. The situation can be greatly simplified by considering the geometry of the three-roll bending process.

For a workpiece that is loaded in a roll bending apparatus, the exact moment distribution along the sheet is complex but can be approximated as a linear function of arc length assuming that no moment is generated between the drive rolls and the workpiece (Figure 4). As indicated for three-point bending, the bending moment applied to the workpiece increases from zero at the input roll to a maximum at the center-roll contact point and then decreases to zero at the output roll. This loading sequence can be traced on the moment-curvature diagram (Figure 3), the moment-position diagram (Figure 4), and on a machine diagram (Figure 5). At the input roll the workpiece has zero moment and, assuming an initially flat workpiece, zero curvature (Point A). The moment and curvature increase and the workpiece deforms elastically until the yield point is reached (Point B). The slope of the elastic loading line in Figure 3 is the effective bending stiffness. As the moment increases from Point B to a maximum at Point C the sheet deforms plastically. The moment and curvature decrease linearly as the sheet moves from maximum

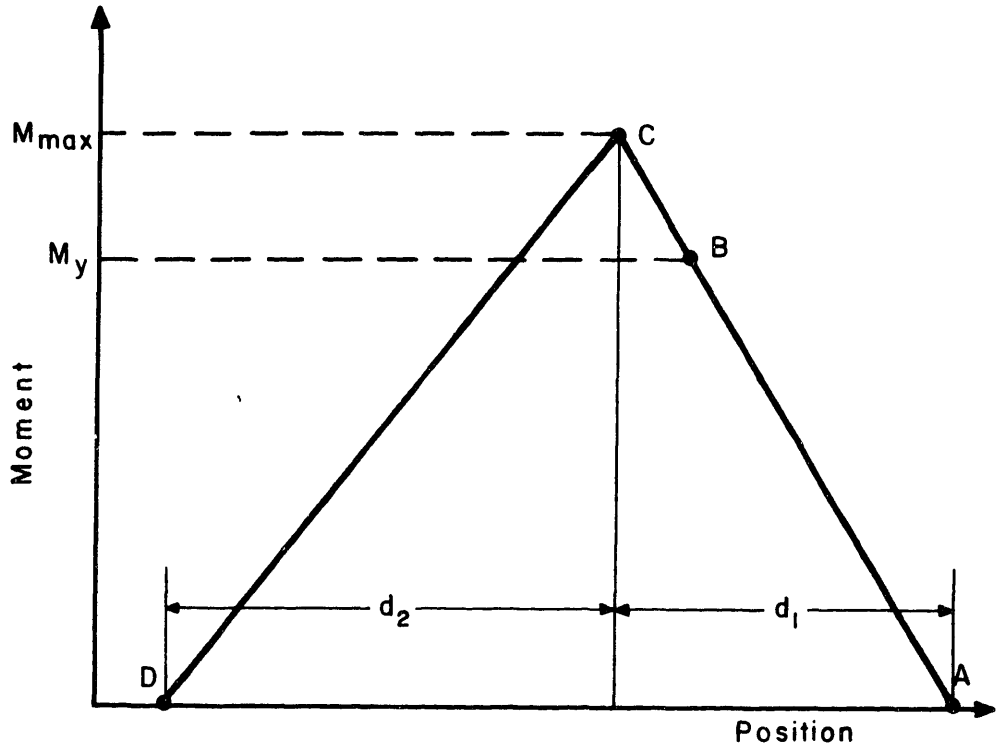

Figure 4. Moment vs. Workpiece Position

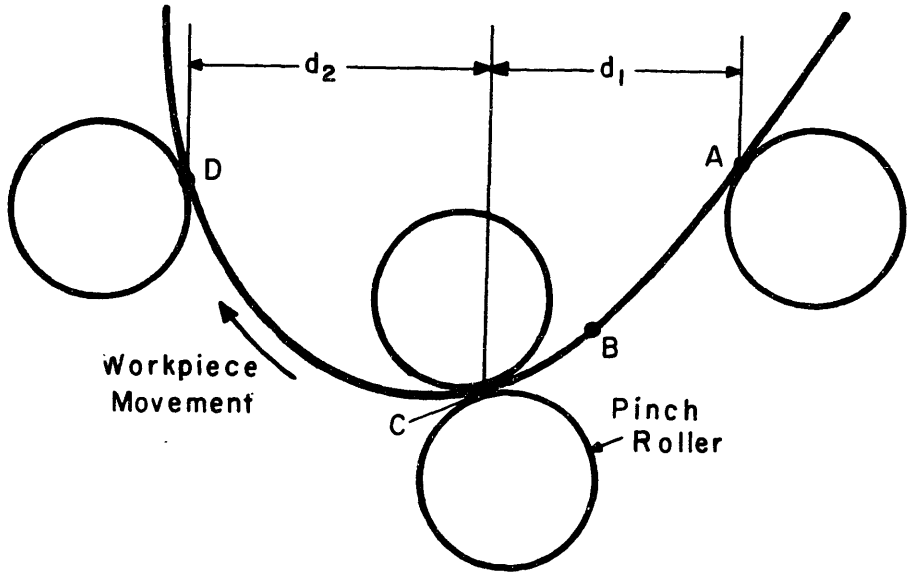

Figure 5. Roll Bender Configuration

loading (Point C) to the output roll (Point D) where the moment is again zero but the curvature is not because the workpiece has been plastically deformed. The slope of the unloading line in Figure 3 is the same as the elastic loading line. The workpiece springback as a function of distance, s, along the workpiece is the difference between the maximum loaded curvature and the final unloaded curvature and is found from Figure 3 to be:

$$\Delta K(s) = K_L(s) - K_u(s) \tag{1}$$

where K_L is the maximum loaded curvature and K_u is the unloaded curvature. The springback can also be expressed in terms of the moment. As shown in Figure 3 the unloading path is a linear function of the moment and so the springback can be expressed:

$$\Delta K(s) = M(s)/(dM/dK) \tag{2}$$

where M(s) is the moment distribution along the sheet and dM/dK is the slope of the elastic loading line. This equation points out one of the major advantages that the roll bending process has over the brakeforming process. For brakeforming, where the workpiece is formed at discrete loca-

tions, it is necessary to obtain the full moment-curvature distribution along the workpiece in the forming region to predict accurately the distributed springback. For roll forming, however, every point along the workpiece is loaded to the maximum moment as it passes under the center roll, and by controlling the maximum moment, each point along the workpiece can be formed individually.

As shown in [22], if the loaded curvature and the springback are known for a given point, then the unloaded curvature is found by rearranging Equation 1:

$$K_u = K_L - \Delta K \tag{3}$$

This can be combined with Equation 2 to yield:

$$K_u = K_L - M_{max}/(dM/dK) \tag{4}$$

where it is understood that these two equations apply to each point along the workpiece. Equation 4 shows that it is possible to calculate the unloaded curvature of the workpiece while the workpiece is in the loaded condition if the moment and curvature at the contact point under the center roller are known together with the bending stiffness of the workpiece. In other words it is possible to measure the

material springback in real time. Because the measurement is made at the center roll where the forming occurs, there is no measurement lag as there is with post-forming measurements as presented in [17]. A closed-loop controller can be designed using the unloaded curvature as the loop feedback. A general block diagram of such a control scheme is presented in Figure 6. A control system based on the real-time measurement of springback has many advantages over systems based on delayed measurement or springback prediction, such as in [16]. The primary advantage is that one-pass forming of arbitrary shapes is possible because the controller can use the actual system output, unloaded curvature, for feedback. Thus the system shown in Figure 6 can be thought of as a closed-loop curvature servo. Changes in material properties such as yield point, which can differ from workpiece to workpiece and even along the same workpiece, are reflected in the moment and curvature measurements and compensated for automatically. This was demonstrated for the static case by Hardt, Roberts, and Stelson in [18] and Roberts in [22].

Straightening

Another significant advantage of real-time measurement of unloaded curvature is evident in the straightening application. Consider a workpiece that is initially curved. The effect of the initial curvature on the moment-curvature diagram is shown in Figure 7, which is drawn for a single

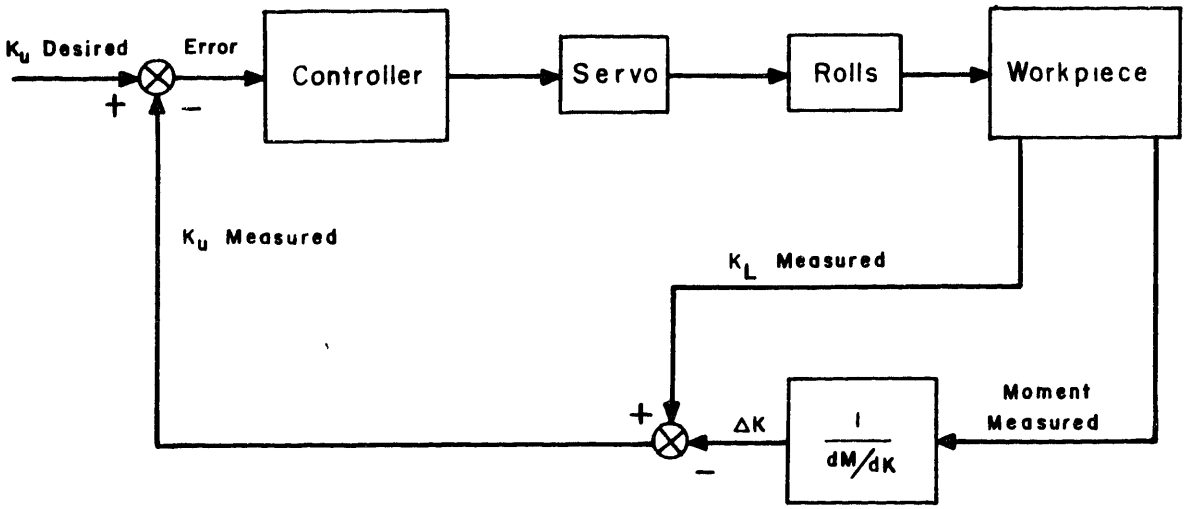

Figure 6. Closed-Loop Control Block Diagram

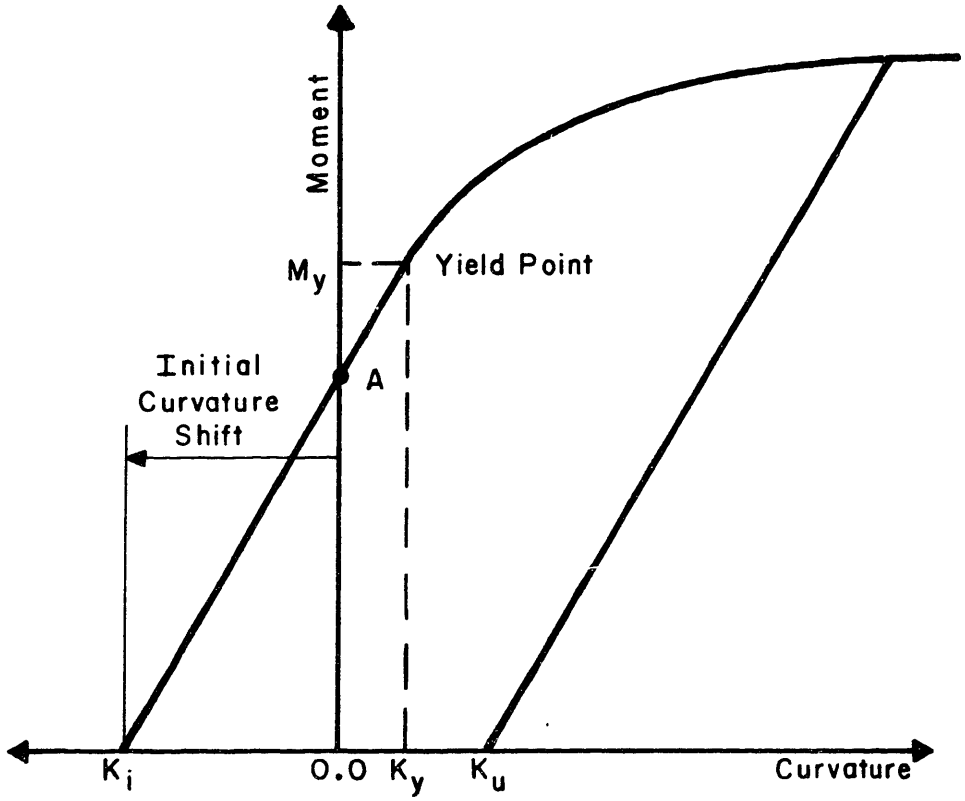

Figure 7. Shifted Moment-Curvature Diagram

point on the workpiece where the initial curvature is negative. The initial curvature simply shifts the origin of the curve. In the unloaded state (zero applied bending moment) the loaded curvature is no longer zero and the curve shifts to reflect this initial condition. The actual shape of the nonlinear portion of the curve depends on the initial stress state in the workpiece. The slope of the loading and unloading lines does not change though, so the control scheme is unaffected by initial stresses. In the closed-loop controller, initial curvature can be described as a system disturbance. A model of this disturbance is developed more fully in Chapter 3. The closed-loop control scheme will sense the disturbance and react to eliminate it. Because the disturbance is measured under the center roll, the control system can react while the workpiece is still loaded. Thus, with the closed-loop controller, straightening is no different than bending to zero curvature and can be accomplished in a one-pass operation without prior knowledge of the disturbance. This is clearly not possible using predictive methods of calculating the springback unless the disturbances are fully known beforehand. Prior knowledge of the disturbances requires a separate operation and additional instrumentation, and even then, multiple passes may be required because a controller based on predicted springback is open-loop and cannot compensate for material property variations.

Unsymmetrical Sections

For a workpiece with a cross-sectional area that is symmetric about a given axis and material properties that are constant along the workpiece and symmetric about the axis, a pure moment acting in the plane of symmetry will produce a deflection only in the plane of symmetry. These conditions are very restrictive though, and apply only to a limited number of industrially relevant cases. The general case of three-dimensional bending is much more complex. For an arbitrary cross-section with a bending moment applied in an arbitrary direction, it is possible for the workpiece to twist about the longitudinal axis and bend about two orthogonal transverse axes. In other words, the two-dimensional bending and the twisting are all coupled and may all occur from a one-dimensional loading.

Consider a triangular rod (Figure 8) that is loaded about the two orthogonal transverse axes. The deflection in the xy plane is related to the loading by Equation 5 (see [23] and [24]):

$$\frac{\partial \alpha}{\partial s} = \frac{M_z I_{zz} + M_y I_{yz}}{E(I_{yy} I_{zz} - I_{yz}^2)} \tag{5}$$

where α is the local beam angle in the xy plane, s is the distance along the beam, E is the modulus of elasticity, M_z

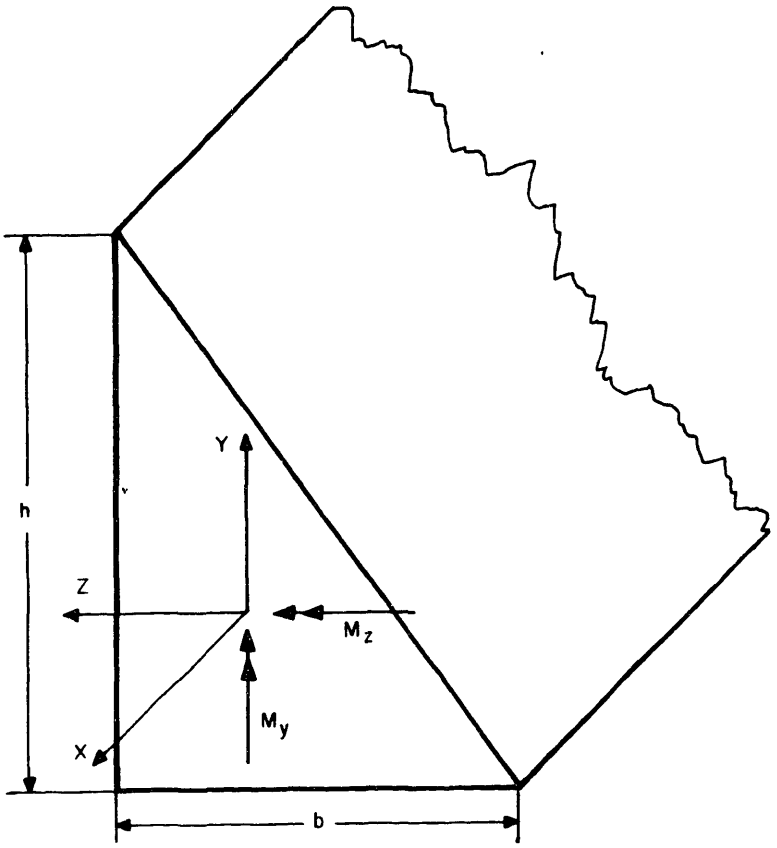

Figure 8. Triangular Rod

and M_y are the moments applied about the z and y axes respectively, I_{zz} and I_{yy} are the area moments of inertia for the z and y axes respectively, and I_{yz} is the area product of inertia for the y and z axes. The deflection in the xz plane is:

$$\frac{\partial \beta}{\partial s} = \frac{-M_z I_{yz} - M_y I_{yy}}{E(I_{yy} I_{zz} - I_{yz}^2)} \tag{6}$$

where β is the local beam angle in the xz plane. It is easy to see that a moment applied only in the z (or y) direction

will produce a deflection in two directions because of the coupling from the product of inertia term, I_{yz}. This multi-dimensional bending is undesirable for the roll bending process because three dimensions must be measured and controlled in order to control the final shape for the general case. Therefore it is important to analyze the coupling effect to determine how it can be prevented or reduced.

From Equations 5 and 6 it is obvious that the bending is uncoupled when $I_{yz} = 0.0$. This is the case if y and z are principal axes, such as the axes through the centroid and parallel to the edges of a rectangular section. Thus bending about a principal axis will result in an uncoupled deformation. For many sections however, this restrictive condition cannot be met. Even if coupling is unavoidable, the effects can be minimized. Because permanent changes in curvature involve plastic deformation, if a moment in one direction produces plastic deformation in one direction and elastic deformation in all other directions, the bending is effectively uncoupled. Although bending occurs in more than one direction, plastic deformation, and therefore permanent curvature changes, will occur in one direction only. The following analysis demonstrates the effect of coupling for a two-dimensional case.

Suppose that the workpiece shown in Figure 8 is initially flat and is loaded in a single direction ($M_y = 0.0$).

Rewriting Equation 6 gives:

$$\frac{\partial \beta}{\partial s} = \frac{-M_z I_{yz}}{E(I_{yy}I_{zz} - I_{yz}^2)} \tag{7}$$

Rewriting Equation 5 yields:

$$\frac{\partial \alpha}{\partial s} = \frac{M_z I_{zz}}{E(I_{yy}I_{zz} - I_{yz}^2)} \tag{8}$$

Substituting Equation 8 into Equation 7 yields:

$$\frac{\partial \beta}{\partial s} = \left(\frac{-I_{yz}}{I_{zz}}\right)\left(\frac{\partial \alpha}{\partial s}\right) \tag{9}$$

From this equation it is easy to see that the coupling is governed by the ratio of the product of inertia to the moment of inertia. A similar development can be used to show that the coupling that occurs when $M_z = 0.0$ is given by:

$$\frac{\partial \alpha}{\partial s} = \left(\frac{-I_{yz}}{I_{yy}}\right)\left(\frac{\partial \beta}{\partial s}\right) \tag{10}$$

Now let K_{xz} be the maximum elastic loaded curvature in the xz

plane and K_{xy} be the maximum elastic loaded curvature in the xy plane. Then the conditions that will ensure uncoupled bending are given by:

$$\left(\frac{-I_{yz}}{I_{zz}}\right)\left(\frac{\partial \alpha}{\partial s}\right) \leq K_{xz} \tag{11}$$

for bending in the xy plane and

$$\left(\frac{-I_{yz}}{I_{yy}}\right)\left(\frac{\partial \beta}{\partial s}\right) \leq K_{xy} \tag{12}$$

for bending in the xz plane. Consider, for example, the triangular cross section shown in Figure 8 where h = 1.75 in, b = 1.25 in, E = 10×10^6 psi and the proportional limit is 35×10^3 psi (Aluminum 6061-T6). If the maximum elastic loaded curvature can be approximated by the loaded curvature of the workpiece when the outermost fibers are stressed to the proportional limit, then:

$$I_{zz} = 0.186 \text{ in}^4$$
$$I_{yy} = 0.095 \text{ in}^4$$
$$I_{yz} = -0.066 \text{ in}^4$$
$$K_{xz} = 0.004 \text{ in}^{-1}$$
$$K_{xy} = 0.003 \text{ in}^{-1}$$

Thus the largest curvatures that can be formed in each direction without affecting the unloaded curvature in the other direction are:

$$\frac{\partial \alpha}{\partial s} \leq \left(\frac{I_{zz}}{I_{yz}}\right)(0.004) = 0.011 \quad in^{-1} \tag{13}$$

$$\frac{\partial \beta}{\partial s} \leq \left(\frac{I_{yy}}{I_{yz}}\right)(0.003) = 0.0043 \ in^{-1} \tag{14}$$

For straightening the triangular beam, it might be possible to keep the curvature below the indicated values because curvature magnitudes are very small. For bending, though, coupling is sure to occur. But the coupling effect can be minimized by careful application of the analysis shown above. By bending first in the direction which is least affected by bending in the opposite direction, the required number of passes will be minimized if an iterative control method is used. Better yet, it might be possible to calculate, using Equations 9 and 10, the overbend or underbend needed to compensate for the coupling. This defeats the purpose of the closed-loop control scheme however, because the coupling is estimated and not measured explicitly. If the closed-loop curvature control scheme could be applied to two or three dimensions then the coupling effects would be measured and compensated for automatically,

much like initial curvature disturbances are handled in straightening. The work presented here will be restricted to one-dimensional uncoupled bending to simplify the experimental apparatus.

Bidirectional Bending

To form arbitrary workpiece shapes in a single pass the bending apparatus must be capable of forming both positive and negative (bidirectional) curvatures. This means that more complex hardware, such as opposing roll pairs, is needed (see Appendix 1). The closed-loop control scheme can be applied to bidirectional bending with no changes. The major difference between unidirectional and bidirectional bending is due to the effect of the elastic deadband region. Equation 4 together with Figure 3 show that there is no change in the unloaded curvature while the workpiece is loaded elastically. Thus for a certain range of center-roll movement the system output does not change. This range of movement is called the deadband region. Figure 9 shows the relationship between center-roll displacement and unloaded curvature for a workpiece that is stationary in the bending apparatus. The points noted in Figure 9 correspond to the loading conditions shown in Figure 3 for the special case of a stationary workpiece. Notice that a large portion of the loading path and the complete unloading path shown in Figure 3 are in the deadband region. For unidirectional bending with no over-

shoot, the system passes through the deadband region only once at the start of bending and the effect on the system response is very small. For bidirectional bending, and especially for straightening where curvature levels are very small, most of the center-roll movement may be in the deadband region. Thus it is possible for the deadband region to dominate the system response. This is of little importance for static bending but becomes very important for the dynamic case where the workpiece moves through the roll bending apparatus. The deadband region has a large effect on system stability and error, especially as the feedrate becomes large. The effect of the deadband region on the system dynamics will be explored in more detail in the next chapter.

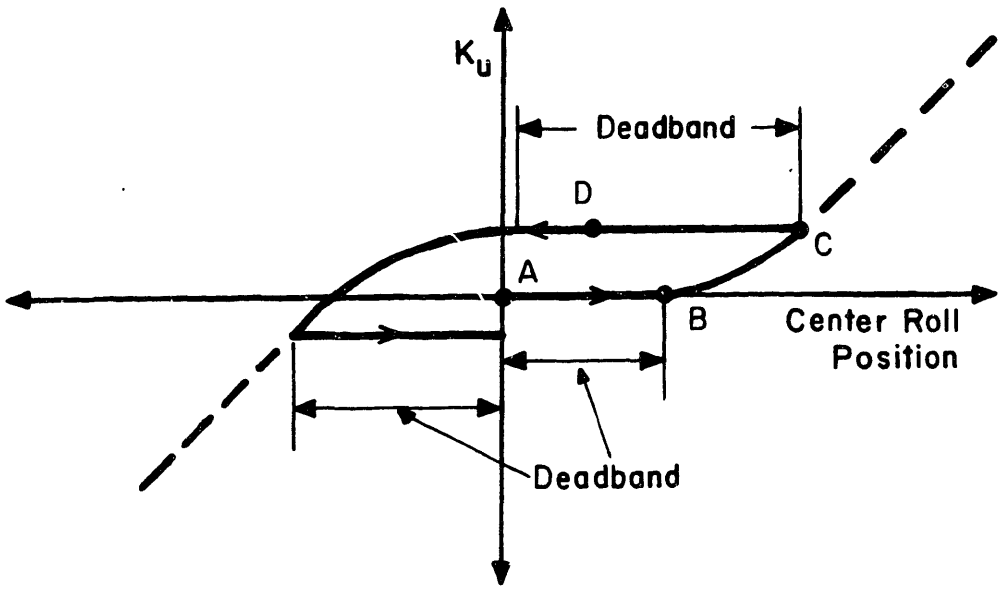

Figure 9. K_u vs. Center-Roll Position

Chapter 3

DYNAMIC ANALYSIS AND MODELING

The research presented in [18], [20], [21], and [22] demonstrated that the closed-loop control scheme described in Chapter 2 works very well for bending and straightening if the workpiece is rolled through the apparatus very slowly. The assumption of very low feedrate allowed the authors to ignore any dynamics associated with the servo system or workpiece. In this chapter a model of the roll bending system that includes dynamic effects will be developed. This model will be used to analyze the dynamic performance of the roll bending operation and predict the performance limits. Then the dynamic model will be used to develop a control algorithm. The system dynamics for any roll bending apparatus will depend on the particular roll bending configuration and hardware under consideration. A general roll bending system must contain several key components to implement the closed-loop controller. The dynamic models of these components are presented in general terms later in this chapter. These models are used to analyze a particular roll bending configuration that was used to perform the experiments in Chapter 5. The experimental roll bending apparatus is used to examine the validity of the dynamic models and also to develop and evaluate different controllers. A short descrip-

tion of the experimental apparatus is given below. More detailed information about the experimental hardware is presented in Appendix 1 and [22].

Experimental Apparatus

The experimental bending apparatus (Figure 10) consists of two outer roll-pairs and a center roll-pair mounted on a Bridgeport milling machine. All of the roll-pairs have a fixed roll and an adjustable opposing roll. Thus the apparatus is capable of bidirectional bending of various sized workpieces. The outer roll-pairs are fixed to the milling machine bed which is driven by DC motors through a ball-screw. The movement of the outer rolls with respect to the center roll provides the forming action needed. The center roll is mounted in and driven by the milling spindle. The workpiece is clamped between the driven center roll and the opposing center roll. Friction between the rolls and the workpiece causes the workpiece to move through the apparatus. Feedrate can be varied by adjusting the spindle speed. As shown in Equation 4, the loaded curvature and the maximum moment must be measured to implement the closed-loop control scheme. Loaded curvature is measured on the experimental apparatus by two linear variable differential transformers (LVDT's) which are mounted next to the center roll. The distance between the LVDT's is adjustable. The maximum moment is measured with a strain-gage force transducer.

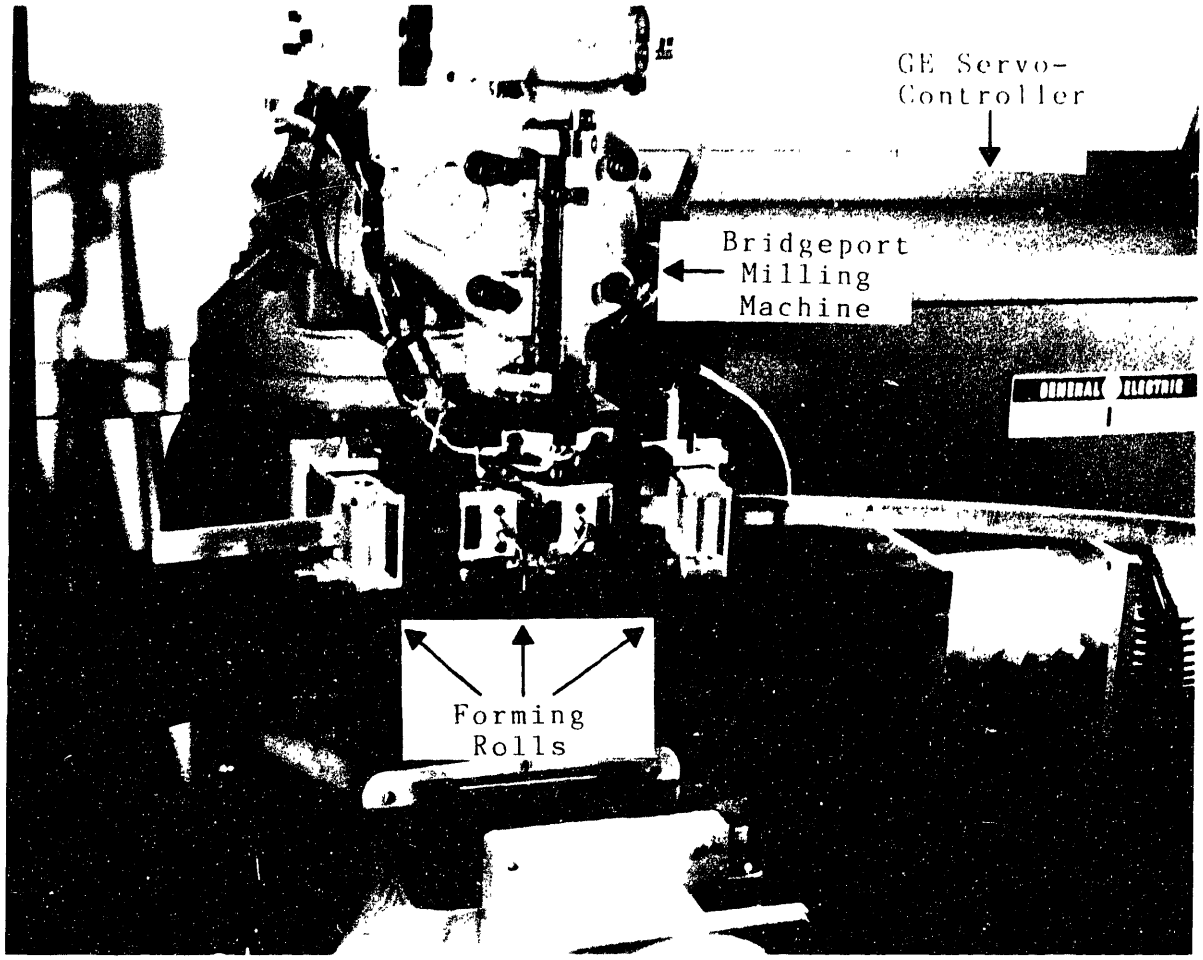

Figure 10. Experimental Roll Bending Apparatus

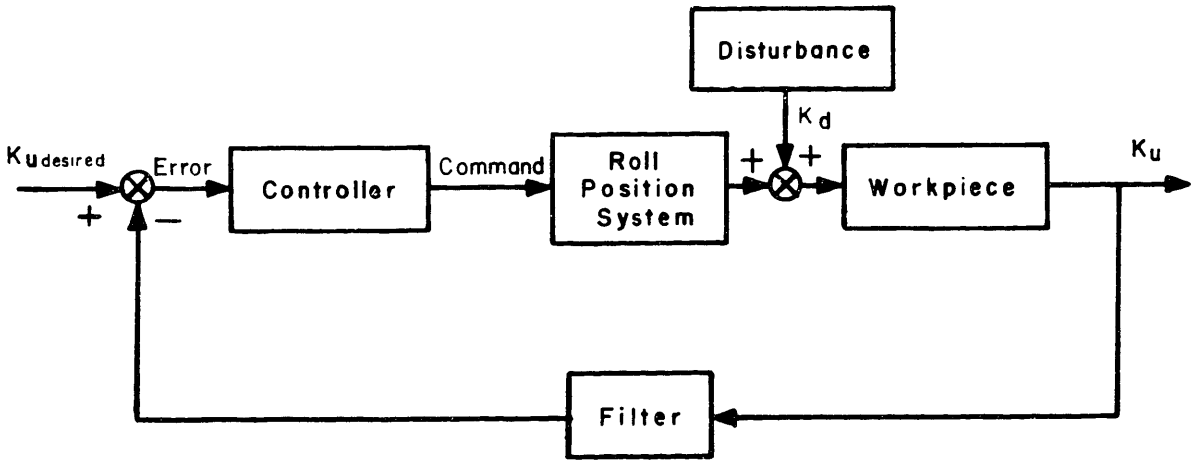

Figure 11. Roll Bending System Block Diagram

Notice that all the roll-pair housings are free to rotate so that no moment is generated between the rolls and the workpiece. The rotation of the roll housings changes the moment arm used to calculate the maximum moment and therefore the rotation must be measured. Rotation of the center-roll housing is measured with a potentiometer. The outer-roll rotations are negligible for the bending experiments reported in Chapter 5 and are not measured. Appendix 3 contains a complete error analysis which shows the effect of neglecting various measurements. Appendix 2 presents some alternatives to the moment and curvature measurements. Analog signals from all transducers are amplified and filtered before being sent to a computer where they are digitized. The computer then uses this information to generate an error signal which is sent to a General Electric servo-controller. The servo-controller is connected to the DC motor that adjusts the roll position and the loop is completed.

Analysis of the machine description and the bending process reveals five system components that appear to contribute significantly to the system dynamics. These five components are the workpiece, the servo system, measurements and filters, disturbances, and the system controller. A block diagram of the roll bending system which includes all these components is shown in Figure 11. A model for each of these components is developed below and verified using the experimental apparatus described.

Workpiece Model

As shown in Chapter 2 it is not necessary to know anything about the plastic deformation of the workpiece as it is being loaded to measure the unloaded curvature. It is only necessary to know the maximum moment and curvature at each point along the workpiece and the slope of the unloading path. For modeling purposes however, it is necessary to know how the workpiece deforms, both elastically and plastically as a function of the center-roll position. For the workpiece model we will assume that the workpiece material is elastic-perfectly-plastic, which means that the stress-strain relationship is as shown in Figure 12. In the elastic region the

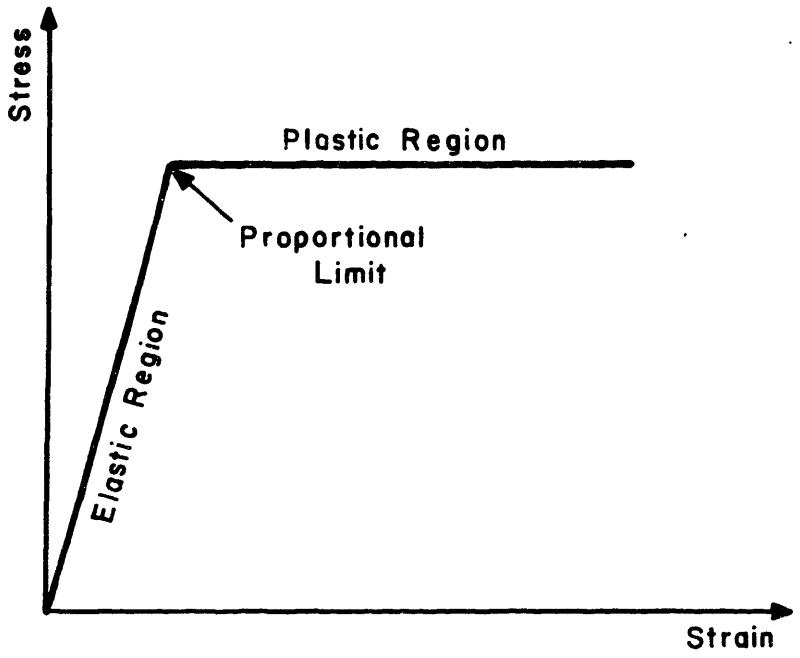

Figure 12. Elastic-Perfectly-Plastic Stress-Strain

moment and curvature are linearly related by the bending stiffness. If we further assume that the workpiece has a rectangular cross section that is constant along the length, then the relationship between moment and curvature for the entire loading path can be described as shown in [23] by:

$$M = K(dM/dK) \qquad K < K_y$$
$$M = 1.5M_y(1 - (K_y/K)^2/3) \qquad K \geq K_y \tag{15}$$

where M_y and K_y are the moment and curvature at yield.

The curvature of the workpiece can also be expressed as a linear function of roll position using the deflection equation of a beam under three-point loading,

$$K = 3z/(L^2) \tag{16}$$

where z is center-roll displacement and L is the distance between the center and outer roll. This relationship is based on linear beam theory, but is a very good approximation well beyond yield as shown in Figures 13 and 14. This equation is not dependent on material properties such as bending stiffness or yield point and is therefore very useful for a general model.

Substituting Equations 15 and 16 into 4 yields the

following relationship between unloaded curvature and center-roll displacement (assuming an initially flat workpiece):

$$K_u = 0.0 \qquad z < z_y$$

$$K_u = \frac{3z}{L^2} - \frac{9z_y}{2L^2} + \left(\frac{3}{2}\right)\frac{z_y^3}{L^2 z^2} \qquad z \geq z_y \tag{17}$$

where z_y is the center-roll position at the yield point of the workpiece. Equation 17 is the desired workpiece model that relates the input (center-roll position) to the output (unloaded curvature). This equation applies to the point on the workpiece that is in contact with the center roller (Point C in Figure 5). As shown in Chapter 2, this point corresponds to the maximum moment and curvature which means that the final curvature of the workpiece is set at this point. Applying Equation 17 to each point on the workpiece as it is rolled through the apparatus provides a model of the workpiece as a function of the distance along the workpiece.

Figures 13 and 14 are plots of measured moment scaled by the bending stiffness, loaded curvature, and unloaded curvature versus roll position for a 1/8" X 1" 2024 aluminum strip and a 1/4" X 1" 2024 aluminum strip, respectively. Equations 15, 16, and 17 are also plotted using the bending stiffness and yield point obtained by experimentation. These plots

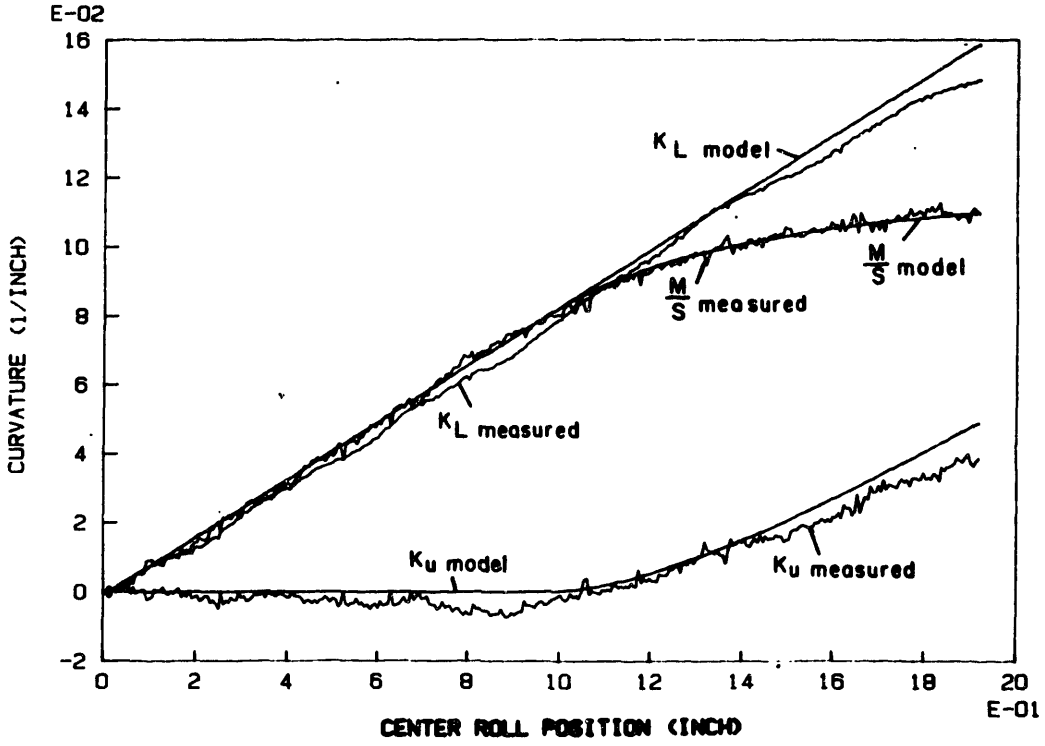

Figure 13. 1/8" X 1" Aluminum Workpiece Model

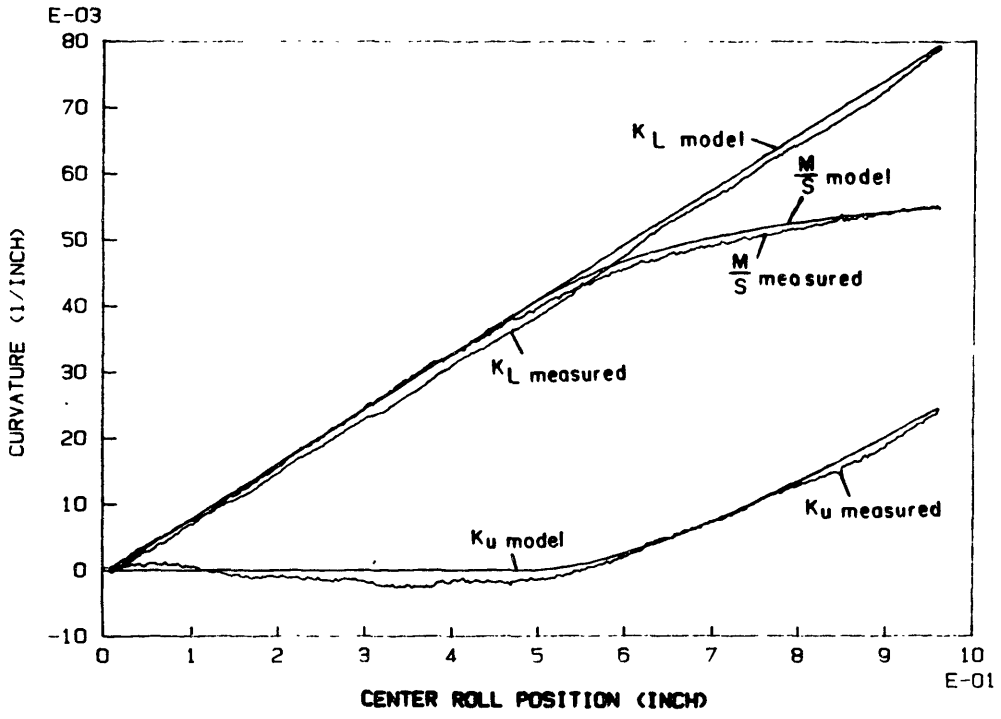

Figure 14. 1/4" X 1" Aluminum Workpiece Model

show that the workpiece model developed above is a reasonable approximation of the actual workpiece.

There are three important features to note from the workpiece model. First, there is a deadband region while the workpiece is elastically loaded. The significance of the deadband region depends on the type of bending and the bending stiffness of the workpiece. For very stiff workpieces the elastic region, and therefore the deadband region, is very small. Flexible workpieces have a much larger deadband region. Forming circular shapes or bending workpieces with curvatures in only one direction involves passing through the deadband region only once. For bidirectional bending or for straightening, the deadband region may dominate the operating region for a particular workpiece.

The second important feature of the workpiece response is that the response has two different forms depending on whether the workpiece is stationary or moving through the rolls. For a stationary or very slow moving workpiece, there is hysteresis in the model as shown in Figure 15. This is because the unloaded curvature does not change while the workpiece is in the elastic loading state or during unloading. If the workpiece is stationary, then the same portion of the workpiece is formed during a forming cycle. For a moving workpiece, each point along the workpiece is formed only once since new material is continually fed into the bending apparatus. Figure 15 shows that a moving workpiece

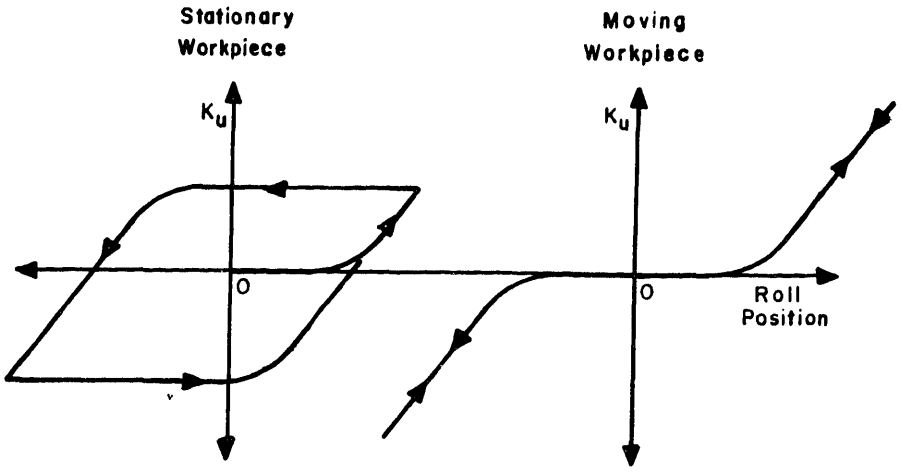

Figure 15. Workpiece Hysteresis

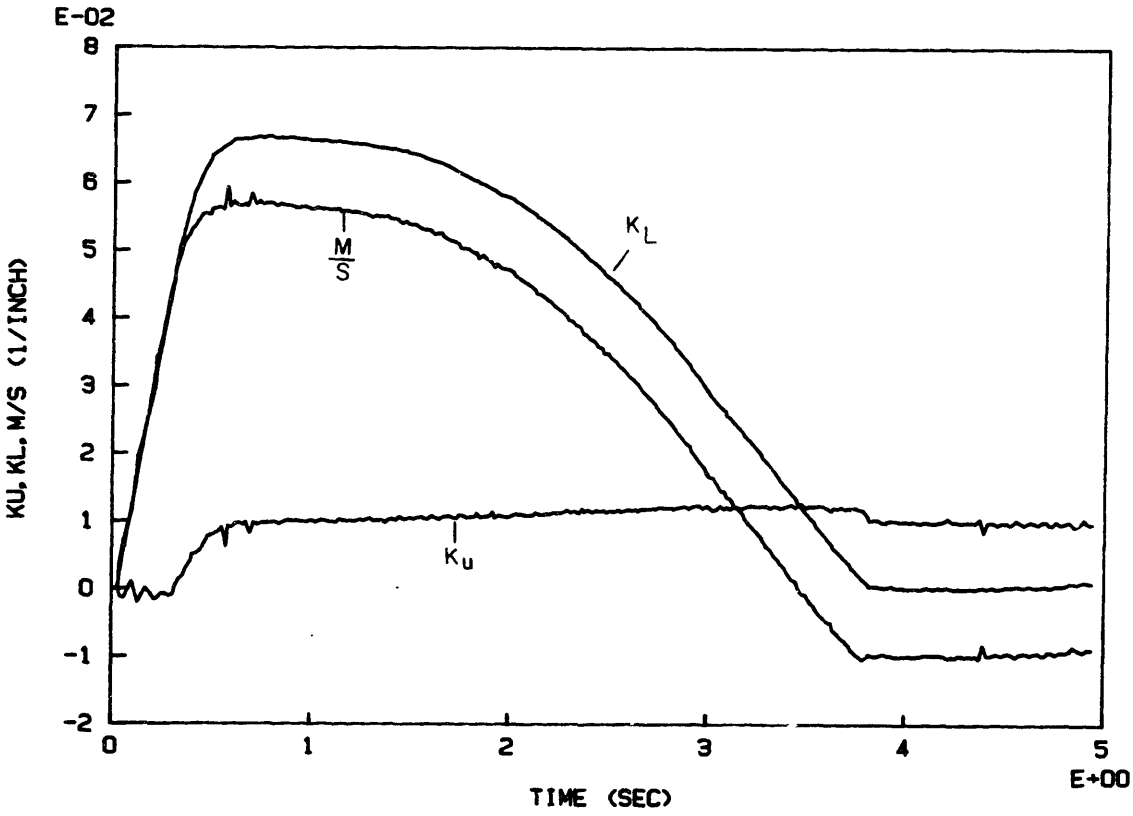

Figure 16. Hysteresis Test

does not have hysteresis but still has a deadband region. Figure 16 shows the dramatic effects of the workpiece hysteresis. This figure shows the loaded and unloaded curvatures and the scaled moment for a stationary 1/4" X 1" aluminum workpiece such as the one described in Figure 14 in response to a step curvature command of 0.01 in^{-1}. The deadband region is apparent in the first 0.25 sec, but then the unloaded curvature responds quickly to move to the commanded value. The system has a very small overshoot and the roll position decreases in an attempt to eliminate the error. But even though the moment and loaded curvature decrease, the workpiece is unloading elastically as indicated in Figure 3 and the unloaded curvature does not decrease. When the workpiece is loaded past the negative elastic limit the unloaded curvature will decrease and the error will be eliminated. This occurs at about 3.75 sec in Figure 16. This response is exactly the response indicated by the hysteresis shown in Figure 15. The results in Figure 16 can be compared to the results of Test 10 shown in Chapter 5, which is the same test with a moving workpiece.

The third important feature to note about the workpiece model is that time is not a variable in the model. The unloaded curvature is a function of center-roll position only. This means that the workpiece can be thought of as a nonlinear gain. This is, of course, an approximation because the workpiece does actually have mass, compliance, and damp-

ing, which will all affect the system dynamics. In the workpiece model these effects are assumed to be negligible. This assumption turns out to be a critical feature of the model, which is valid only under certain conditions as shown in Chapter 5.

Servo Model

The roll bending apparatus works by adjusting the center-roll position to change the loading in the workpiece. Closed-loop control of the roll bender requires automatic control of the center-roll position by a servo system. There are several different roll positioning alternatives available on commercial roll bending machines. Actuation can be achieved using a hydraulic servo system or a DC motor and leadscrew, for example. At low frequencies the servo systems can all be modeled as a standard position servo or velocity servo. The equation for a position servo, expressed in Laplace transform notation, is:

$$\frac{z}{z_c} = \frac{w_n^2}{s^2 + 2\zeta w_n + w_n^2} \tag{18}$$

where z_c is the position command, w_n is the natural frequency, and ζ is the damping ratio. The equation for a velocity servo is:

$$\frac{\dot{z}}{\dot{z}_c} = \frac{K}{Ts + 1} \tag{19}$$

where $\dot{z}$ is the center-roll velocity, $\dot{z}_c$ is the velocity command, K is the servo gain constant, and T is the system time constant.

The GE servo-control system on the experimental bending apparatus can be configured as either a velocity servo or a position servo. Figure 17 is a plot of the center-roll velocity in response to a step input to the velocity servo. Figure 18 is a Bode diagram which shows the frequency response of the velocity servo. The forcing function used to drive the servo and determine frequency response was generated from the control computer. This was done to ensure that all the electronics are included in the dynamic response. The program used to determine the step and frequency response is listed in Appendix 4. Figures 17 and 18 indicate that the velocity servo is a first-order system with a time constant of 0.042 sec. Thus the servo model given by Equation 19 is a very good approximation to the actual system if T = 0.042. The servo gain constant, K, is adjustable on the GE servo-control system. For modeling purposes the servo gain constant is assumed to be 1.0 so that all of the system gains are represented by the controller gain. Figures 19 and 20

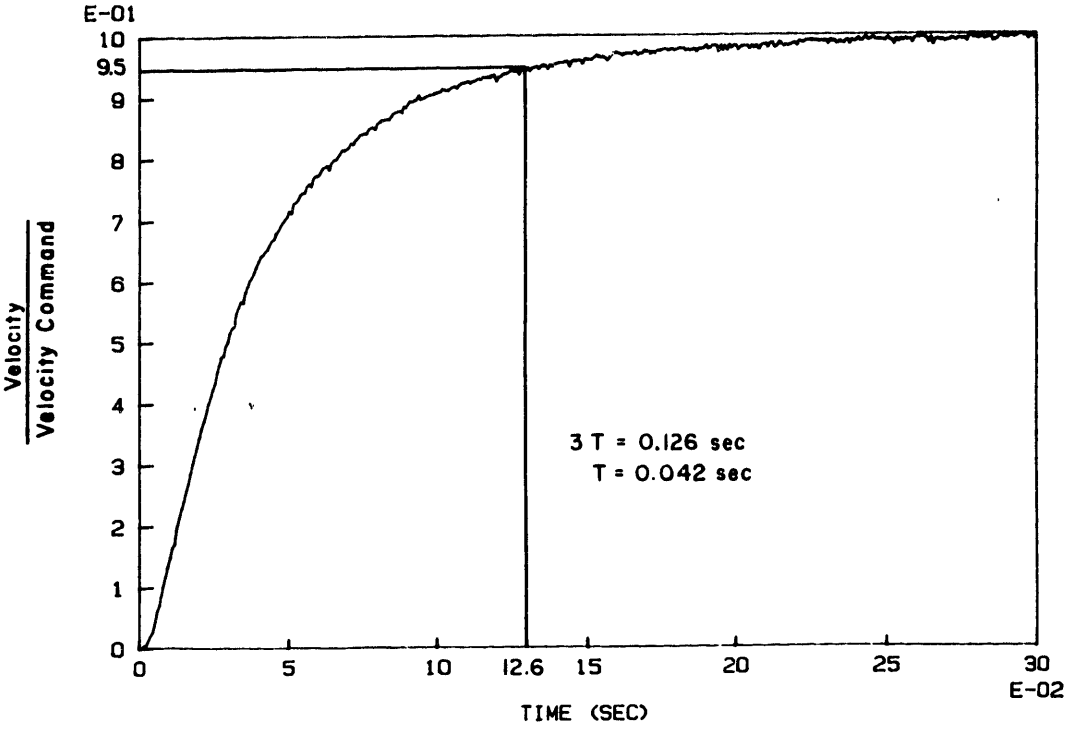

Figure 17. Velocity Servo Step Response

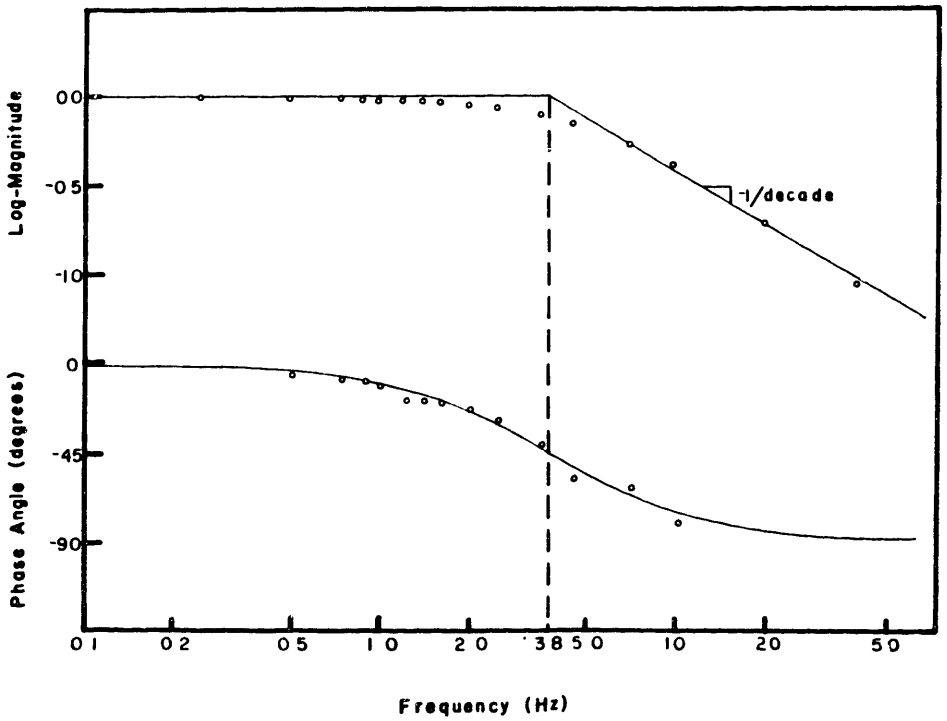

Figure 18. Velocity Servo Bode Diagram

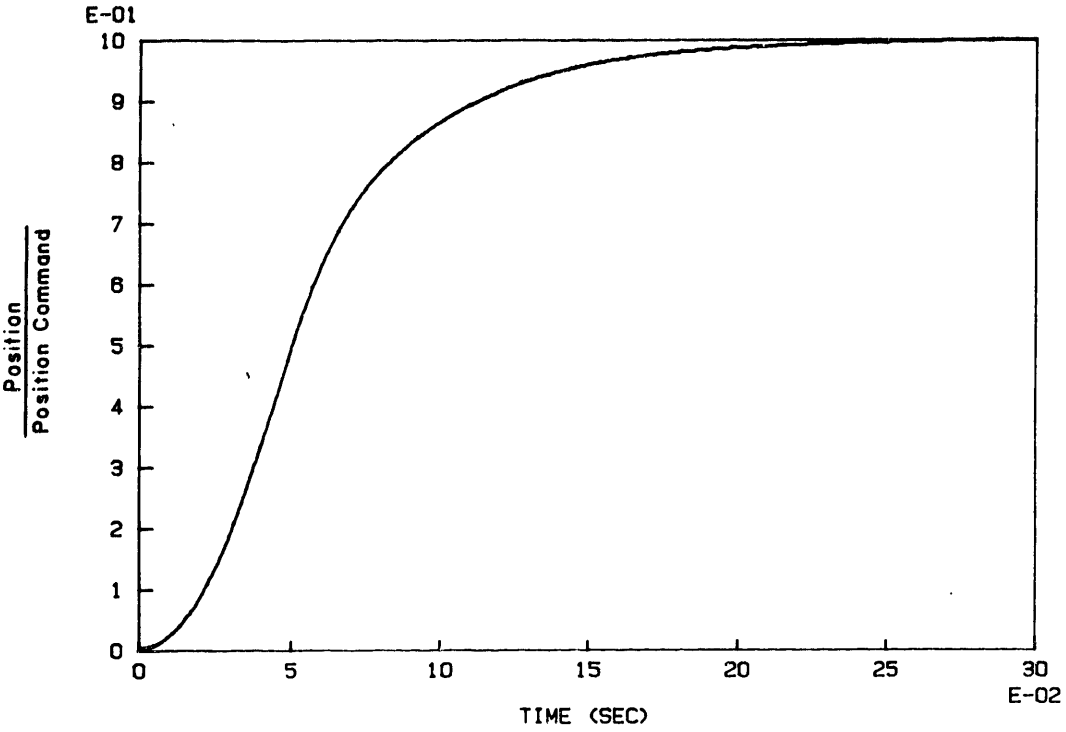

Figure 19. Position Servo Step Response

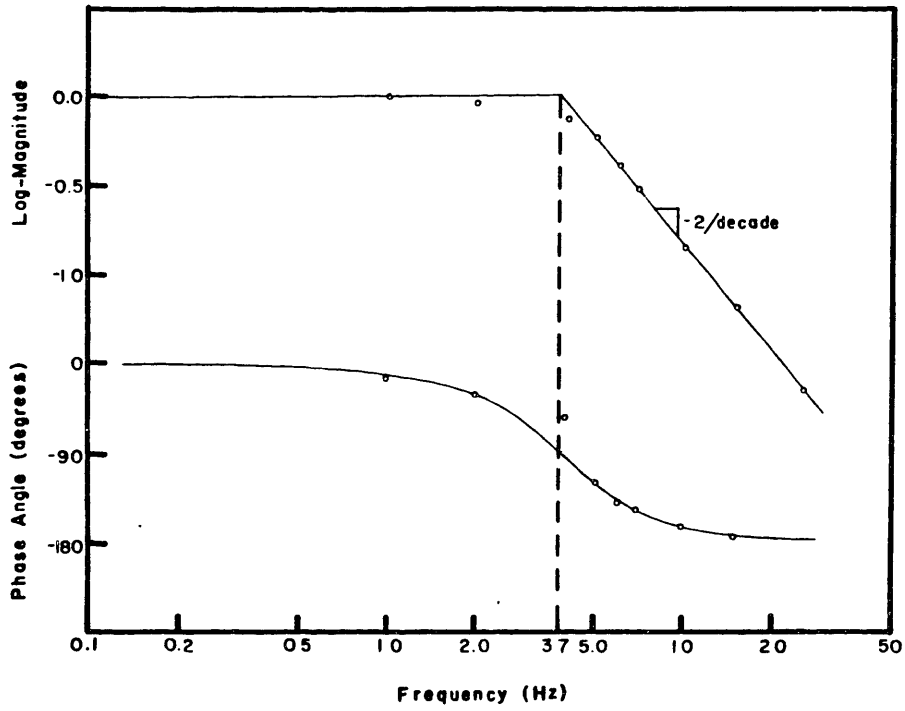

Figure 20. Position Servo Bode Diagram

are the step response and frequency response of the position servo. These plots show that the position servo is a critically damped second-order system with a bandwidth of 3.7 Hz. Thus the model for the position servo given by Equation 18 is a very good approximation if $\zeta = 1.0$ and $w_n = 23.2$ rad/sec.

Measurement and Filter Model

The transducers needed to measure maximum moment and loaded curvature will have a very large bandwidth compared to the servo system, so the dynamics of the measurements can be ignored. The signals must be filtered to eliminate high-frequency noise from the transducer signals and reduce signal aliasing. The amount of filtering necessary and the break frequency of the filters will vary depending on the quality of the transducers, the required accuracy, the type of bending, and the sampling frequency. In any case the filters can be modeled as a combination of first- and second-order differential equations. The filters used on all of the experimental transducers are second-order Butterworth filters with a break frequency of 130 Hz. Figure 21 shows the frequency response of the filters. The response is second-order and can be modeled using Equation 12 with $\zeta = 0.707$ and $w_n = 820$ rad/sec.

Disturbance Model

Disturbances in the system such as initial curvatures in the workpiece can be modeled as a shift of the moment-

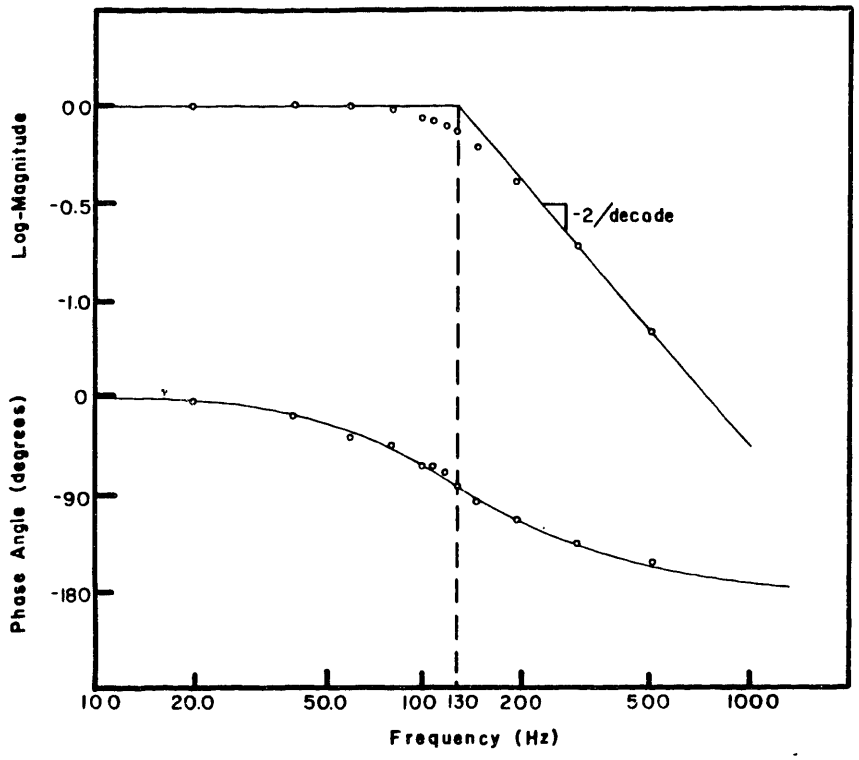

Figure 21. Filter Bode Diagram

curvature curve, as shown in Figure 7. This shift is incorporated into the workpiece model by changing the yield point as shown in Figure 22. The disturbance curvature causes a change in the unloaded curvature which is exactly equal to the disturbance curvature. This is shown as a direct addition in Figure 22. The shift in the yield point is determined by applying Equation 16. This is modeled as an additive term in Figure 22 which affects the input to the workpiece model. Equation 28 is the combined model for the workpiece and curvature disturbance. This is the method used in the simulation program listed in Appendix 4. Figure 23 is a plot of scaled moment, loaded curvature, and unloaded

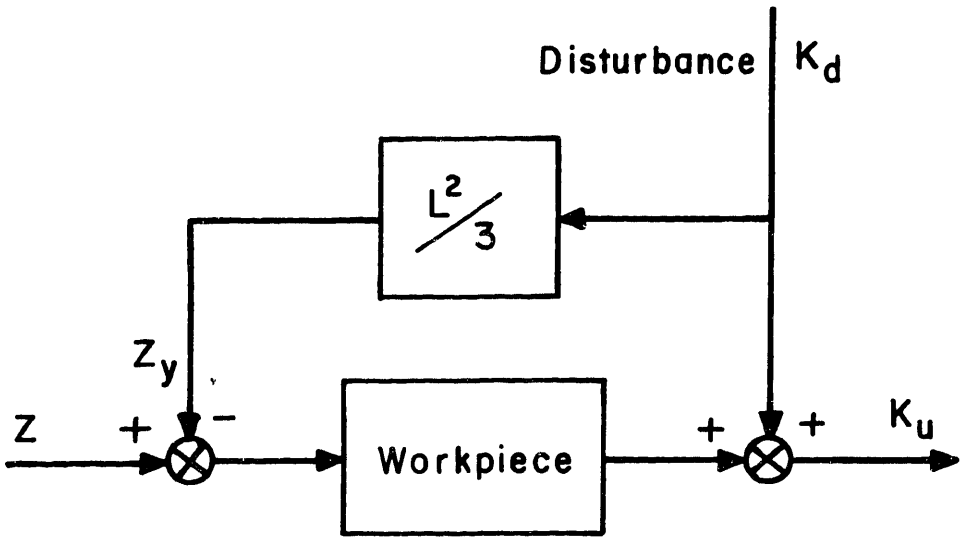

Figure 22. Disturbance Model Block Diagram

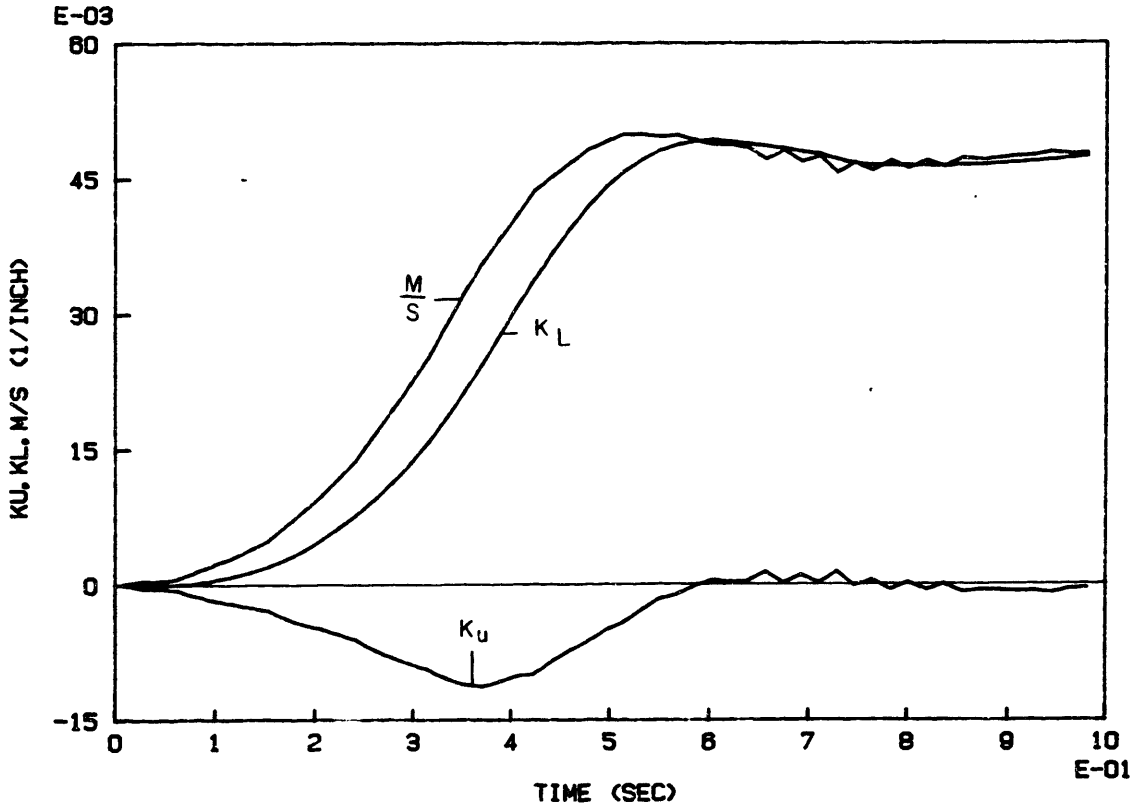

Figure 23. Disturbance Detection

curvature as a workpiece which has an initial bend is straightened by the experimental bending apparatus. This figure shows how the initial curvature disturbance is detected by the closed-loop control scheme. Detection of the disturbance indicates that the disturbance is within the control loop, which means that the disturbance can possibly be eliminated with an appropriate controller. Notice that there is an apparent shift between the moment and the loaded curvature in Figure 23. From Figure 3 it would seem that such a shift is impossible because any change in the moment requires a corresponding change in the curvature. But this is true only if the workpiece has a constant initial curvature, which means that the origin of the moment-curvature relationship is stationary. If the initial curvature changes, then the moment-curvature curve shifts as in Figure 7. This shift can be described as a change in curvature (from zero to some initial curvature) without a change in moment (unloaded in both cases), thus the apparent shift. Figure 23 indicates a change in moment without a change in curvature. This is because of the geometry of the roll bending apparatus which causes the apparatus to sense the disturbance in the moment measurement rather than the curvature measurement. As stated earlier, the curvature is a very strong function of center-roll position. In fact the loaded curvature measurement in Figure 23 is actually proportional to center roll position as given in Equation 16. When a flat

workpiece which contains a kink is rolled through the bending apparatus, the following is observed. As the kink reaches the input roll and begins to enter the system, the workpiece tends to straighten because the rolls are initially stationary, and the curvature of the workpiece tends to remain constant. The moment however, changes to reflect the occurrence of the disturbance. This situation corresponds to Point A in Figure 7 and to the first 0.1 sec in Figure 23. As the moment increases more than the curvature, the system responds to eliminate the disturbance. This corresponds to the response shown in Figure 23 up to 0.6 sec, where the system has nearly reached steady state. This example demonstrates that the closed-loop roll bending system will always detect curvature disturbances with the moment measurement.

Controller Model

A specific controller model will be developed in the next chapter, but the general form of the controller is given here. One important feature of the controller that must be taken into account if the controller is to be implemented by a digital computer, is the discrete nature of the control signal. Even though the mechanical system is a continuous system, the control signal from the computer will change only at discrete intervals. This discretization can be modeled by a zero-order hold equivalence. This model assumes that the control signal is held constant over each interval until

updated at the next sampling time as shown in Figure 24. Using Laplace transform notation the zero-order hold (ZOH) can be described by:

$$ZOH = \frac{e^{-\tau s}}{s} \qquad (20)$$

where τ is the time in seconds of the interval between control signals and s is a complex variable defined in the Laplace operator. For the computer and controllers used with the experimental apparatus, τ varied from 0.009 to 0.012 depending on the amount of computation required by the controller.

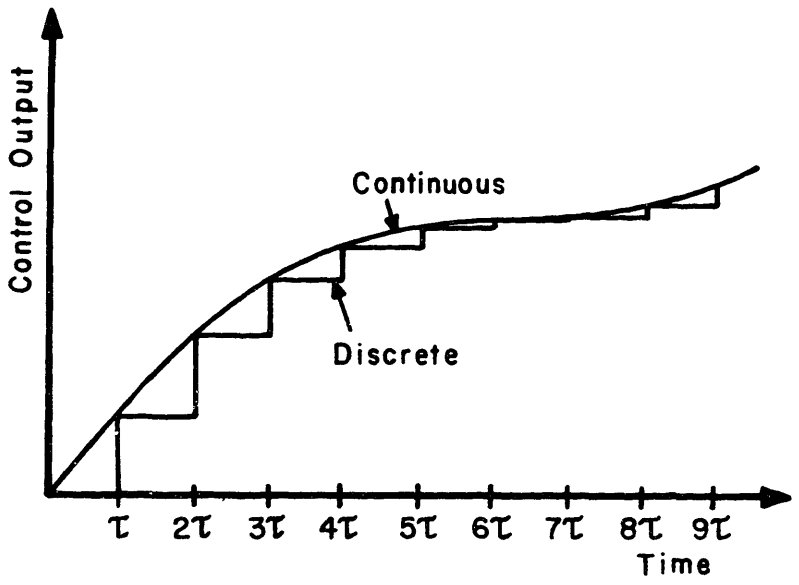

Figure 24. Discretized Control Output

Chapter 4

CONTROL

The models developed in Chapter 3 indicate that the roll bending system is very much like a standard servo system. The servo is the major component of the system and contains most of the significant dynamics. If the non-zero portion of Equation 17 is a perfect description of the relationship between servo movement and unloaded curvature, and if all the parameters are known exactly, then the roll bending control design nearly reduces to a standard servo controller. But the details of the servo/workpiece interaction introduce unique dynamic effects which require more detailed analysis than the standard servo control problem. In particular, the deadband region represented by the zero portion of Equation 17 and the presence of disturbances in the form of initial curvature are unique properties of the roll bending system.

Although the workpiece model is nonlinear, there is some insight to be gained from a linear control analysis. If the workpiece can be described as a variable gain, then a linear analysis should indicate the general form of the system response to a specific controller. For this reason the roll bending system will first be analyzed using linear control techniques. These techniques are well known and will be used without derivation (see for instance [25] or [26]). The control schemes suggested by this analysis will then be eval-

uated by using a computer simulation of the roll bending system which includes the nonlinear workpiece model and the discrete controller. This nonlinear control analysis should produce a more realistic simulation of the actual system response.

Control Objectives

The feasibility of closed-loop control of the roll bending operation has been demonstrated using rudimentary control in [18], [20], and [21]. The purpose of the control analysis in this chapter and the experiments described in Chapter 5 is to determine, if possible, the ultimate limits of the roll bending system response and the practical factors unique to the roll bending process that limit the response. The control objective is to determine what control scheme or schemes can be used to attain this ultimate response. The problem is defining "ultimate response", because on a practical level the required system response will vary depending on the type of bending, part shape, feedrate, and error tolerance. The control objective can be stated in general terms, however, with individual objectives taking on more or less importance for a specific application. To compare the various control schemes the following control criteria will be used to evaluate system response.

1) Stable system

Obviously any controller should be designed so that the

roll bending system is always stable. There are several areas of particular concern. First, the nonlinearities cause stability problems. Because the workpiece is a variable gain dependent on bending stiffness and servo position, a control scheme that is stable for a particular workpiece and bending condition might not be stable for different workpieces and conditions. Second, unmodeled dynamics can cause instability if the system bandwidth is large enough. There are unmodeled dynamics in all components, but particularly in the servo system and workpiece. The servo system has unmodeled dynamics associated with friction, backlash, and compliance in the coupling between the DC motor and the ballscrew. The workpiece is modeled as a variable gain, but actually contains mass, compliance, and damping. These unmodeled workpiece dynamics are especially troublesome as shown in Chapter 5.

2) Zero steady-state error

This objective is very important for straightening applications or for other types of bending where a high degree of accuracy is required. Steady-state error is generally associated with a particular input. The steady-state error properties of the control schemes developed in this chapter will be evaluated in response to a step input. Linear control theory shows that a free integrator in the open-loop transfer function (Type I system) is enough to guarantee zero steady-state error to a step input. Note that

a free integrator does not necessarily guarantee zero steady-state error in response to system disturbances, depending on where the disturbances enter the system in relation to the integrator. This becomes important for the straightening operation, since initial curvature is a disturbance to the closed-loop roll bending system.

3) High bandwidth

The high bandwidth criterion is really a measure of how well the system can follow a command. The required bandwidth of the system is determined largely by the frequency content of the input command and the disturbances. For the roll bending system the input command and the disturbances are in the form of curvature as a function of the distance along the workpiece. In other words the input commands and disturbances have a constant spatial frequency, but the time frequency is variable depending on the feedrate. For example, consider a workpiece that contains an initial curvature that is a sine wave of unit amplitude and 1.0 cycle/ft of length frequency along the workpiece. If the workpiece is rolled through the bending apparatus using a feedrate of 1.0 ft/sec, then the controller will measure a disturbance which has a frequency of 1.0 cycle/sec. If the same workpiece is rolled through the apparatus using a feedrate of 2.0 ft/sec, then the disturbance seen by the controller is at a frequency of 2.0 cycle/sec. This shows that the feedrate actually deter-

mines the temporal frequency content of the input or disturbance. The frequency response of the roll bending system is purely time based which means that it is independent of the feedrate. The system will respond to a command in the same manner regardless of the feedrate. Consider the implications of the spatial/time relationship. Any increase in system bandwidth will allow a proportional increase in feedrate. Reverse the example above. A system with a 1.0 cycle/sec bandwidth is capable of forming a unit magnitude, 1.0 cycle/ft frequency curvature with maximum feedrate of 1.0 ft/sec. If the feedrate is increased for this system, the output curvature will have less than unity magnitude. If the system bandwidth is increased to 2.0 cycle/sec, then the system can form a unit magnitude, 1.0 cycle/ft frequency curvature using a feedrate of up to 2.0 ft/sec. Conversely, a high spatial frequency curvature can be formed by a small bandwidth system if the feedrate is small enough. The control systems developed in this chapter will be analyzed on the basis of time frequency only, with the intention of increasing productivity of the roll bending system by increasing feedrate.

4) Disturbance rejection

Initial curvature, friction, and external forces all enter the roll bending system as disturbances which cause the unloaded curvature to deviate from the commanded curvature. The closed-loop control scheme must be able to reject these

disturbances. This objective is most important in straightening applications where the only requirement of the controller is to eliminate disturbances. But some other applications such as bending an initially curved workpiece, also require good disturbance rejection.

Linear Control Analysis

The transducer filters have been designed so that the break frequency of the filters is very large compared with break frequency of the position or velocity servo. This means that the filter dynamics should be negligible compared with the servo dynamics. The filter poles can then be ignored in the control analysis. All of the following control analysis and design is done under the assumption of negligible filter dynamics. The validity of this assumption will be examined in the next chapter.

The only nonlinearity in the component models derived in Chapter 3 is in the workpiece model. All other components are well represented by linear models. For the linear analysis it is necessary to linearize the workpiece model. Because the nonlinearity is going to be included explicitly in the computer simulation, it is sufficient to obtain only a rough approximation of the nonlinear model. Because the unloaded curvature is a nonlinear function of roll position only, the simplest linearized model is a constant gain operating on the roll position.

Consider the difference between a roll bending system based on position servo and one based on a velocity servo. If the center roll is controlled by a position servo, then a change in servo position will result, through interaction with the workpiece, in a change in curvature if the system is past the deadband region. This correlates well with the workpiece model of a pure gain. If, however, the center roll is controlled by a velocity servo and the workpiece is a pure gain, then a step change in servo velocity should result in a change in the rate of change of unloaded curvature. In fact this does occur, but the controller is still measuring unloaded curvature and not rate of change of unloaded curvature. This means that an integration has occurred somewhere in the velocity servo interaction with the workpiece. In other words, because the unloaded curvature is a function of roll position only and not roll velocity, the workpiece operation on the servo velocity is actually a gain and an integration. Therefore the workpiece model must be modified to include a free integrator as well as a gain for a roll bending system based on a velocity servo. The location of the integrator is important because the location has implications for the steady-state error in response to a disturbance. Consider the general second-order system shown in Figure 25. The disturbance D_1 occurs before the integrator. This disturbance might correspond to a torque disturbance on the velocity servo of the experimental roll bending apparatus

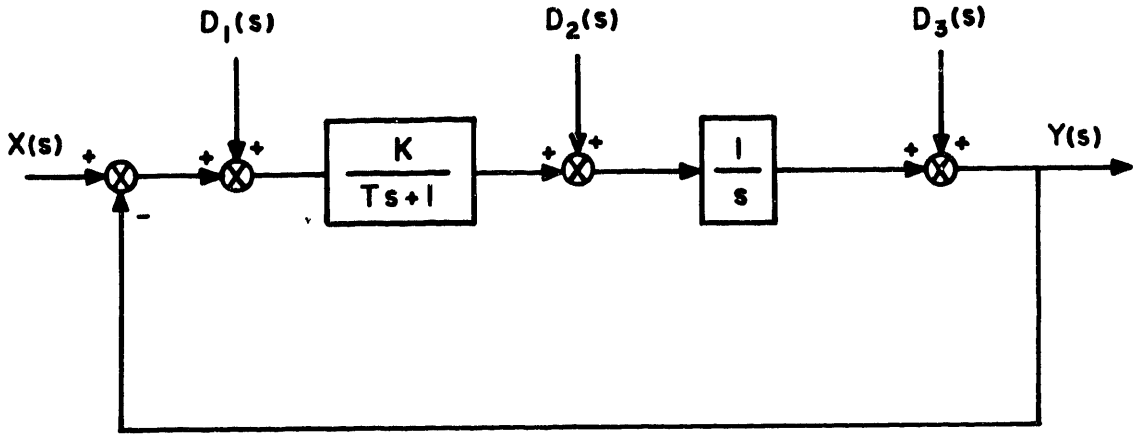

Figure 25. Disturbance Block Diagram

caused by friction or to the load applied to the servo by the workpiece. Disturbances D_2 and D_3 might correspond to an initial curvature disturbance in the roll bending system. The transfer functions from each of the disturbances to the output are given below in Equations 21 to 23.

$$\frac{Y(s)}{D_1(s)} = \frac{1}{Ts^2 + s + K} \tag{21}$$

$$\frac{Y(s)}{D_2(s)} = \frac{Ts + 1}{Ts^2 + s + K} \tag{22}$$

$$\frac{Y(s)}{D_3(s)} = \frac{Ts^2 + s}{Ts^2 + s + K} \tag{23}$$

From these equations the steady-state (s = 0) response of the system to each of the disturbances can be determined:

$$\frac{Y(s)}{D_1(s)_{ss}} = \frac{1}{K} \tag{24}$$

$$\frac{Y(s)}{D_2(s)_{ss}} = \frac{1}{K} \tag{25}$$

$$\frac{Y(s)}{D_3(s)_{ss}} = 0.0 \tag{26}$$

As indicated above, if the disturbance enters before the integrator, the output has a finite error. Disturbances which enter the system after the integrator are rejected completely and do not cause any steady-state error. It is not obvious where an initial curvature disturbance enters the velocity-based roll bending system in relation to the workpiece integrator. The disturbance model in Figure 22 shows that the curvature disturbance operates on center-roll position indicating that an integration must occur before the

disturbance. This assumption will be explored in more detail in the experiments of Chapter 5.

Figures 26 and 27 are block diagrams of the roll bending system based on a position servo and a velocity servo, respectively. The position servo block in Figure 26 is drawn to emphasize the fact that the servo integrator is within the servo loop and is not a free integrator, which is necessary for zero steady-state error. The workpiece model in Figure 26 is operating directly on position and cannot contain an integrator. The workpiece model in Figure 27 does contain a free integrator which means that the system based on a velocity servo has the required zero steady-state error. A free integrator could be included in the controller of the position-servo based system, but this degrades system response and decreases the relative stability of the system. This can be seen more easily on the root-locus diagrams shown in Figures 28 and 29. The root-locus plots are drawn with the same scale in the S-plane. The numbers used are from the experimental apparatus models in Chapter 3. The controller is actually discrete, as discussed earlier, but these continuous root-locus diagrams are sufficient to point out the differences between the position- and velocity-servo based systems. Figure 28 is the root locus of the position-servo based system with an integral controller. Figure 29 is the root locus of the velocity-servo based system with only a proportional controller. Notice that the addition of the

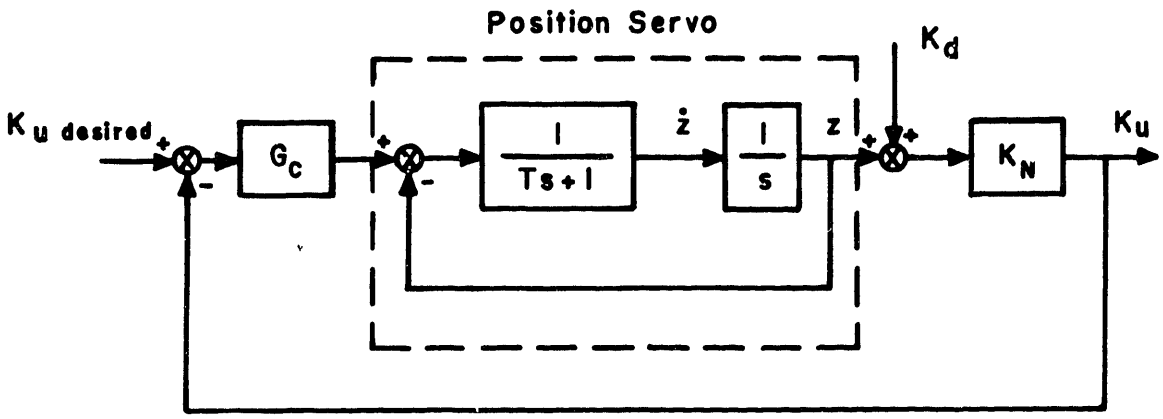

Figure 26. Position-Servo Based Block Diagram

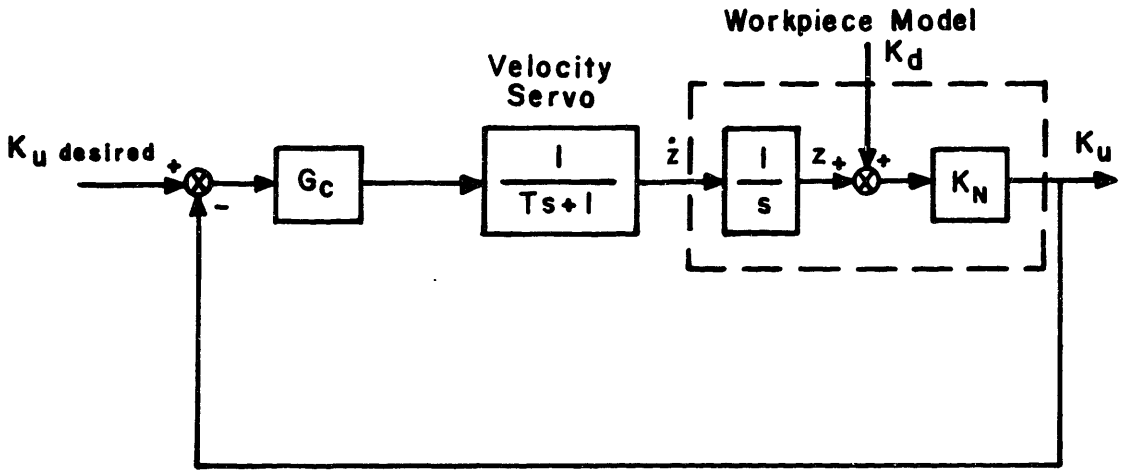

Figure 27. Velocity-Servo Based Block Diagram

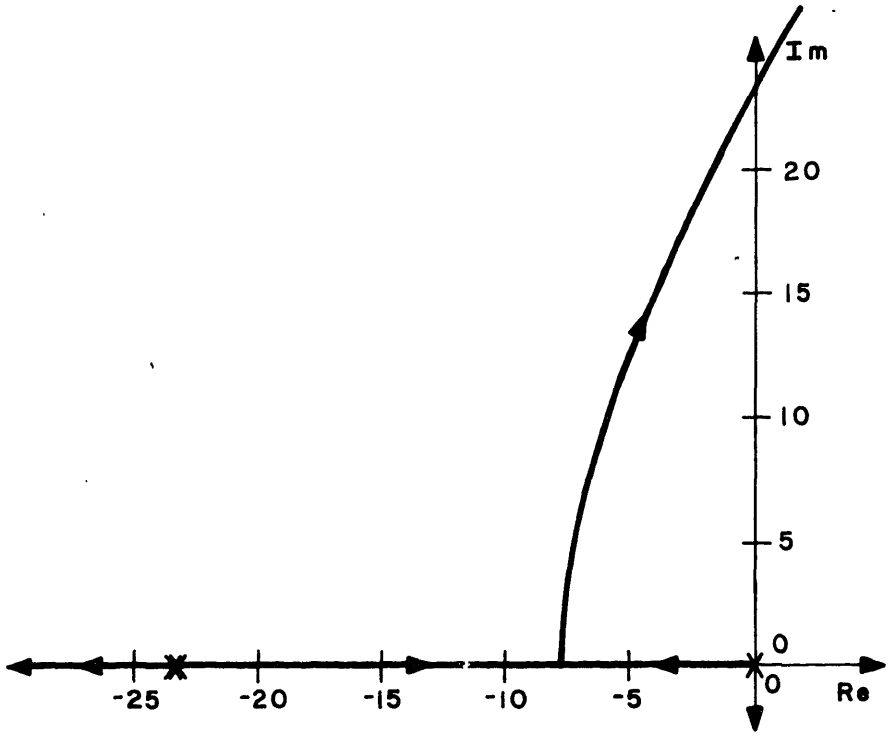

Figure 28. Position-Servo Based Root Locus

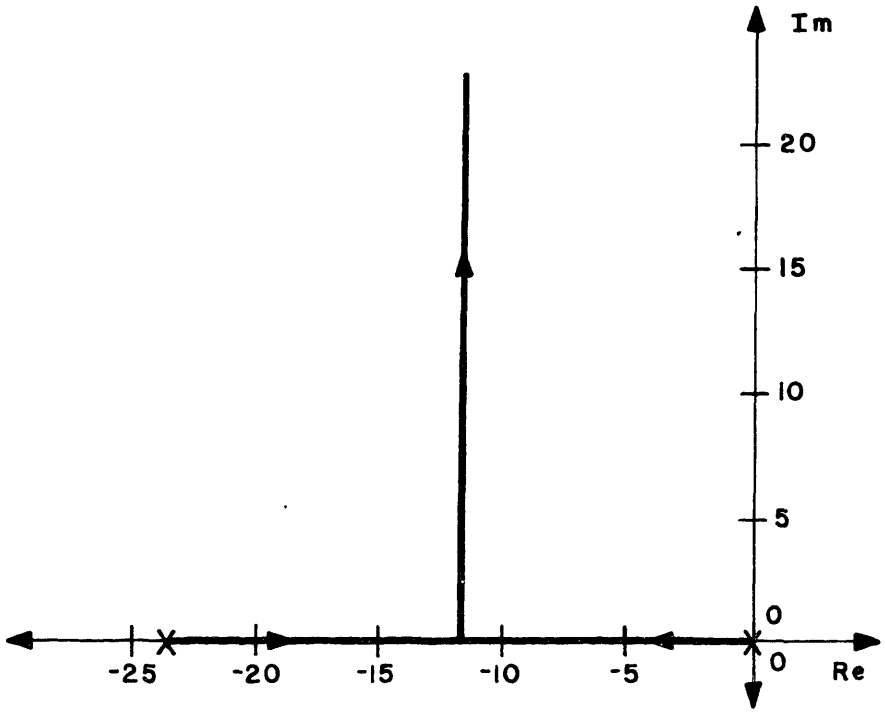

Figure 29. Velocity-Servo Based Root Locus

integrator in Figure 28 increases the order of the system. Notice also that the higher-order system becomes unstable as the gain is increased. The system in Figure 29 is only second order and will never go unstable. Remember that the stability of both systems is overstated in this simplified linear analysis. Nevertheless, the roll bending system based on a velocity servo appears to have many advantages over the position-servo based system. It has good inherent steady-state error and stability properties. For these reasons, the roll bending system based on a position servo will be discarded at this point and the control analysis will be continued for the velocity-servo based system only.

As indicated above the continuous controller assumption overstates the actual system stability. This can be shown by using discrete-time control analysis. For the discrete analysis the continuous physical system must be converted to an equivalent discrete system and described using Z transforms. There are many different methods used to convert continuous systems to discrete form (see [25]). The easiest method is a mapping technique whereby the poles and zeros in the continuous S-plane are mapped to the discrete Z-plane according to the rule $z = e^{sT}$ where z and s are the location of the pole or zero in the Z-plane and S-plane respectively and T is the cycle time for the discrete controller. There is also a scale factor applied to the Z transform to match final values of the discrete and continuous models, but that

will be ignored here. Figure 30 shows the map of the continuous system shown in Figure 29 in the Z-plane using a sample time of T = 0.01 sec. The shape of the root locus is the same but the interpretation is different. The stability limit in the Z-plane is the unit circle. As seen in Figure 30, the system becomes unstable at higher gains. This instability is caused by the discrete nature of the sampling and control. The control signal and the transducer readings are only updated at discrete intervals. As the system bandwidth approaches the sampling frequency, the controller receives and sends outdated information. The effect is similar to a phase lag in continuous systems and the result is instability.

If the velocity servo bandwidth is high enough, it might be possible to achieve an acceptable roll bending system bandwidth using a simple proportional controller at very low gains. Better system response could be attained by adding a zero to the system and drawing the poles to a position of higher bandwidth and greater stability as shown in Figure 31. A zero can be added to the system either by including it in the controller or by feeding back the rate of change of output as well as the output. In a discrete controller, however, there can never be more zeros than poles because this would require information from future time steps that the computer does not have. This problem can be solved by including a very fast pole, but this increases the order of

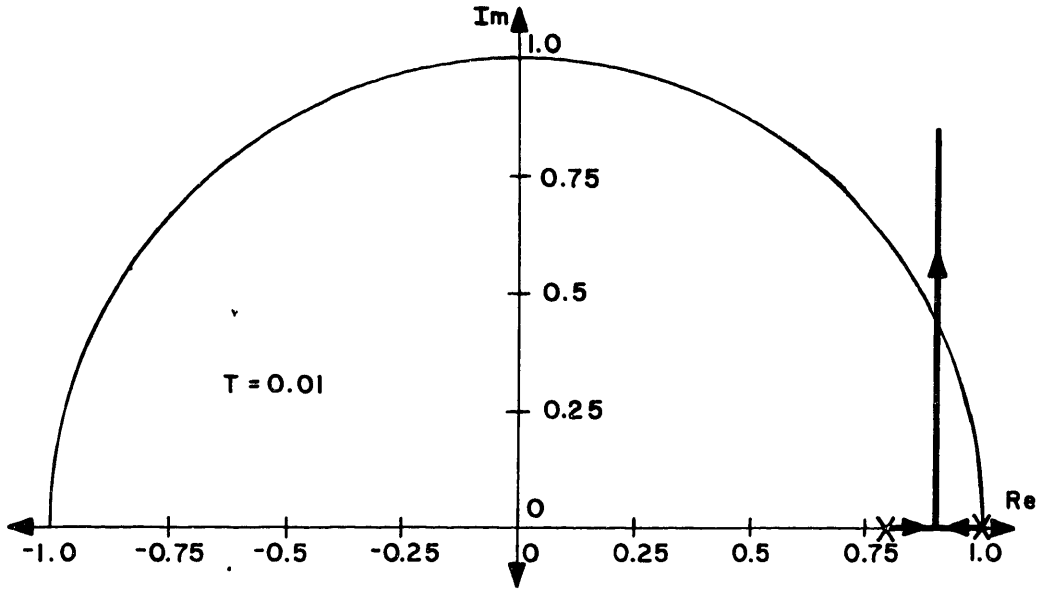

Figure 30. Velocity-Servo Based Z-Plane Root Locus

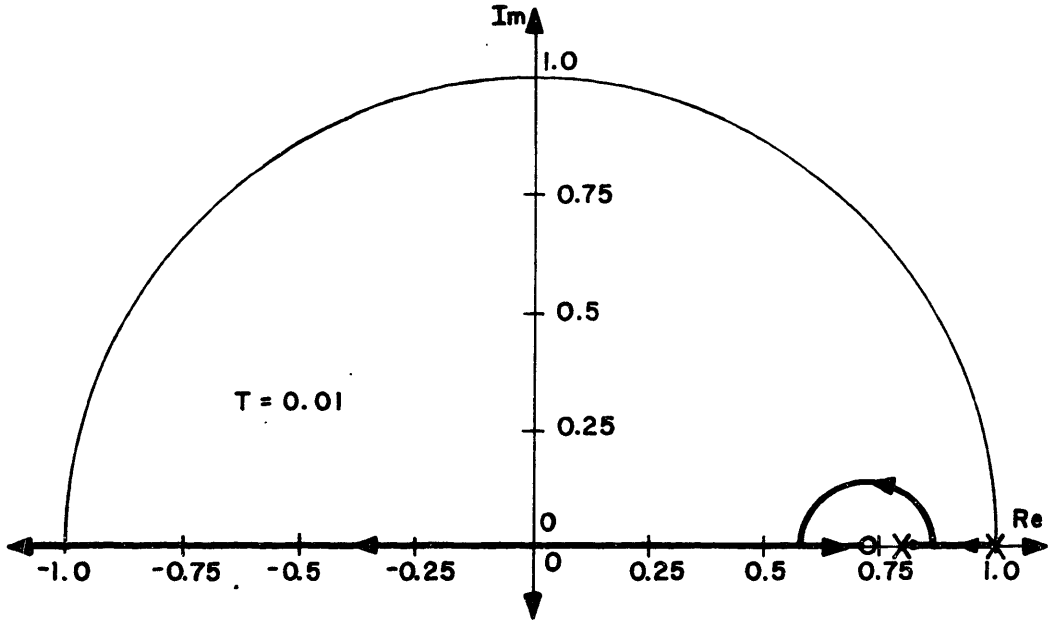

Figure 31. Z-Plane Root Locus with a Zero

the system and introduces greater complication. In addition, since a zero implies that the controller is taking the derivative of the input signal, any noise in the system can cause large fluctuations in the controller output.

Measuring the rate of change of the output is a more attractive method of adding a zero to the system because it is less affected by noise and also because the transient response has less overshoot for similar systems. For the roll bending system the output is unloaded curvature, which is measured as detailed in Appendix 1. The rate of change of unloaded curvature is much more difficult to measure. It is possible, however, to obtain a reasonably good approximation of the rate of change of unloaded curvature by either of two methods. One method is to divide the difference between two subsequent unloaded curvature measurements by the time interval between the measurements as shown in Equation 27:

$$\dot{K}_u(nT) = [K_u(nT) - K_u((n-1)T)]/T \qquad (27)$$

where $K_u(nT)$ is the unloaded curvature at time nT and $\dot{K}_u(nT)$ is the rate of change of the unloaded curvature at time nT. This is actually not a measurement of the rate of change of output but a backward difference. Therefore it is more like a zero in the controller and is subject to the same noise problems. In addition it is always delayed by half a time

step because it uses unloaded curvature information from the current and the previous time steps. More elaborate differentiation schemes are available, but they require considerably more computation. A better measurement method is to use roll velocity as an approximate measure of rate-of-change of unloaded curvature similar to the way that roll position can be used to estimate unloaded curvature. The relationship between roll position, z, and unloaded curvature, K_u, is given by Equation 17. If the effect of disturbances is included, the equation becomes:

$$K_u = K_d \qquad z < (z_d + z_y)$$

$$K_u = \frac{3}{L^2}(z - z_d) - \frac{9z_y}{2L^2} + \frac{3z_y^3}{2L^2(z - z_d)^2} + K_d \qquad z \geq (z_d + z_y) \tag{28}$$

where K_d is the curvature disturbance and z_d is given by:

$$z_d = K_d L^2/3 \tag{29}$$

Taking the derivative of Equation 28 gives:

$$\dot{K}_u = \dot{K}_d \qquad z < (z_d + z_y)$$

$$\dot{K}_u = \frac{3}{L^2}(\dot{z} - \dot{z}_d) - \frac{3z_y^3(\dot{z} - \dot{z}_d)}{L^2(z - z_d)^3} + \dot{K}_d \qquad z \geq (z_d + z_y) \tag{30}$$

The rate of change of unloaded curvature depends on four variables: the roll position, z; roll velocity, $\dot{z}$; the curvature disturbance, K_d; and rate-of-change of curvature disturbance, $\dot{K}_d$. Notice that in the second term the z and z_d terms are cubed in the denominator which indicates that the relative magnitude of the second term will quickly become much smaller than the first term. The rate of change of curvature is determined by the feedrate as well as the distribution of curvature along the workpiece. But for most bending applications $\dot{K}_d$ will be small compared with $\dot{z}$. Therefore it is likely that roll velocity can be used to estimate rate of change of unloaded curvature using only the linear terms.

$$\dot{K}_u = 3\dot{z}/(L^2) \tag{31}$$

Notice that a controller using Equation 31 as an estimate of $\dot{K}_u$ should provide slightly more damping and greater stability in the deadband region than if the true $\dot{K}_u$ were used. This

is because although $\dot{K}_u$ is zero in the deadband region (if $\dot{K}_d$ is zero), Equation 31 indicates a rate of change in unloaded curvature proportional to the roll velocity.

If Equation 31 is an accurate model of $\dot{K}_u$ and if the workpiece does actually perform an integrating function on the center-roll velocity, then a control scheme which uses a proportional controller and K_u plus $\dot{K}_u$ feedback should result in a roll bending system which has a root locus as shown in Figure 31. Figure 31 indicates that the system bandwidth can be increased to the Nyquist frequency, but practical considerations such as transducer noise, servo saturation and unmodeled dynamics will limit the maximum bandwidth to considerably less than the maximum theoretical limit. Nevertheless the control scheme as described is quite attractive because, with proper placement of the zero, the system will have very good stability robustness, zero steady-state error, high bandwidth, and good disturbance rejection. Also, a wide range of second-order system responses is possible by manipulation of the gain and the zero location. The linear control analysis indicates that this control scheme will give very good system response. The next step is to perform a nonlinear analysis to determine the effect of the nonlinearities on system response.

Nonlinear Control Analysis

A computer program has been developed to simulate the

roll bending system and to include the nonlinear workpiece model and the discrete controller. The program, detailed in Appendix 4, uses a fourth-order Runge-Kutta integration technique to model the continuous system. The discrete controller is modeled using difference equations exactly as they would appear in the actual controller. The control signal is updated only at the Runge-Kutta time steps corresponding to the sampling interval of the controller.

The nonlinear workpiece model used in the simulation program is given by Equation 28. Notice that this equation models the loading deadband region, but does not include any hysteresis. This means that the program can simulate a moving workpiece assuming that each point on the workpiece is formed only once, but cannot model a stationary or slow moving workpiece. A more complex workpiece model could be used to model stationary workpieces but because the objective of this research is to increase the productivity of the roll bending process by increasing the maximum feedrate, the moving-workpiece model is adequate. Equation 28 must be calibrated for a specific workpiece since the bending stiffness and the yield point are different for different materials and workpiece shapes. For the simulations shown below the workpiece modeled is a 1/4" X 1" aluminum strip. The calibration factors used are taken from the experiment shown in Figure 14. The form of the discrete controller which would implement the control scheme described above is given

by:

$$U = G1[K_u\text{desired} - K_u - (G2)(\dot{K}_u)] \qquad (32)$$

where U is the controller output, G1 is the controller gain, G2 is used to determine the location of the zero, and $\dot{K}_u$ is given by Equation 31. The discrete controller time step is assumed to be T = 0.01 sec in the simulation.

Figure 32 is a simulation of the roll bending system response to a step command input curvature of 0.01 in^{-1}. The factors G1 and G2 in the simulated controller are as listed on the figure. For this simulation the zero is located between the two poles so the response should always be overdamped. The response shown in Figure 32 is as expected. The initial response is zero because of the deadband as the workpiece moves through the linear elastic region. Once past the deadband region, the system moves quickly to the commanded curvature. The error at steady-state is zero, as predicted. The speed of response increases with increasing gain, but the system can limit cycle or even become unstable at very high gains. The fastest response in Figure 32 in on the verge of a limit cycle. A small increase of G1 will result in a limit cycle around the commanded curvature. A large increase of G1 will cause the system to become unstable. Figure 33 shows even faster system response,

although the deadband region has not been eliminated. The zero location for this simulation is as shown in Figure 31. This system shows a faster response because the zero does not trap the slow pole, but draws both poles to a faster location. There is a possibility of overshoot with this zero location and in fact the response for G1 = 350 shows an overshoot of about 1% even though it is difficult to see on the plot. The system remains stable for larger gains with the zero location as shown in Figure 31. Again, higher gains result in faster response and also in smaller steady-state errors to some disturbances. The computer simulation has no provisions for modeling saturation effects, so very fast responses are possible if very large gains are used. But the control power needed to achieve this faster response is very large which means that the velocity servo system would have very large power requirements. In other words there are no theoretical limits to system response using this control scheme if the models used are accurate and if the servo system has infinite power. Figure 34 shows the system response to an initial curvature step disturbance of -0.005 in^{-1}. The curvature command is zero. The zero location is the same as for Figure 32. The system again shows good response and zero steady-state error.

The nonlinear control analysis does not reveal any stability problems with the control scheme developed in the linear control section. The analysis also does not predict

any limits to system response. But as mentioned above the analysis assumes perfect conditions. The roll bending experiments detailed in the next chapter provide more insight into the practical limits of the roll bending system response.

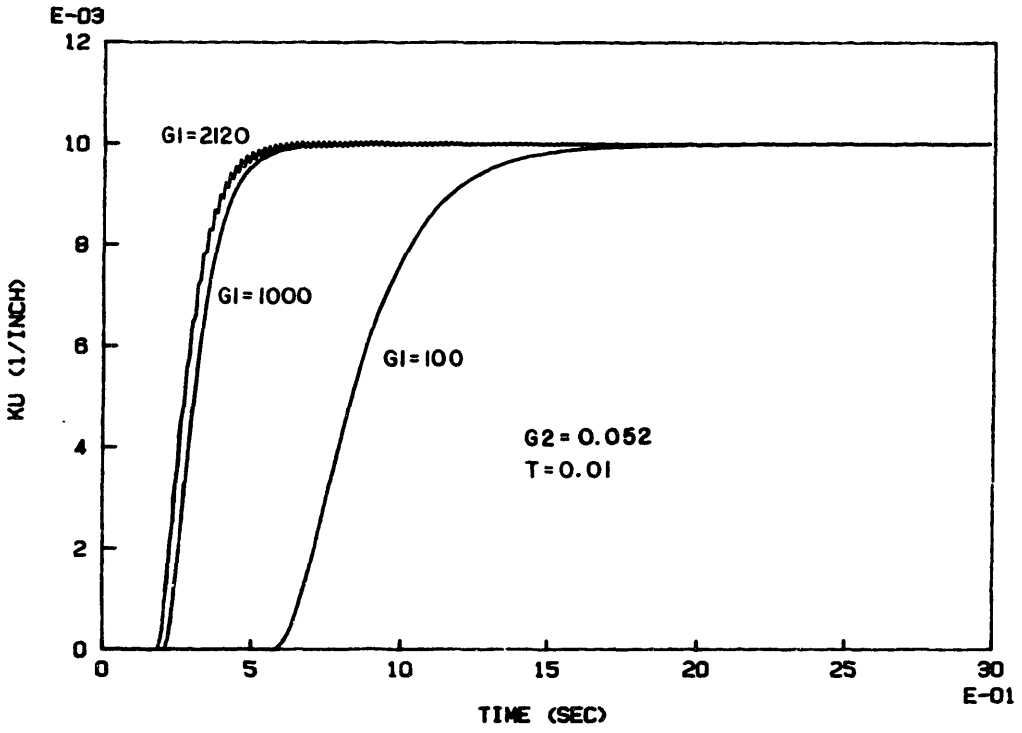

Figure 32. Simulated System Step Response

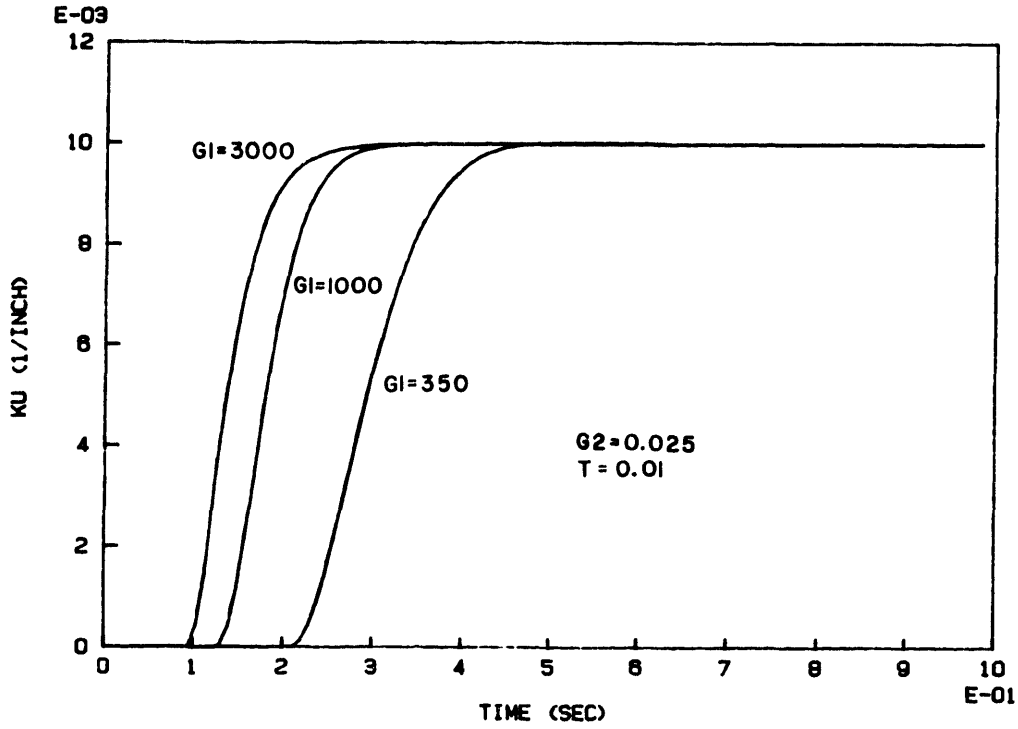

Figure 33. Simulated System Step Response

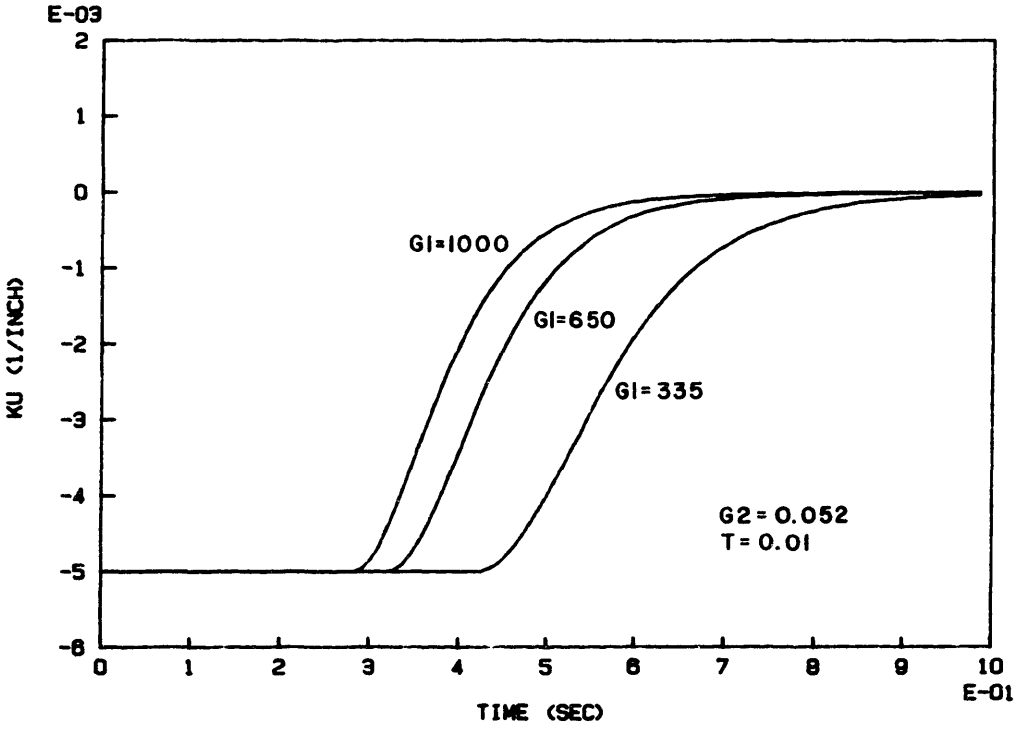

Figure 34. Simulated System Disturbance Response

Chapter 5

EXPERIMENTATION

Experimental Objectives

There are several key assumptions in the control analysis developed in Chapter 4 which need to be examined experimentally. First, the assumption that the workpiece performs an integrating function is crucial for zero error at steady-state. The position of the integrator in the control loop is also important for the analysis of steady-state error to disturbances. Furthermore, the integrating workpiece assumption is the basis for choosing a velocity- rather than position-servo based system. If the workpiece model is incorrect then the control analysis is invalid. Second, the control scheme developed uses a measurement of rate-of-change of unloaded curvature in the feedback signal. As mentioned earlier, $\dot{K}_u$ cannot be measured directly, but is assumed to be proportional to center-roll velocity. Since the $\dot{K}_u$ feedback is used to increase system damping and stability as well as increase the system bandwidth, if the assumption is incorrect there might be stability problems. One objective of the experiments detailed below is to determine if these assumptions are valid and if so, under what conditions.

If the assumptions listed above are valid, then the simplified control analysis in Chapter 4 implies that the upper limits on system performance will be determined by

model accuracy. A second experimental objective will be to determine the practical upper limits of the roll bending system response. There are many practical factors which limit system performance. For the roll bending system, possible limitations are imposed by transducer bandwidth and noise, servo bandwidth and power, and controller design. In many real systems these factors define the limits of system performance, because the cost of high quality transducers and servos often does not justify the performance gain. But because the objective is to explore the performance limits of the roll bending process, the experiments are designed to eliminate, as far as possible, limitations imposed by the hardware. The results provide some insight into the process limitations or the maximum system performance that can be attained given optimal conditions. If the conditions are indeed nearly optimal, then the experiments should also reveal the robustness of the control scheme to the unmodeled dynamics. The implementation details given below show some of the compromises made to reduce hardware limitations.

The velocity servo actuation system, described in Chapter 3 and Appendix 1, is oversized in relation to the workpieces formed in the experiments. This means that the problem of servo power saturation is greatly reduced and will not be a limiting factor in the experiments. The major hardware limitations are the computer speed and transducer noise. The computer speed is a problem because the discrete

controller update frequency and the sampling frequency should be at least twice, and preferably several times as large as the roll bending system bandwidth. Any reduction in the computation needed will increase the controller frequency, but simplifying the computations reduces system accuracy (see Appendix 2). For these experiments the accuracy is not a major concern. The objective is to determine the limits of the control scheme assuming optimal conditions, so for the purpose of these experiments the simplified calculations can be assumed valid. The results using the simplified calculations should provide some information about when the simplifying assumptions are acceptable. The transducer noise problem is more difficult to deal with because the noise contains significant energy across a large frequency range (see Appendix 1). The transducers can be filtered, but heavy filtering places limits on system bandwidth. Of all the possibilities the measurement method with the least noise will be preferable even if some accuracy is lost.

There are several ways to measure loaded curvature, each with specific advantages and disadvantages (see Appendix 2). In some of the experiments described below, loaded curvature is measured using the center-roll displacement according to Equation 16. The remaining experiments are based on an LVDT loaded curvature measurement calculated as shown in Equation 39. The center-roll displacement is measured by a rotary encoder mounted on the DC motor shaft. Loaded curvature

determined by this measurement is not as precise as by some other methods, but has no noise since it is a digital measurement. In addition, the loaded curvature measurement based on center-roll position requires much less computation in the discrete controller than does the LVDT curvature measurement method. Therefore this method for loaded curvature measurement is ideal for the purposes of these experiments. But the experiments show that in some cases, the inaccuracy of the center roll position loaded curvature measurement has very large effects on system response. In these cases the LVDT curvature measurement results in more predictable system response even though this measurement is noisy.

The moment measurement is scaled by the bending stiffness in order to determine the unloaded curvature as shown in Equation 4. Since the force transducer noise is nearly constant for all workpieces, the signal to noise ratio increases dramatically for stiffer workpieces. For this reason, the bending experiments use the stiffest workpieces possible with the experimental hardware. The force transducer signals are also filtered to eliminate high frequency noise. The low pass filters have a break frequency of about 130 Hz. This frequency is much too high to eliminate aliasing according to the sampling theorem, but the input to the transducers is limited to a much lower frequency so the aliasing errors will be small. Again, the objective is to

achieve maximum system bandwidth, not ultimate accuracy. Placing the filters at such a high frequency will ensure that they do not affect system dynamics. The complete equation used to compute the maximum moment is given by Equation 34. The sine and cosine terms are included to reflect the change in the moment arms due to rotation of the roll pairs. For stiff workpieces formed to low curvatures, these terms are negligible. Ignoring these terms increases the computation speed considerably. The moment equation employed in the experiments retains the sine term for D_x because the command curvatures are relatively large. In the computer program the sine term is not calculated using the trigonometric function, but a first-order, small-angle approximation is used instead. This compromise works well because the inclusion of the sine approximation increases the precision, but does not slow the computation down noticeably.

Experiments

The experimental procedure consisted of bending and straightening workpieces using the apparatus described in Appendix 1 and the control program described in Appendix 4. A short description of the experimental procedure is given below. The procedure is presented in more detail in Appendix 4 along with complete discussion of the control program logic. The tests were performed using 2024-T6 aluminum workpieces with a rectangular cross-section 1.0 in wide and

0.25 in thick. The workpiece length varied from 3 to 6 ft. The experimental procedure for forming a workpiece is:

- Load the workpiece in the bending apparatus and start the computer program.
- Enter the control gains and other necessary input from the computer keyboard.
- Measure the bending stiffness of the workpiece (see Appendix 2).
- Turn on the center-roll drive motor to feed the workpiece through the bending apparatus.
- Begin real-time control of the unloaded curvature using the control algorithm developed in Chapter 4 and shown in the program listing in Appendix 4.
- At the end of the workpiece, turn off the drive motor and return the apparatus to the zero position.
- Store the experimental data for future evaluation.

Step Tests

Figures 35 to 38 show the system response for the first test where the input command is a step curvature change of 0.01 in^{-1}. The workpiece is initially flat. In this test the loaded curvature is measured using the center roll position according to Equation 16. The feedrate is 3.3 in/sec. The results of all the experiments shown in this chapter are plotted using every other data point. The controller gains for this test are shown on Figure 35 and correspond to the gains for the simulation in Figure 32. With these gains the zero is located between the open loop poles at z = 0.84. The simulated response from Figure 32 is plotted in Figures 35,

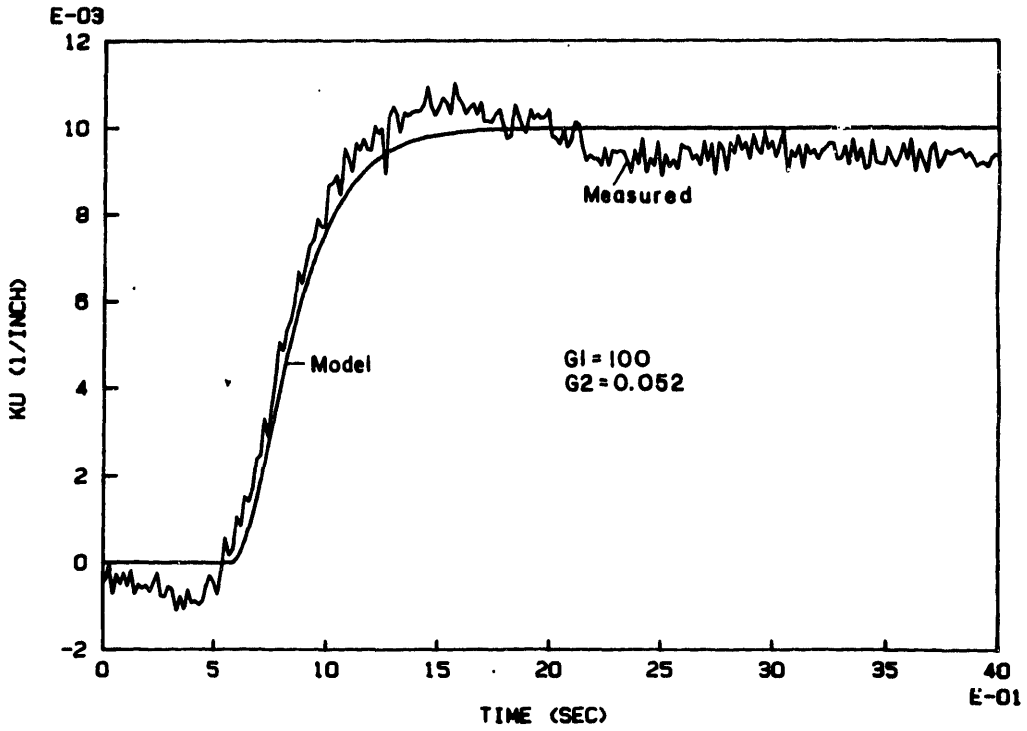

Figure 35. Test #1 Plot #1

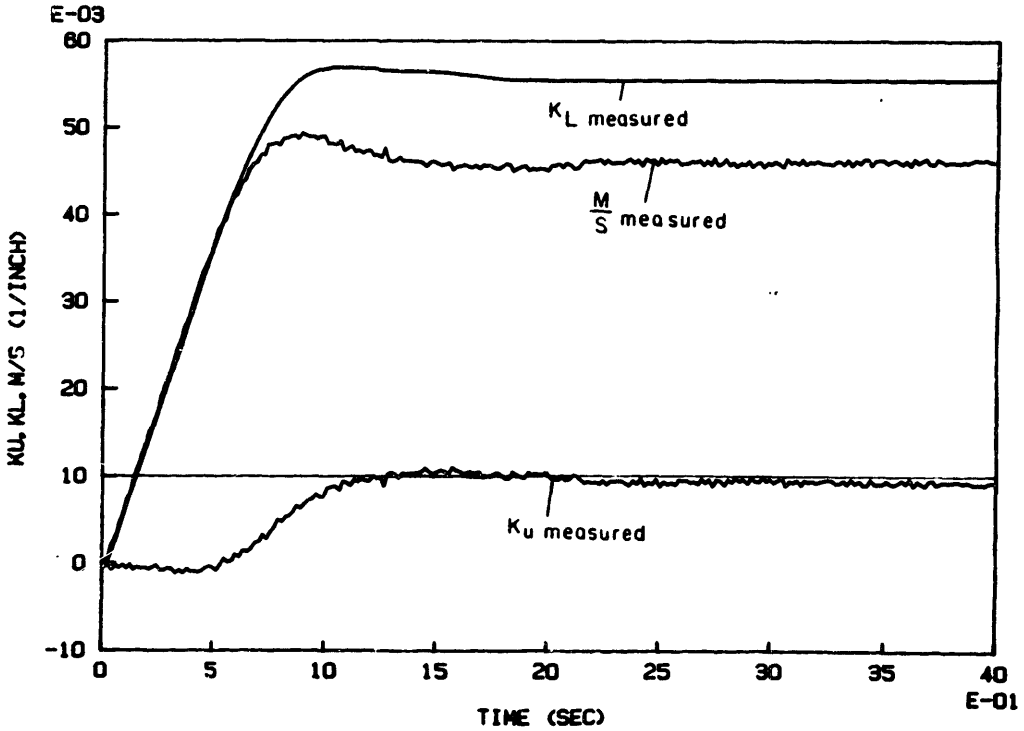

Figure 36. Test #1 Plot #2

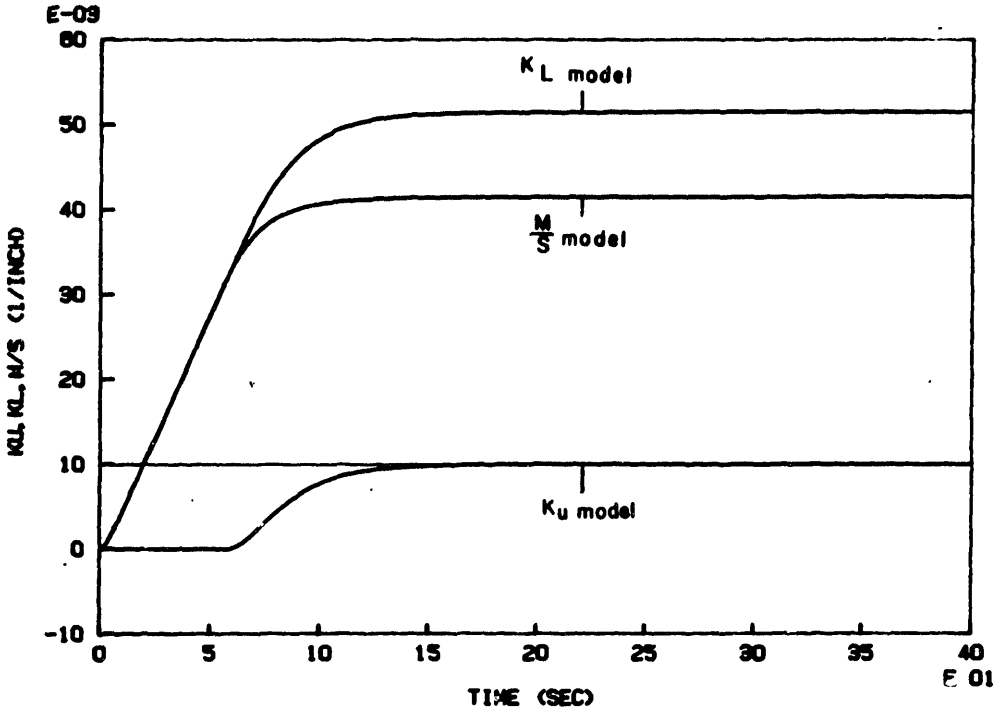

Figure 37. Test #1 Plot #3

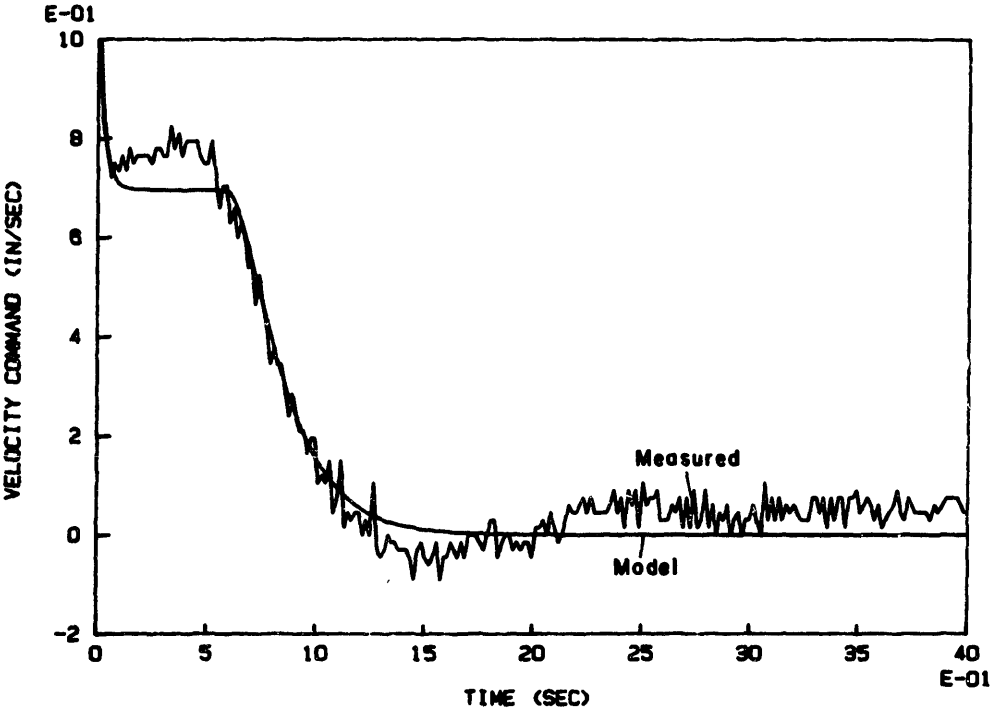

Figure 38. Test #1 Plot #4

37 and 38 for comparison. Although the simulated response has essentially the same form as the actual response, there are three areas where the two responses differ significantly. First the measured initial unloaded curvature is not zero as predicted. This is caused by two factors. The first factor is the initializing procedure for the transducers. For this test the transducers were initialized while the sheet was stationary. When the drive motor is started, a small moment is developed between the center drive roll and the workpiece. This small moment results in an increase in measured moment from the "zero" position which results in a small negative unloaded curvature measurement. This error was eliminated in subsequent tests by initializing the transducers after the drive motor was started.

A second factor which results in errors in the deadband region is the error due to simplifying assumptions in the moment and loaded curvature measurements. Figure 36 shows the loaded and unloaded curvature and the scaled moment for this test. According to bending theory, the loaded curvature and the scaled moment should be exactly the same through the elastic region. Figure 36 shows that the loaded curvature and scaled moment are indeed nearly the same until about 0.6 sec. But notice that where there are differences between the two measurements in the elastic region, the unloaded curvature reflects the error. And because of the steep slope, a small error between the two measurements results in a large

error in the unloaded curvature. The magnitude of the unloaded curvature error will increase as the speed of response increases because the slope of the loaded curvature and scaled moment will increase. This error is due to the simplifying approximations made for the measurement calculations and can only be eliminated by increasing the precision of the measurements. The effect of the error on system response is small, although the damping is reduced somewhat because the initial change of the unloaded curvature is negative while the command is positive. For the purposes of these experiments, the error in the deadband region is not significant and will be acknowledged and ignored.

A second area where the actual response does not conform exactly to the simulated response is the steady-state error. The actual response shows a steady-state error of about 0.0005 in^{-1} or 5%. This could be caused by a disturbance entering the roll bending system before the workpiece integrator as shown in Chapter 4 or possibly the assumption of a workpiece integrator is inaccurate. The velocity servo model in Chapter 3 was developed under the assumption that the internal friction and external load applied by the workpiece are very small compared to the inertia of the servo. This is essentially true, but the small disturbances caused by the friction and external load will result in a small steady-state error even though there is a free integrator in the open-loop transfer function. If this is the

case, then there will be a finite steady-state command to the servo which results in a torque which exactly offsets the torque applied by the disturbances. Figure 38 shows that there is indeed a finite steady-state command to the velocity servo, but as seen in Figure 35 the system does not move. This means that there is a disturbance torque acting on the system. The steady-state velocity command in Figure 38 is about 0.075 in/sec. Experiments with the velocity servo show that in the unloaded state, a command velocity of about 0.12 in/sec is required to overcome friction. Thus in Test 1 the system is measuring an error at steady-state, but because of the low gain, the command input is not large enough to overcome friction and the system remains stationary.

There are several steps which can be taken to reduce the error due to the disturbances although the only way to eliminate the error is to move the free integrator so that it appears before the disturbances in the system as shown in Chapter 4. Including an integrator in the controller would eliminate the steady-state error due to the torque disturbances, but this would create two free integrators in the velocity-servo based roll bending system which would degrade system response and nullify many of the advantages of the velocity-servo based system over the position-servo based system. Other options are more attractive. Equation 24 shows that the error is inversely proportional to the open-loop gain. Increasing the controller gain will decrease the

steady-state error. Figure 39 shows the results of Test 2 which was conducted using the same conditions as Test 1 except that the controller gain was increased from 100 to 335. Also the loaded curvature is measured using the LVDT measurement method according to Equation 39. The reasons for this are explained later. The results show that the steady-state error is much reduced, if not zero. There is some noise in the loaded curvature measurement so the unloaded curvature appears to oscillate, but the oscillation is around the commanded value and it is easy to see that increasing the gain does reduce the steady-state error due to the disturbances. But the increased gain does have side effects which might be undesirable, such as the large overshoot observed in

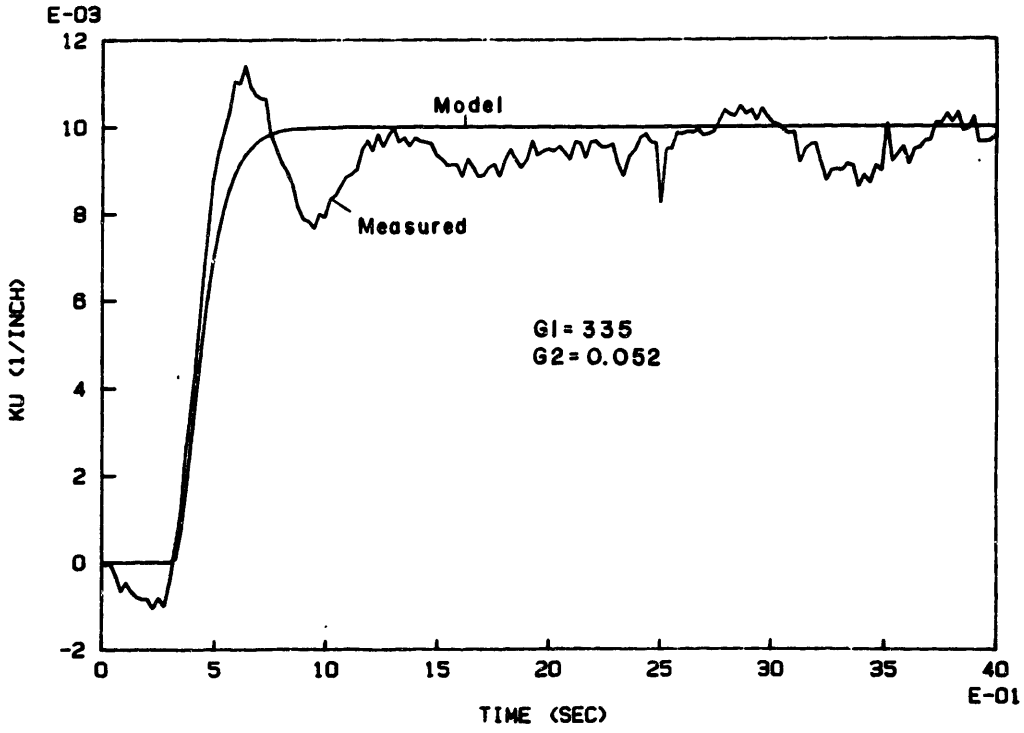

Figure 39. Test #2

Figure 39.

Velocity feedback could also be used to reduce steady-state error by closing the loop around the velocity servo. This is a standard item on most commercial servo systems, but is not included on the velocity servo used for these experiments because of noise problems. It is possible, instead of using velocity feedback, to make an open-loop compensation for the friction effects in software. This is accomplished by adding an amount which represents the frictional effects to the velocity command. Figure 40 shows the results of Test 3 which was conducted using the same conditions as Test 1 except that loaded curvature is measured using the LVDT method and an open-loop software compensation was used to eliminate the effects of friction on the steady-state error. The results show that steady-state error is reduced even though the controller gain is the same. Again there is some oscillation due to noise in the loaded curvature measurement but the oscillation is around the commanded value. This open-loop compensation does not affect the error due to the disturbance from the external load applied by the workpiece. Figure 41 shows the effect of using a higher gain and the open-loop compensation for frictional effects. The controller gain is the same as for Test 2: all other parameters are unchanged. Figure 41 shows nearly zero steady-state error to a step input even in the presence of friction and external load disturbances. The open-loop friction

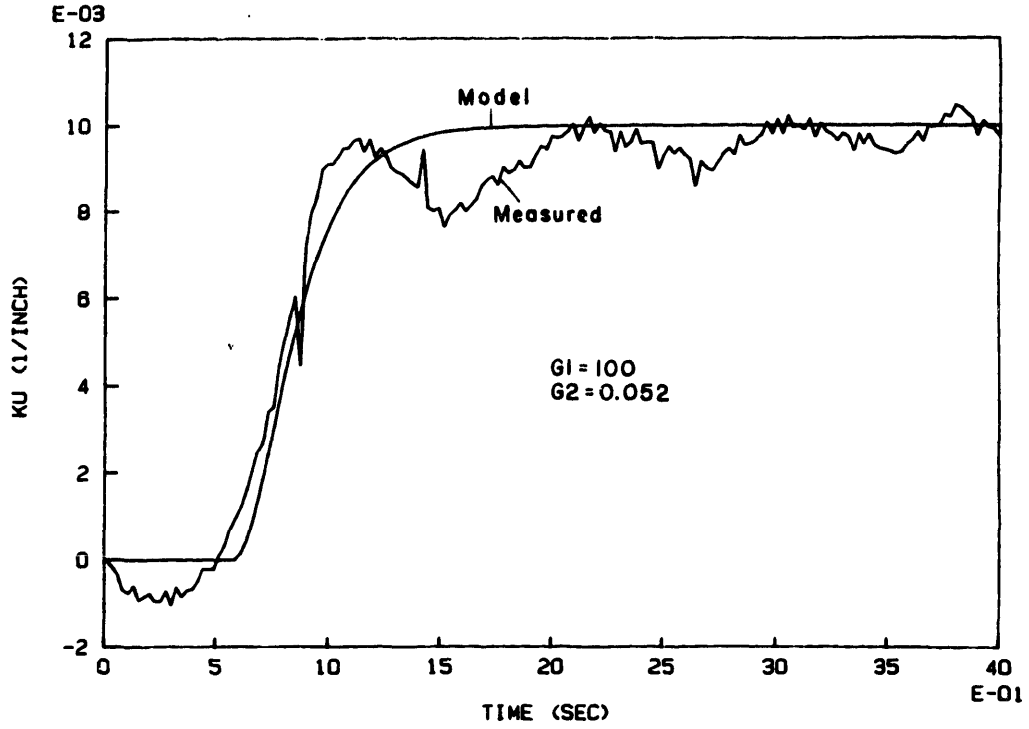

Figure 40. Test #3

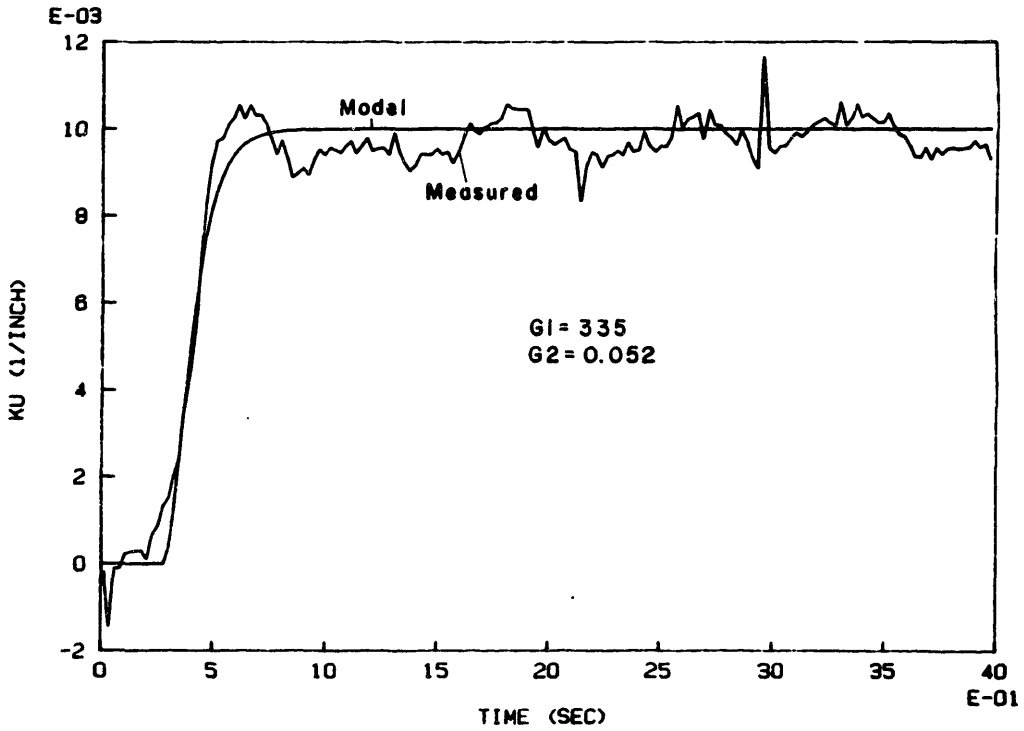

Figure 41. Test #4

compensation is used in all the subsequent experiments. Tests 2, 3, and 4 show that the workpiece does perform an integrating function as predicted and the control scheme suggested in Chapter 4 will satisfy the steady-state error requirement if the effect of the disturbances can be sufficiently reduced. There is still some question whether the initial curvature disturbances will enter the system before or after the workpiece integrator. This question is explored in more detail later.

The third significant variation of the actual response from the predicted response shown in Figure 35 is that the actual response has some overshoot. Even though the overshoot is small, it is significant because the gain and zero location were picked specifically so that the system would be overdamped. As discussed in Chapter 4, if the zero is located between the poles then the system should always be overdamped and the response should never overshoot. There are several factors which could be causing the overshoot. One is that the actual gain and zero location are not as predicted although this is unlikely because the actual response so closely resembles the simulated response and the parameters for the test are taken from the simulation. It is also possible that the unloaded curvature error in the deadband region is contributing to the overshoot. As mentioned earlier the negative unloaded curvature in the deadband region causes the control command to be larger than it would

be otherwise. Another possibility is that the assumption that center-roll velocity can be used to estimate $\dot{K}_u$ is invalid. The $\dot{K}_u$ feedback is used to increase the damping, but if the $\dot{K}_u$ measurement is wrong then the damping will be affected. Figures 36 and 37 suggest another cause for the overshoot. The underlying assumption used for the simulated system response is that the workpiece is moving through the bending apparatus fast enough so that each point along the workpiece is unaffected by any previous forming. Essentially this means that if the workpiece is initially flat, then the scaled moment and loaded curvature are always related as shown in Figure 3 and these two measurements cannot change independently. But Figure 36 indicates that the moment and curvature do change independently. The system responds as predicted until the scaled moment and loaded curvature level off at about 1.0 sec. At this point in the simulation shown in Figure 37 the moment and curvature remain constant and the system reaches steady-state. The actual response in Figure 36 shows that the scaled moment, rather than leveling off, decreases after reaching a peak at 1.0 sec but the curvature does not change. The decrease in the scaled moment without a corresponding decrease in the loaded curvature results in an increase in the unloaded curvature which accounts for the observed overshoot. The problem is determining why the moment and curvature move independently.

The most likely reason for the independent movement is

that the moment and curvature measurements are in error and do not reflect the true state of the loaded workpiece. Figure 42 shows the results of a test which was conducted using exactly the same parameters as Test 1 except the workpiece is stationary. The results are nearly exactly as predicted in Figure 37. Obviously the measurement inaccuracy noted in Figure 36 which causes the overshoot only occurs when the workpiece is moving. Thus it is likely that the moving workpiece assumption made for the system simulation is not valid for these forming conditions.

Another possibility is that the step command actually causes a kink to be formed in the workpiece. This kink could affect the forming of the following workpiece until the kink exits from the bending apparatus. With a feedrate a 3.3 in/sec and a roll spacing of 6 in, a point on the workpiece would take nearly 2 sec to move from the center roll to the outer roll. The curious behavior of the moment and curvature in Figure 35 occurs between 1.0 and 2.5 sec which is the same time frame necessary to move a point from the center to the outer roll. If a kink is being formed, this should be reflected in both the moment and loaded curvature measurements. In Test 1 the loaded curvature is assumed to be proportional to center roll position, but it is possible for a kink to exist in the forming region which would be undetected by the center roll loaded curvature measurement. The LVDT loaded curvature measurement should be able to detect

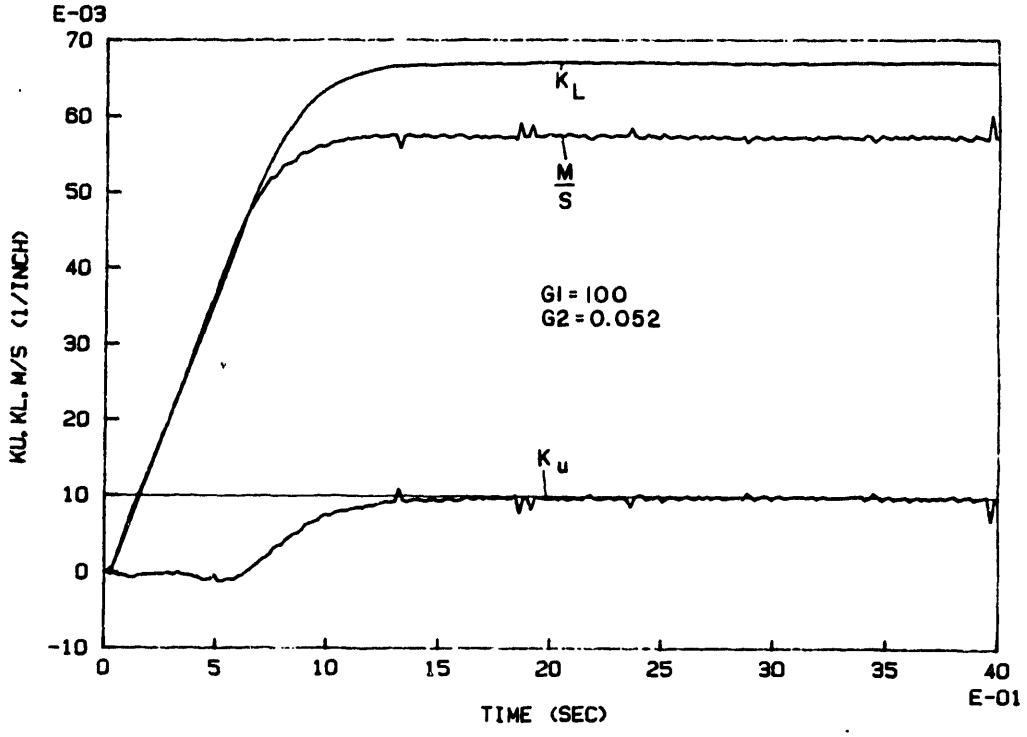

Figure 42. Test #5

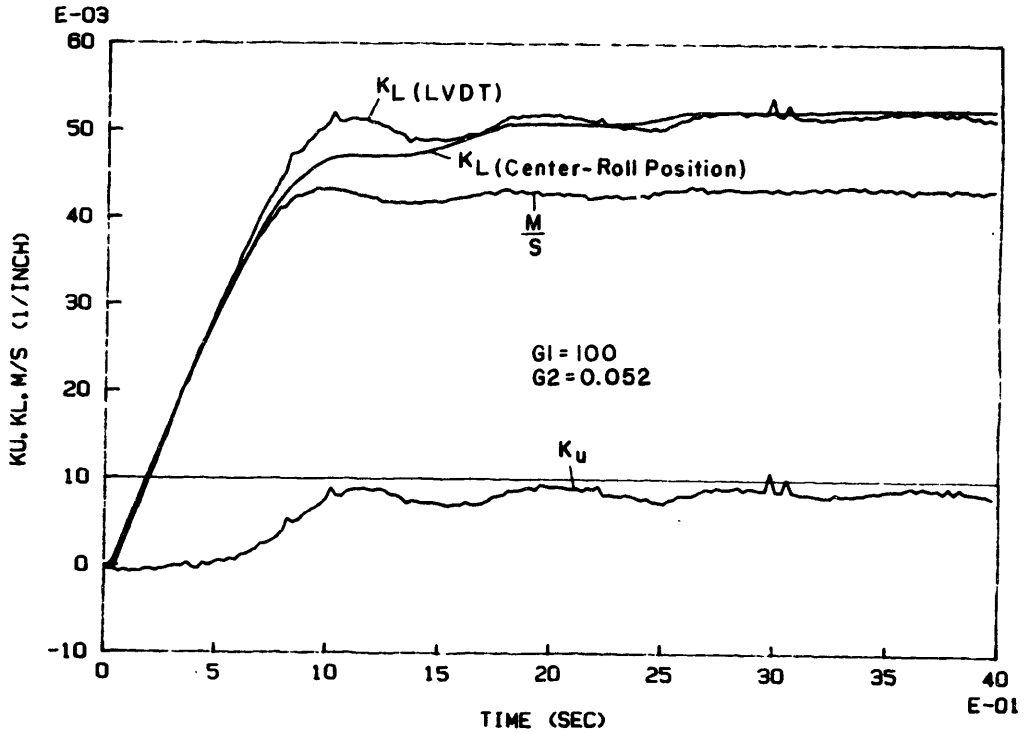

Figure 43. Test #6

the kink since the LVDT's measure the curvature closer to the point of interest, which is the contact point on the center roll.

Test 6 was conducted using the same parameters as Test 1 except that the LVDT curvature measurement method was used. The key result of Test 6 is shown in Figure 43. Again, the scaled moment decreases after reaching a maximum at 1.0 sec, but the loaded curvature also decreases. Thus the moment and curvature do not actually move independently as suggested in Test 1, but only appear to do so because of error in the loaded curvature measurement method based on center-roll position. Notice that the system response in Figure 43 does not have any overshoot. Notice also that the two curvature measurement methods converge once the kink has passed through the system. This suggests that it might be possible to reduce the effects of the kink if the feedrate is increased so that the kink is past the outer roll before the unloaded curvature reaches the commanded value.

For Test 7 and all subsequent tests the feedrate is increased to 13 in/sec. Figure 44 shows the results of Test 7 which used the same parameters as Test 1 except for the faster feedrate and the LVDT curvature measurement. Figure 45 shows the results for a similar test except the controller gain is increased to 335. Both tests show that the effect of the kink is nearly eliminated with the higher feedrate and neither test shows any overshoot. In other words the actual

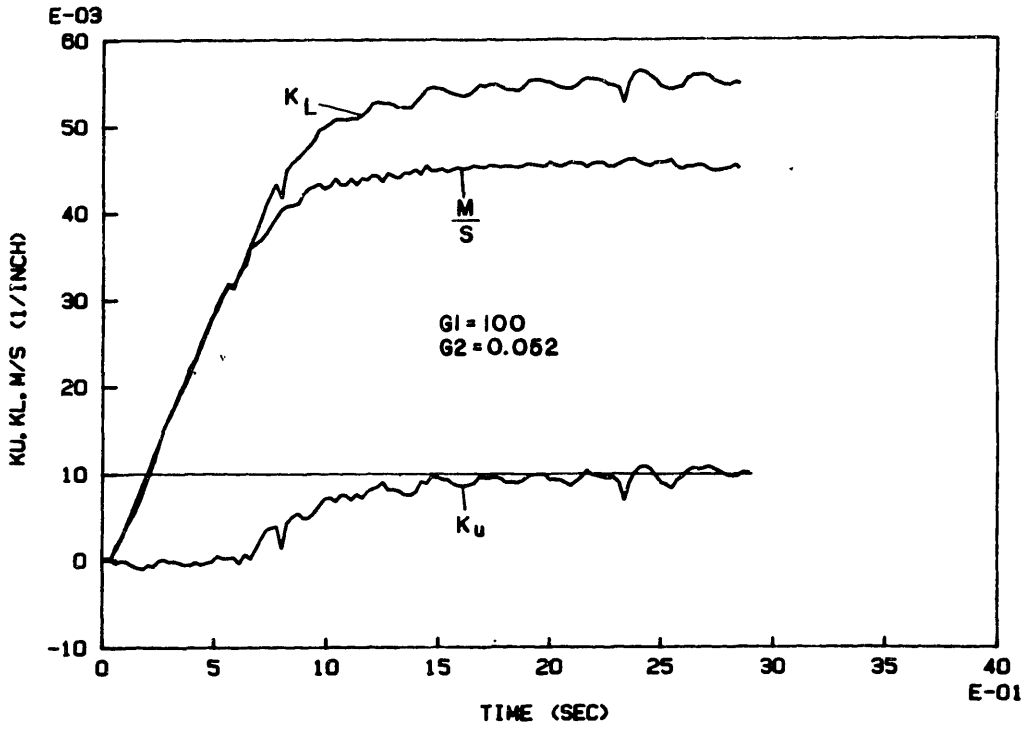

Figure 44. Test #7

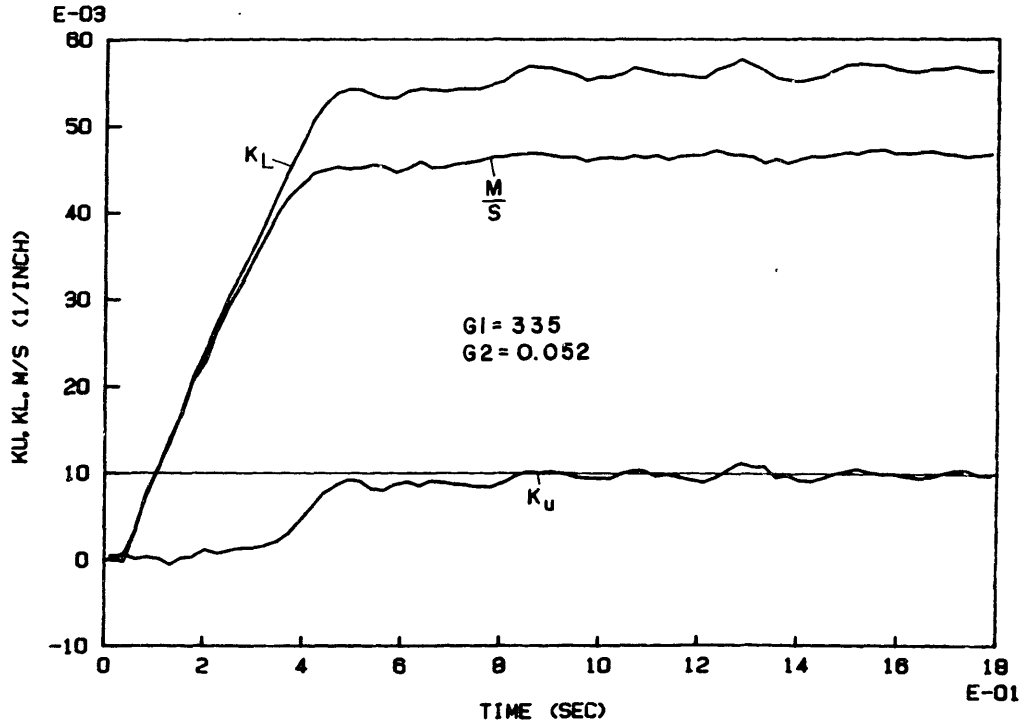

Figure 45. Test #8

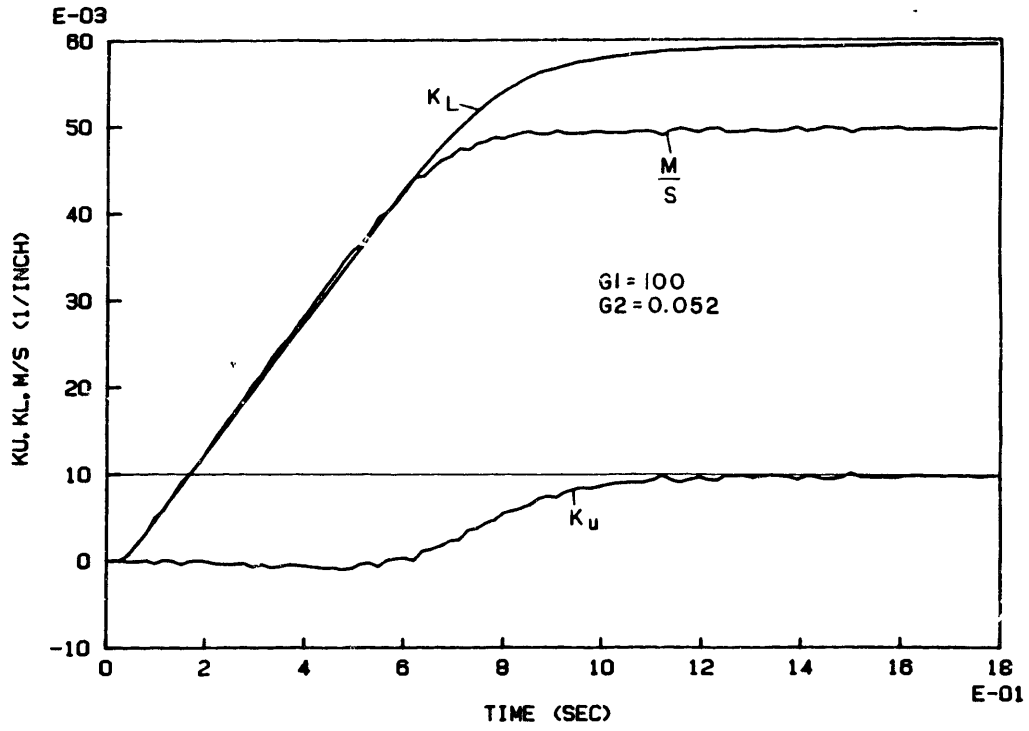

Figure 46. Test #9 Plot #1

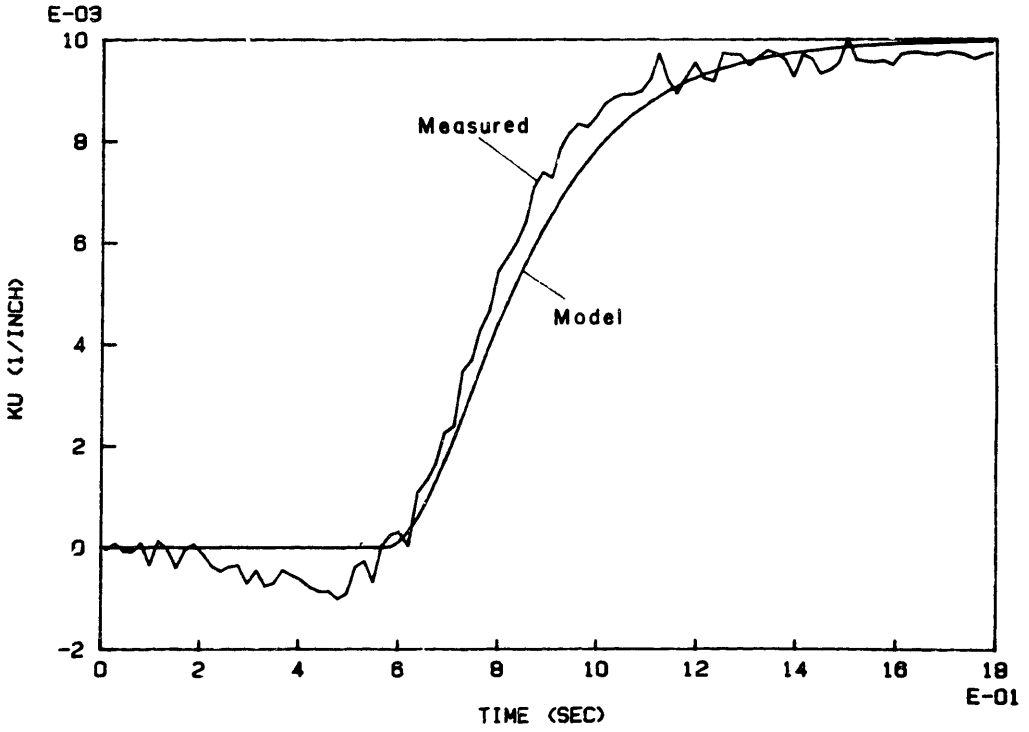

Figure 47. Test #9 Plot #2

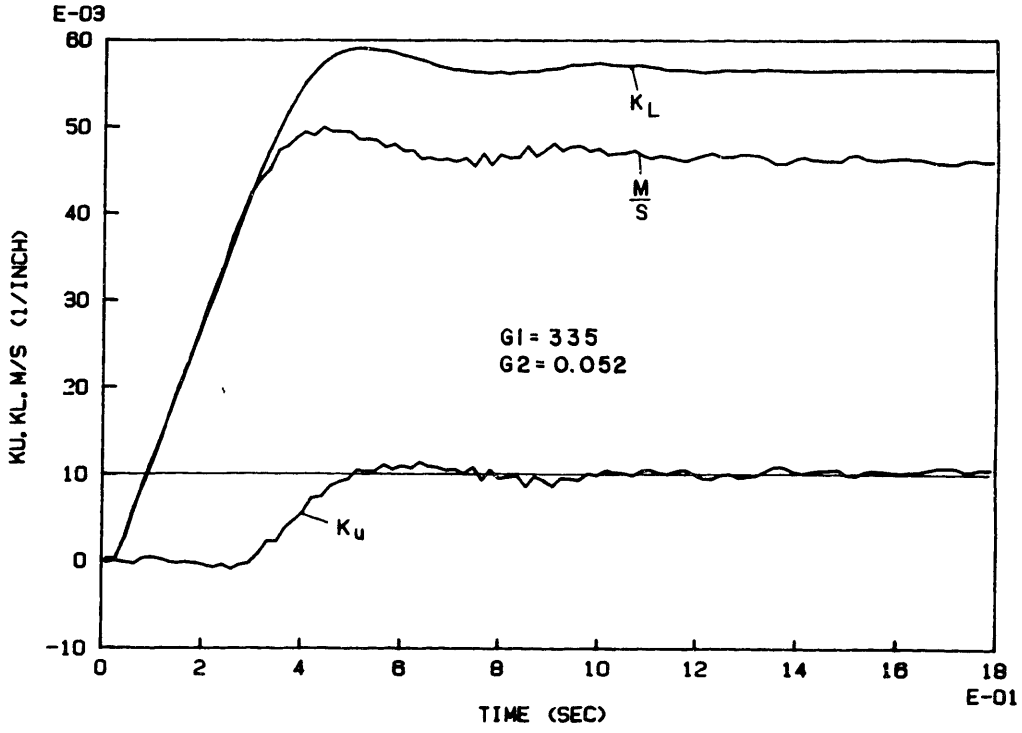

Figure 48. Test #10

system response is very nearly the same as the simulation predicts when the simulation assumptions are valid. The parameters of Tests 7 and 8 are used in Tests 9 and 10 respectively except that the center roll position curvature measurement is used in the later two tests. The results of Test 9 shown in Figures 46 and 47 correspond very well with the simulated response shown in Figure 37 and also in Figure 47. The response is well damped and there are no visible effects due to the kink since the kink takes less than 0.5 sec to pass through the system. Figure 46 shows that the unloaded curvature takes about 0.8 sec (from 0.6 to 1.4 sec) to settle which means that the kink is out of the system

before the system settles. As the gain is increased in Test 10 the speed of response increases. If the rise time is smaller than the time it takes for the kink to move through the system, then the effect of the kink will be visible. The response in Figure 48 is fast enough so that some small effects of the kink are visible in the decrease of the scaled moment even with the very fast feedrate. The overshoot is very much reduced from that of Test 2 shown in Figure 39 which used the same parameters as Test 10 except for a slower feedrate.

The conclusion from these experiments is that the overshoot observed in Test 1 is caused by measurement errors in the loaded curvature measurement. Tests 5, 7, 8, and 9 indicate that the $\dot{K}_u$ approximation is not at fault, but works exactly as predicted in the simulations. The center roll approximation contains significant error during the transient response when the rise time of the system is less than the time found by dividing roll spacing by feedrate. The error shown in the tests is the worst case because the large step command causes a kink to be formed in the workpiece. The presence of the kink causes some interaction in the forming region between the point being formed currently and previously formed points still in the forming region. The analysis of the kink effects is quite complex, but it is of little practical interest since the step command is a rather extreme command and the kink affects the transient response only.

The following tests were all conducted using the center roll position curvature measurement and the fast feedrate. This curvature measurement is more desirable because the lower noise allows a better reading of steady-state error and the faster feedrate reduces the overshoot due to the approximation error.

Although Test 10 shows excellent system response, Figure 33 suggests that even better system response is possible using a zero location as shown in Figure 31. In addition this zero location allows larger controller gains without stability problems which will decrease the steady-state error due to disturbances. Figure 49 shows the system step response using the same controller gain as in Test 10, but the zero location is moved to z = 0.77. The deadband and rise time have both decreased in this test as predicted. There is some overshoot, but this is expected with the center roll position curvature measurement and ignored. The system quickly settles with essentially zero steady-state error. Increasing the controller gain to 670 should increase the speed of response even more as shown in the simulation for Test 12 in Figure 50. The results do show a faster response very close to the predicted response, but the system does not settle. After the transient response the unloaded curvature oscillates around the commanded curvature. Moreover the oscillation appears to be at two different frequencies. A higher frequency oscillation occurs between 0.6 and 1.0 sec

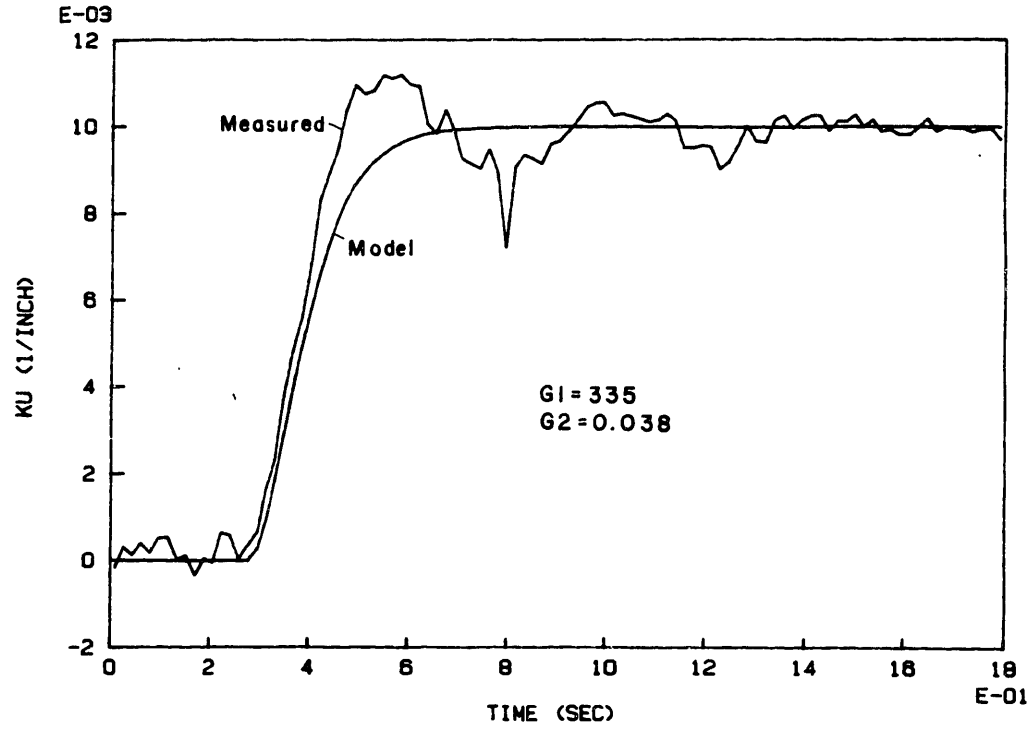

Figure 49. Test #11

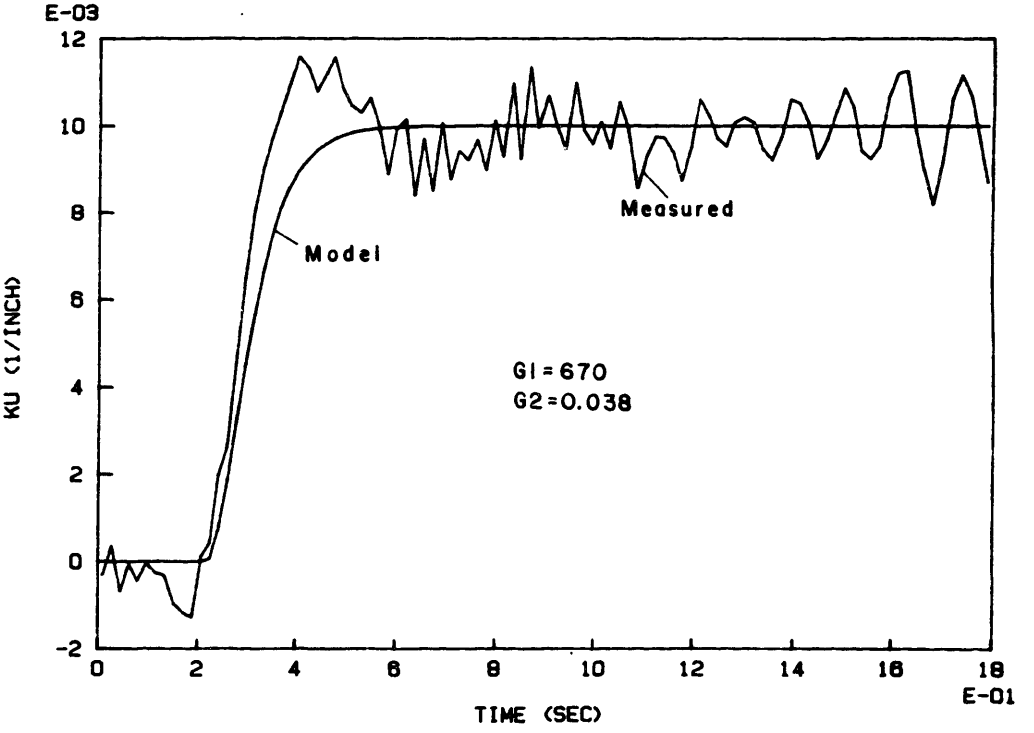

Figure 50. Test #12 Plot #1

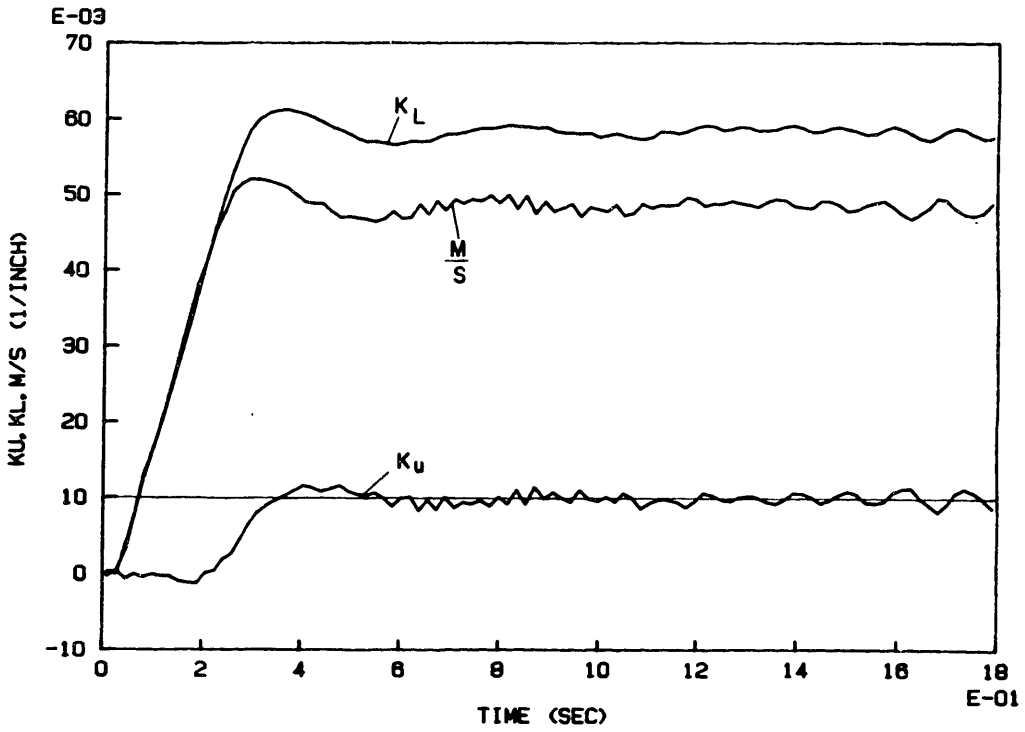

Figure 51. Test #12 Plot #2

and a lower frequency oscillation occurs from 1.2 to 1.8 sec. This oscillation is caused by unmodeled dynamics, vibration of the workpiece. The vibration of the workpiece that is on the outfeed side of the bending apparatus causes false readings on the force transducer that are interpreted through the moment measurement as fluctuations in the unloaded curvature. The actual workpiece shows no sign of the indicated curvature fluctuation but, because it is indicated in the measurements, the controller responds to the apparent disturbances. The fluctuation in the moment and loaded curvature measurements is obvious in Figure 51. Remember that the curvature measurement is proportional to

center-roll position so the response of the system is also visible in this measurement. Notice that the system bandwidth is fast enough so that the system responds to eliminate the lower frequency "disturbance" but the high frequency oscillation passes through the system unchanged. This experiment shows that the workpiece dynamics, which are not considered in the system model, become significant as the system bandwidth is increased. A simple dynamic model of the workpiece can be used to explain the high and low frequency vibration shown in Test 12.

The dynamics of the portion of the workpiece on the outfeed side of the bending apparatus can be modeled very simply as the vibration of a cantilever beam. Because the workpiece is a continuous beam, there will be an infinite number of vibration modes and frequencies. The fundamental mode and natural frequency will be sufficient to explain the experimental results shown in Figure 50. The natural frequency of the fundamental mode for a cantilever beam, using the Euler beam model and assuming a uniform rectangular beam, is given by:

$$w_n = 3.52 \left(\frac{EI}{\rho L^4} \right)^{1/2} \qquad (33)$$

where w_n is the natural frequency, EI is the bending stiffness, ρ is the material density, and L is the length of the

beam. The workpiece dynamics can be modeled by a pair of lightly damped poles with a natural frequency given by Equation 33. Notice that the natural frequency is a function of beam length. This means that the natural frequency of the section of the workpiece on the outfeed side of the apparatus changes as the workpiece is fed through the machine. This explains why the oscillation frequency changes partway through the experiment. At the beginning of the experiment the overhanging workpiece is very short and has a very high natural frequency. The dynamics of the workpiece are at a frequency much higher than the system bandwidth and therefore the oscillation of the moment measurement caused by the workpiece vibration is sufficiently attenuated so that the vibration has very little effect on the system. As the workpiece moves through the apparatus, the natural frequency of the overhanging portion decreases and at some point the lower frequency vibration becomes significant and interferes with the dynamics of the bending apparatus and controller.

The zero location in Tests 13, 14, and 15 is shifted to $z = 0.67$. The controller gain in Test 13 is the same as in Test 11. From the results shown in Figure 52 it is obvious that moving the zero in this manner results in faster system response just as predicted by the simulation, also shown in Figure 52. In Test 14 the controller gain is increased to match that in Test 12. Again an increase in the speed of response is shown in Figure 53 but vibration is not nearly as

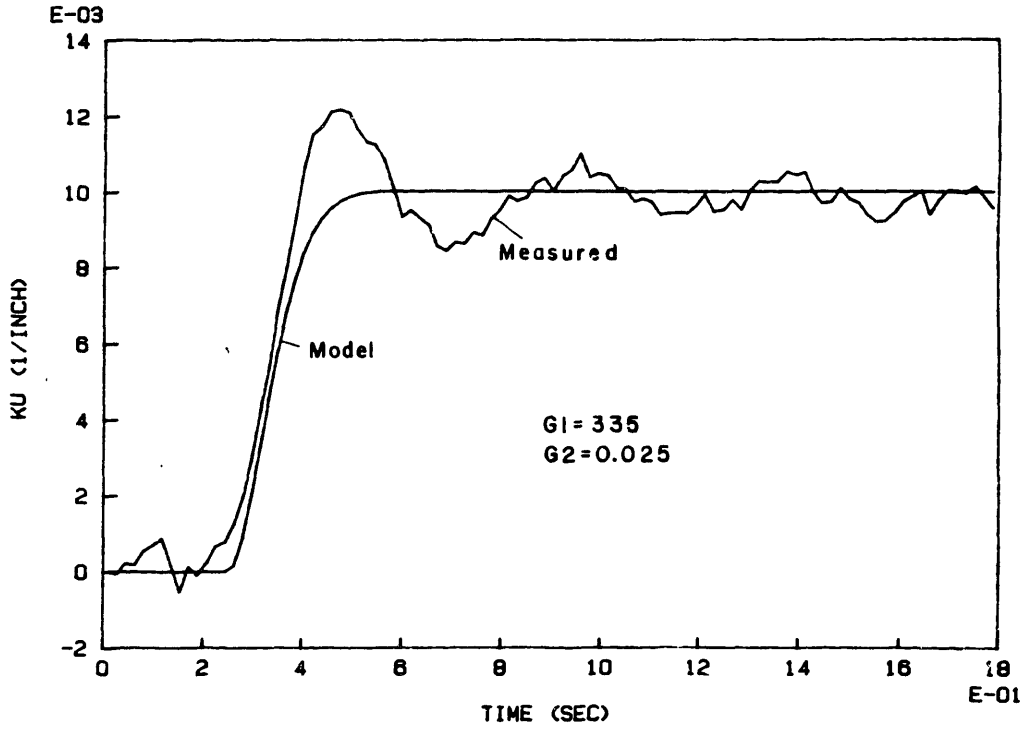

Figure 52. Test #13

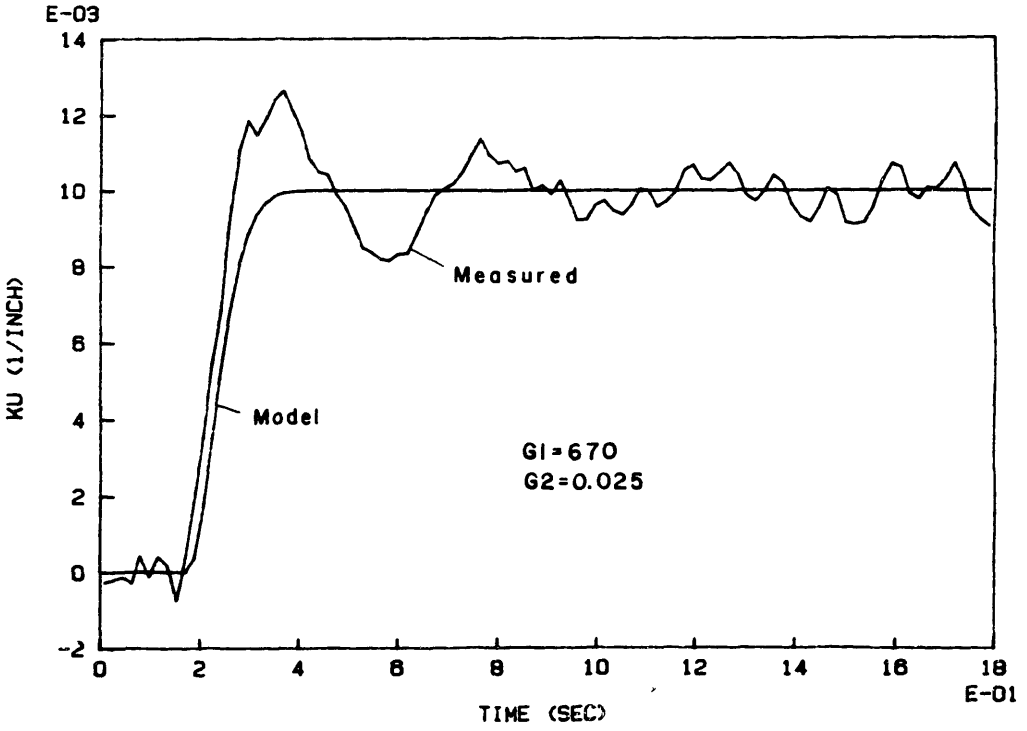

Figure 53. Test #14

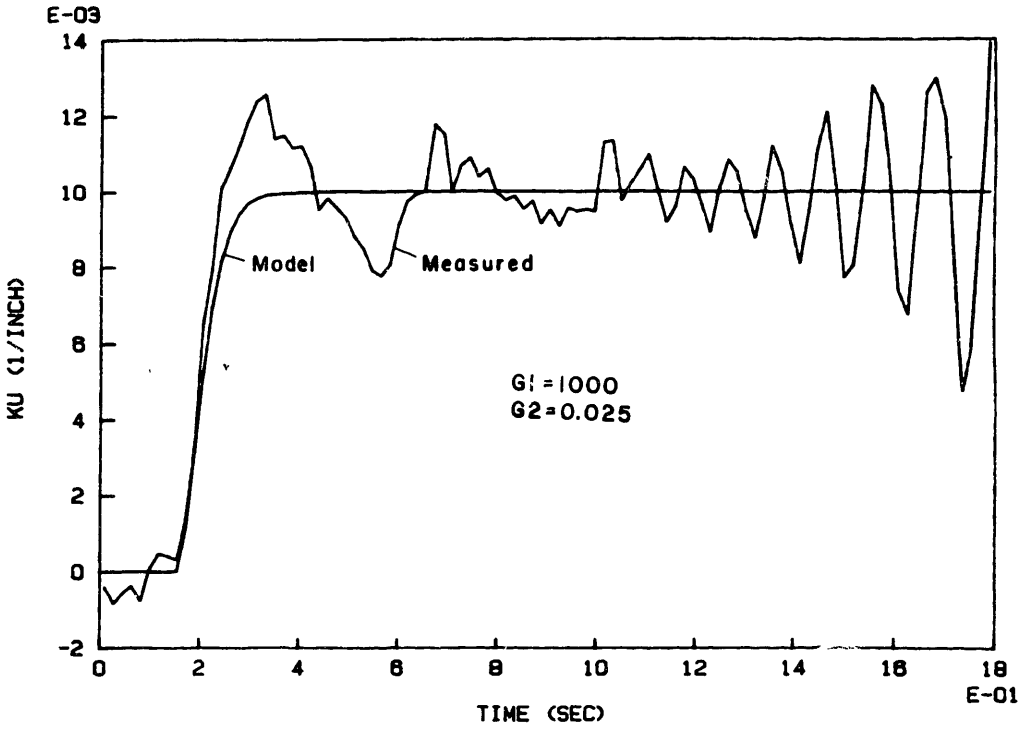

Figure 54. Test #15 Plot #1

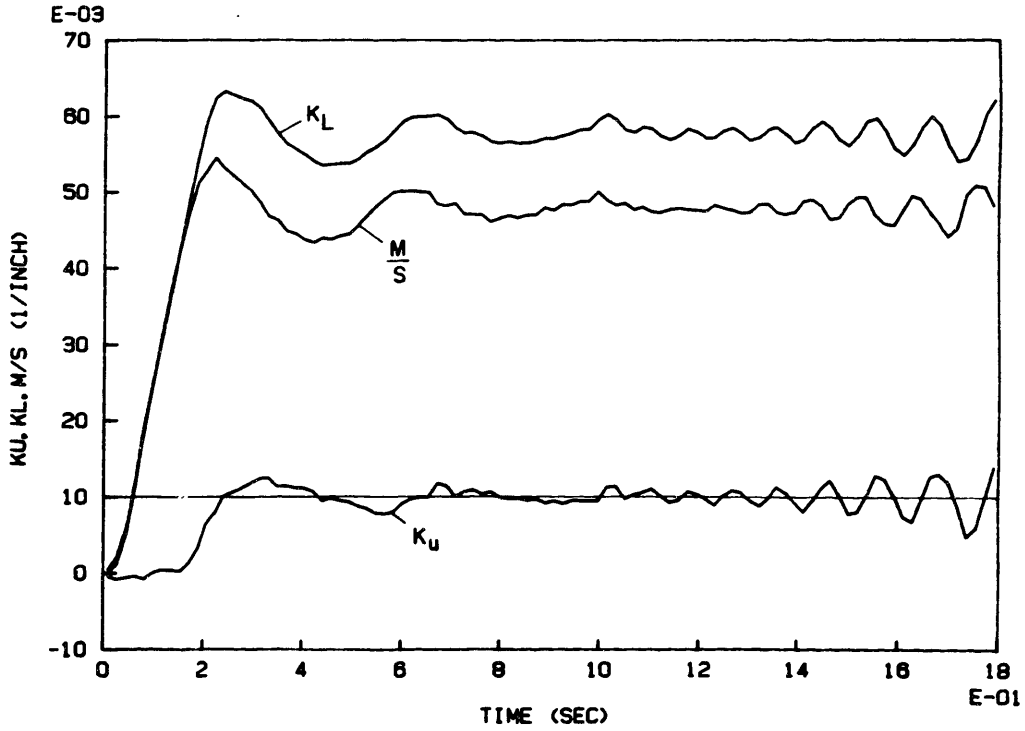

Figure 55. Test #15 Plot #2

large as in Test 12. As the controller gain is increased to 1000 in Test 15, vibration increases. Figures 54 and 55 show that even though the vibration may be a small percentage of the total moment measurement, the effects of the vibration can easily dominate the unloaded curvature measurement.

Tests 11 through 15 all respond to changes in the discrete control algorithm just as predicted by the control theory and simulation in Chapter 4. This means that the roll bending system model is accurate and contains all the significant dynamics except for the workpiece dynamics. As shown above, the workpiece dynamics become important as the length of the overhanging workpiece increases and as the roll bending system bandwidth increases. The one unanswered question is how the closed-loop control system will respond to initial curvature disturbances.

Disturbance Tests

Tests 16, 17, and 18 show the disturbance response of the roll bending system. The workpieces used for these disturbance tests are the same workpieces that were formed in Tests 11, 12 and 14 respectively. Thus for these disturbance tests the workpieces have an initial curvature. The distribution of the initial curvature for each workpiece is shown in the results of the corresponding step tests. After the forming tests, the workpieces were reinserted into the bending apparatus and the disturbance experiments were run using

a zero command for unloaded curvature. The controller parameters used were the same as in the corresponding tests.

Figures 56 and 57 show the results of Test 16. Notice that the scaled moment and loaded curvature do move independently as predicted by the disturbance model in Chapter 3. Figure 57 shows that the disturbance increases initially even though the system is moving to reject the disturbance because the system still must move through the deadband region. The workpiece reaches the yield point at about 0.4 sec and the system settles to zero steady-state error in 1.0 sec. Notice that this response appears much cleaner than the response shown in Test 11. This is because the disturbance is much smoother than the step command in Test 11. It is reasonable that the system should respond much better to the disturbance since the disturbance is really the step command "filtered" by the system dynamics. Test 17 shows faster response in Figures 58 and 59 because of the increased gain. Although it might appear that the oscillation in Test 17 occurs because the system is rejecting disturbances formed into the workpiece in Test 12, this is not actually true. The oscillation shown in Test 12 is the result of measurement error and does not reflect any physical curvature changes. The oscillation in Test 17 is also caused by measurement error due to vibration of the workpiece. The zero location in Test 18 is shifted to match that in Test 14 and the results in Figures 60 and 61 show that the vibration is

reduced just as in Test 14. The disturbance response is again smoother than the corresponding step response because the input has been filtered by the system dynamics.

The disturbance tests demonstrate excellent disturbance response characteristics with good transient response and zero steady-state error. These tests also show that the actual system response is much closer to the predicted response if the system is not hampered by the "kink effects" caused by the step command. The major conclusions from all the experiments are summarized in the next chapter.

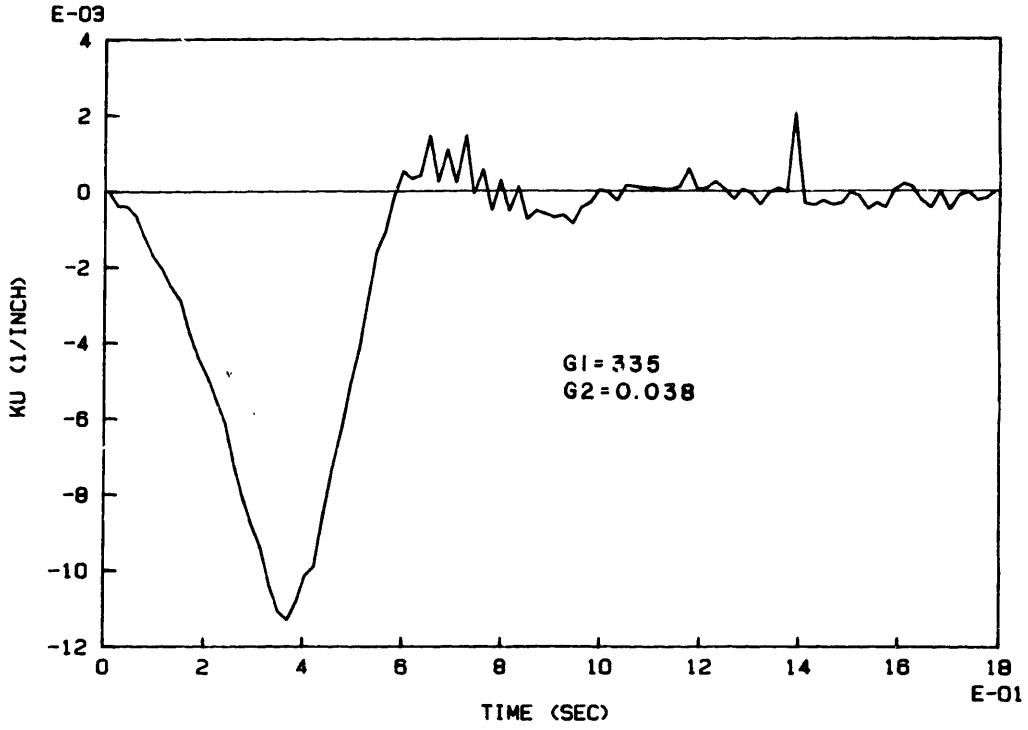

Figure 56. Test #16 Plot #1

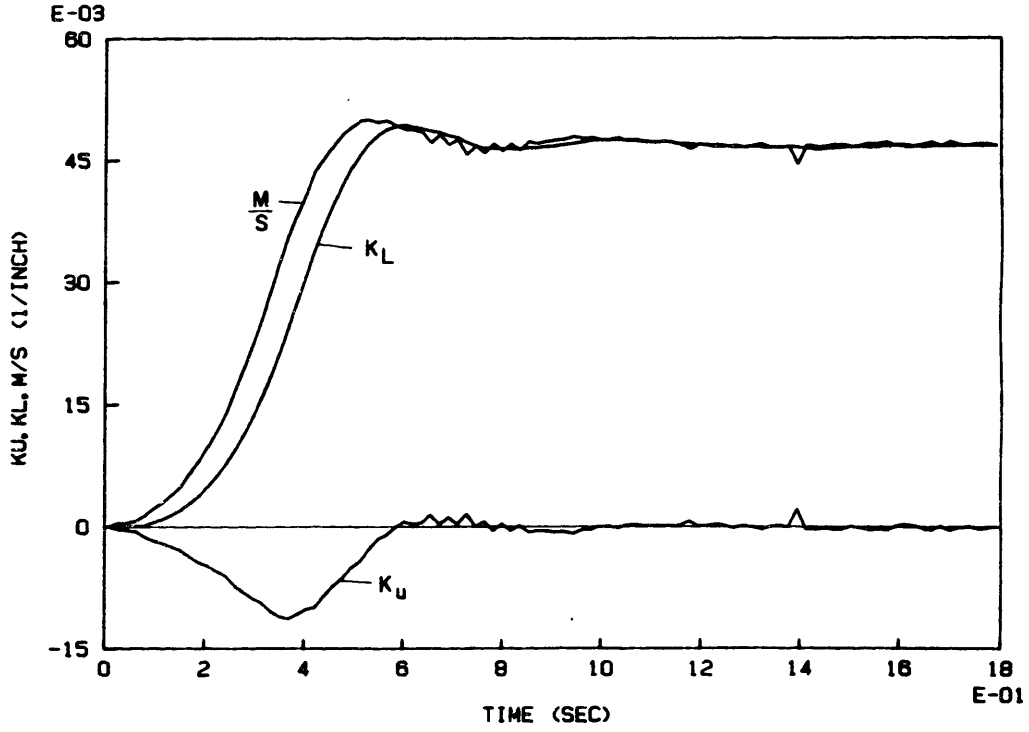

Figure 57. Test #16 Plot #2

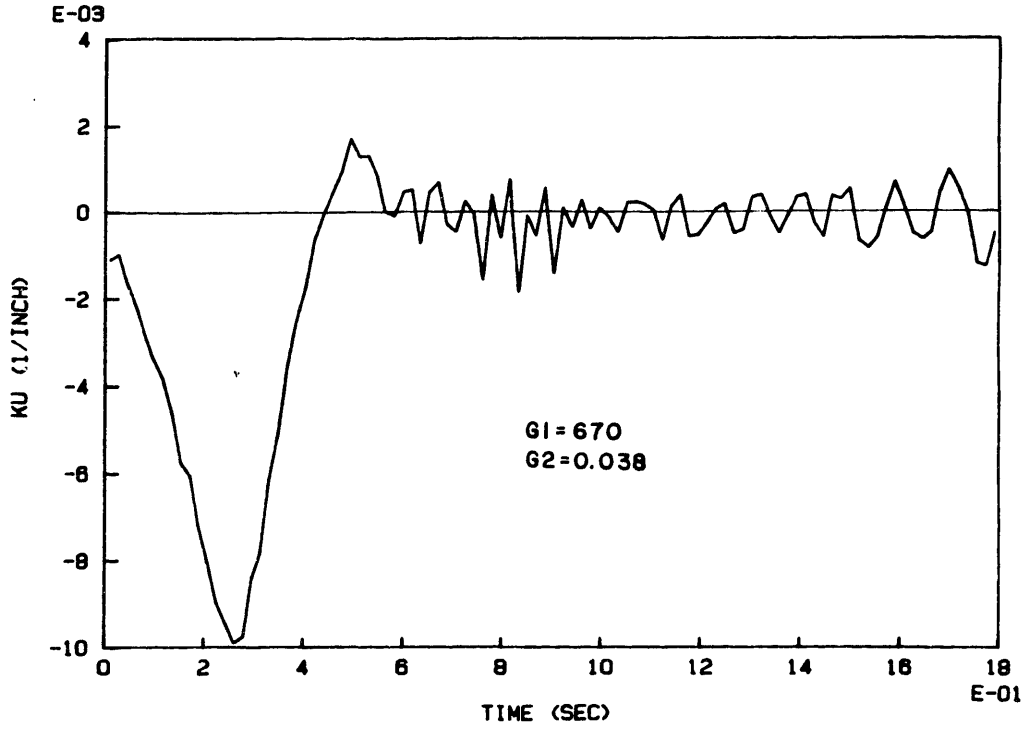

Figure 58. Test #17 Plot #1

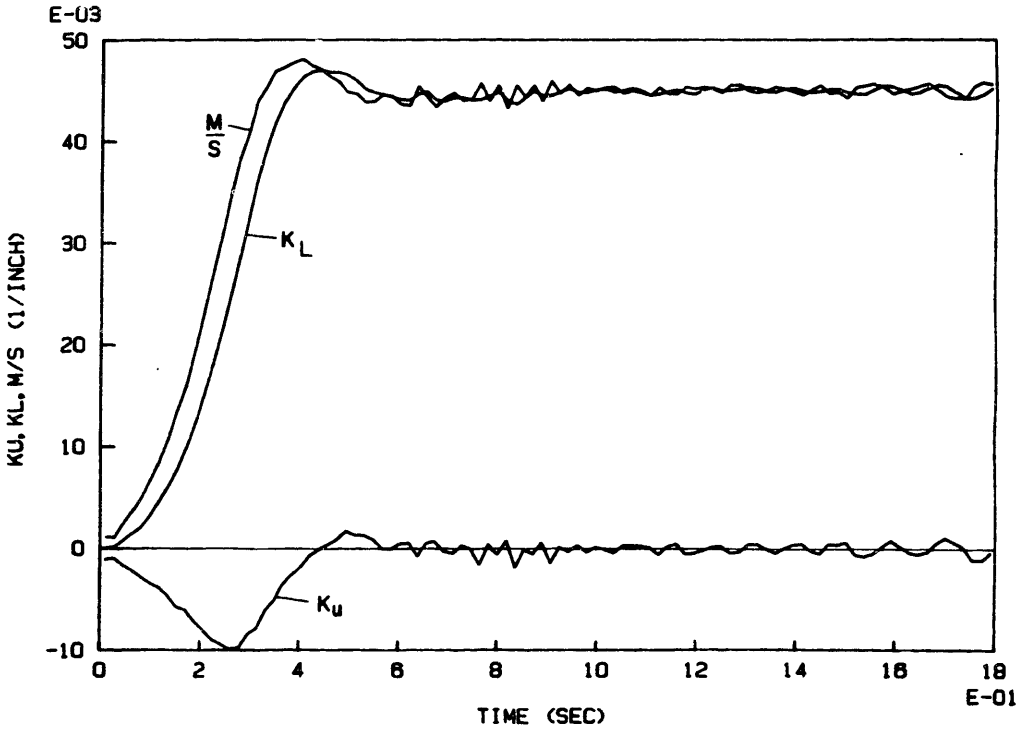

Figure 59. Test #17 Plot #2

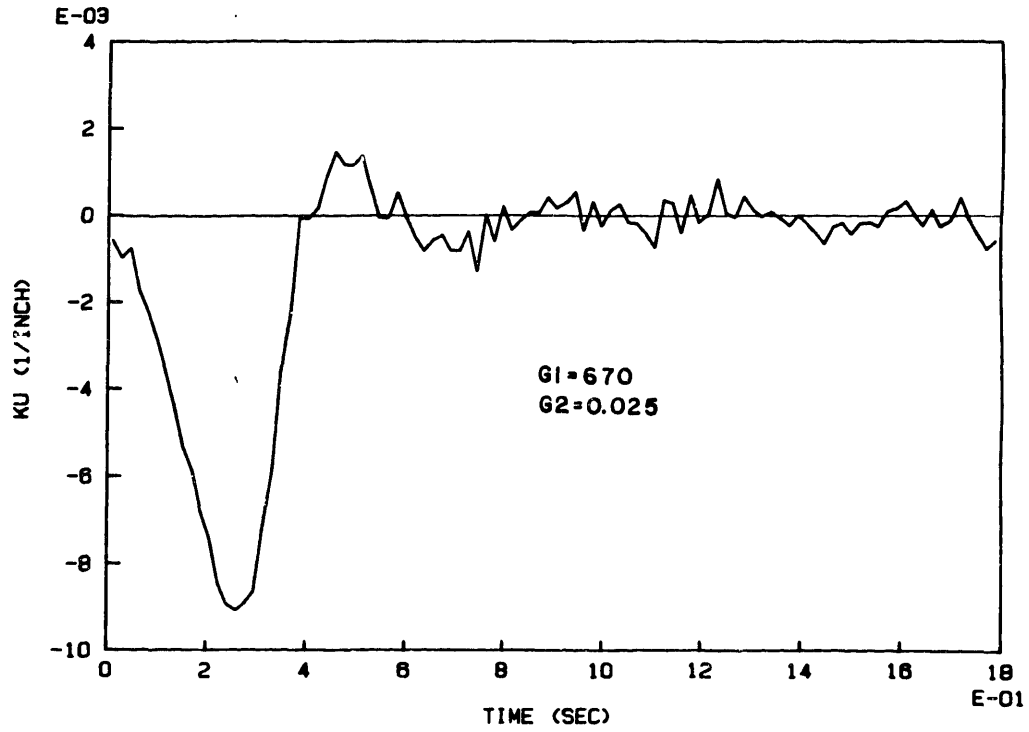

Figure 60. Test #18 Plot #1

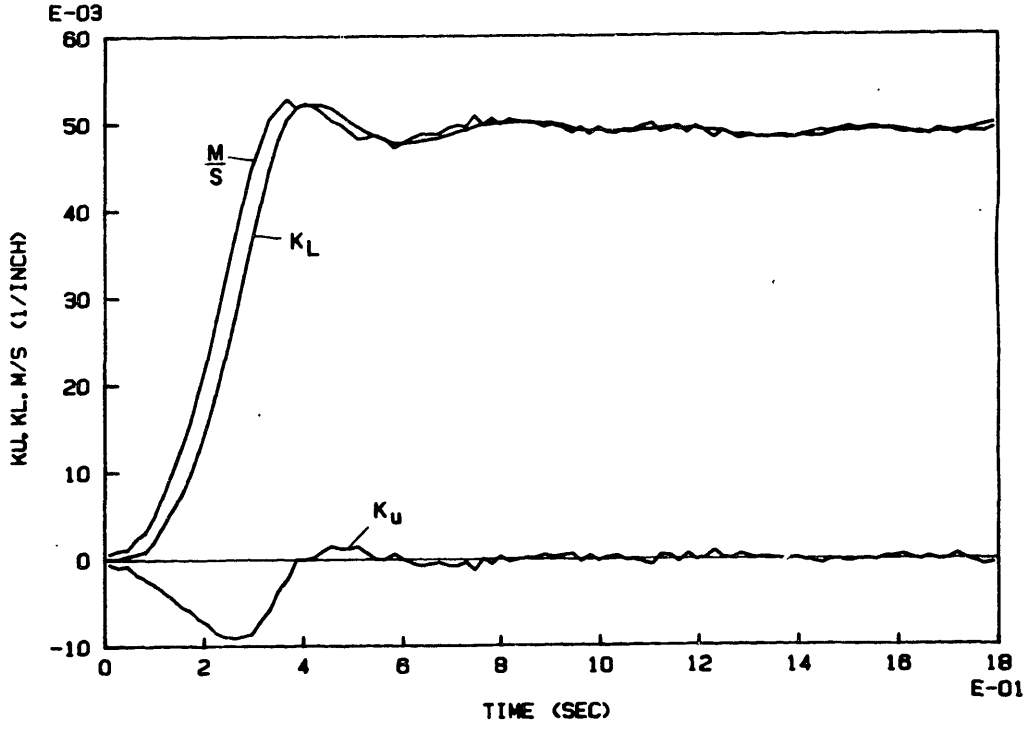

Figure 61. Test #18 Plot #2

Chapter 6

CONCLUSIONS

The experiments in Chapter 5 demonstrate that the roll bending system models developed in Chapter 3 are an accurate representation of the low order dynamics of the roll bending process. The overall experimental system response corresponds very well with the simulated response, although there are small differences. This is to be expected however, because the simulation is based on fixed workpiece material properties while the actual workpiece properties vary. The material property variance is, in fact, a primary motivation for this research, because if the material properties are constant and well defined, an open-loop control system would work just as well and be much simpler to implement than the closed-loop controller presented in this research. Therefore, the control analysis in Chapter 4 and the computer simulation in Appendix 4 are valuable for determining trends and comparing controllers, but not for final tuning of the controller to a particular bending process or workpiece.

Nevertheless, the control scheme developed in Chapter 4 worked essentially as predicted in the simulations. The primary assumptions used to develop this control scheme are that the workpiece performs an integrating function when the roll bending system is based on a velocity servo and that the center-roll velocity is a good approximation of the rate of

change of unloaded curvature. The experiments show that the steady-state error in response to a step input goes to zero if the disturbances are small which indicates a free integrator in the open loop transfer function and verifies the workpiece model. Disturbances which enter the system before the free integrator will always cause a finite error at steady-state which is inversely proportional to the open-loop gain. The experiments show that the error due to disturbances is insignificant.

The use of center-roll velocity feedback to simulate $\dot{K}_u$ feedback was also very successful as demonstrated by the experiments. The system responded to the velocity feedback in exactly the same manner as would be expected with true $\dot{K}_u$ feedback, increasing the bandwidth and stability with a judicious choice of controller parameters. This approximation is somewhat less successful at higher gains or as the system performance is pushed to the limit because the error inherent in the approximation becomes more significant, as do all errors at higher gains. The small overshoot seen in the step tests is due in part to the errors from the velocity feedback although the majority of the overshoot is due to errors in the measurements.

Another result of the experiments which has practical applications is the effect of the approximations in the loaded curvature measurements. The loaded curvature measurement based on center-roll position works very well for most

applications but this measurement method contains significant error during the transient response if the input command changes rapidly. The LVDT curvature measurement method is more accurate during fast transients but is much noisier and more difficult to implement.

The experiments also show that the unmodeled higher-order dynamics, such as workpiece vibration, are significant except at relatively low gains. The vibration problem appears to be a rather severe process-related limitation on the maximum system response. As noted earlier, there are many hardware-related limitations which can generally be overcome by the use of more powerful (and more expensive) hardware. Higher-order dynamics are physical limitations of the particular process. In most control system designs, these higher-order effects can safely be ignored because they occur above a certain high frequency. The controller can be designed so that the system bandwidth is always safely below this critical frequency. As explained in Chapter 5 the higher-order effects due to workpiece vibration do not occur at a constant frequency, because the natural frequencies of the workpiece are a function of beam length. This means that the dynamic behavior of the workpiece changes during the bending operation. To safely ignore the vibration effects, the system bandwidth must be kept well below the lowest natural frequency of the overhanging workpiece. Therefore the controller must be designed for the worst case. This

imposes severe restrictions on maximum system performance which cannot be removed by the use of better hardware. Discovery of this limitation of the roll bending system response accomplishes the major objective of the control analysis, which was to determine the upper limits of system response.

The particular control scheme used in the experiments was able to meet the four specific control objectives listed in Chapter 4. The linear control analysis suggested that a simple proportional controller in a velocity-servo based roll bending system would give the required performance if center-roll velocity feedback is an accurate approximation to true $\dot{K}_u$ feedback. The nonlinear simulation showed that the velocity is indeed a valid approximation to $\dot{K}_u$. The simulations also showed that the system has good stability with this control scheme, even with the nonlinear workpiece model. The experiments proved that the control scheme does produce the expected response. This control scheme results in very good system response, with the roll bending system bandwidth limited ultimately only by the workpiece dynamics.

Future Research

The system response possible using the controller designed in Chapter 4 is a vast improvement over the responses reported in [18], [20], and [21]. The maximum roll bending system response seems to be limited ultimately by

vibration of the workpiece, at least with the simple control scheme used in the experiments. As noted above, this means that system bandwidth can never be greater than the lowest natural frequency of the overhanging beam. It might be possible, however, to improve system response somewhat by using a model reference adaptive controller (MRAC) or a self-tuning regulator. The MRAC allows the controller gains to be changed depending on changes in the physical system. Rather than being designed for the worst case, the controller can be designed to give the best system response throughout the whole bending process. It is also obvious from the workpiece model in Chapter 3 and the simulations in Chapter 4 that the system gains, and therefore the controller gains, are a function of the bending stiffness. Thus the controller gains must be changed for different workpieces. An MRAC or some other adaptive controller might be able to adapt the controller to different workpieces so that the best system response can be attained for each workpiece. An adaptive controller might also give better response for bidirectional bending if the deadband region is large. The controller could increase the gains in the deadband region to move the system quickly through the region and then reduce the gains outside the region. A possible variation of the MRAC is the use of scheduled gains, which can be used to detune the controller as the overhanging workpiece natural frequency lowers and becomes significant. This would have the same effect as

the MRAC but might be simpler to implement.

Another control technique which could be explored in future research is disturbance preview. The experiments show that the disturbance response of the system using the proposed controller is good. But the disturbance response characteristics are most important for the straightening process, which also generally requires the greatest precision of all the roll bending processes. Therefore, to increase the system response for straightening and still retain the precision, it is necessary to have the best disturbance response possible. A control system that includes disturbance preview holds promise for improving disturbance response for those applications which require the best disturbance rejection possible.

In addition to control system improvements, there are some other areas which can be explored to improve system response. As explained earlier, one objective of the experiments was to determine limitations on maximum system response. To do that certain tradeoffs were made in the hardware and measurement methods. One of the major tradeoffs is the measurement of loaded curvature. The loaded curvature is assumed to be a linear function of center-roll position for both elastic and plastic bending. Errors in this approximation result in errors of the same magnitude in the unloaded curvature, so a better approximation or a better measurement of loaded curvature will result in a more precise

final product. Thus there is a need for more detailed study of the bending process from an engineering mechanics perspective. In particular, a simple or computationally efficient relationship between loaded curvature and center-roll displacement for the full loading range would be ideal. This would require a more detailed study of the mechanics of bending in both the plastic and elastic regions. In addition, a complete study of the mechanics of bending should include a more detailed look at the effects of coupling in the bending of unsymmetrical workpieces. This is a necessary step in order to expand the research presented to include control of two- and three-dimensional bending, which is a natural continuation of this research. Closed-loop control of three-dimensional roll bending would make one-pass forming of arbitrary workpiece shapes possible. This would not only increase the productivity of the current roll bending process, but would also greatly increase the versatility of the process.

BIBLIOGRAPHY

1. Hardt, D.E., "Shape Control in Metal Bending Processes: The Model Measurement Tradeoff", editor, D.E. Hardt, Information Control Problems in Manufacturing Technology 1982, Fourth IFAC/IFIP Symposium, pp. 35-40.

2. Allison, B.T., and Gossard, D.C., "Adaptive Brakeforming", Proc. 8th North American Manufacturing Research Conference, May 1980, pp. 252-256.

3. Stelson, K.A., "Real Time Identification of Workpiece Material Characteristics From Measurements During Brakeforming",Trans. of ASME, Journal of Engineering for Industry, Vol. 105, No. 1, February 1983, pp. 45-53.

4. Sachs, G., Principles and Methods of Sheet Metal Fabricating, 2ed., Reinhold, New York, 1966, p. 103.

5. Shanley, F.R., "Elastic Theory in Sheet Metal Forming Problems", Journal of the Aeronautical Sciences, Vol. 9, No. 9, July 1942, pp. 313-333.

6. Lubahn, J.D., and Sachs, G., "Bending of an Ideal Plastic Metal", Trans. of ASME, Vol. 72, No. 1, January 1950, pp. 201-208.

7. Gardiner, B.F.J., "The Springback of Metals", Trans. of ASME, Vol. 79, 1957, pp. 1-9.

8. House, R.N., Jr., and Shaffer, B.W., "Displacements in a Wide Curved Bar Subjected to Pure Elastic-Plastic Bending", Trans of ASME, Journal of Applied Mechanics, Vol. 24, No. 1, March 1957, pp. 447-452.

9. Marshall, J., and Woo, D.M., "Spring-Back and Stretch-Forming of Sheet Metal", The Engineer, August 28, 1959, pp. 135-136.

10. Shaffer, B.W., and Ungar, E.E., "Mechanics of the Sheet Bending Process", Trans. of ASME, Journal of Applied Mechanics, Vol. 27, No. 1, March 1960, pp. 34-40.

11. Bassett, M.B., and Johnson, W., "The Bending of Plate using a Three-Roll Pyramid Type Plate Bending Machine", Journal of Strain Analysis, Vol. 1, No. 5, 1966, pp.398-414.

12. De Angelis, R.J., and Queener, C.A., "Elastic Springback and Residual Stresses in Sheet Metal Formed by Bending",

Trans. of ASME, Vol. 61, No. 4, December 1968, pp. 757-768.

13. Palazotto, A.N., and Seccombe, D.A., Jr., "Springback of Wire Products Considering Natural Strain", Trans. of ASME, Journal of Engineering for Industry, Vol. 95, No. 3, August 1973, pp. 809-814.

14. Kobayashi, S., and Oh, S.I., "Finite Element Analysis of Plane-Strain Sheet Bending", International Journal of Mechanical Sciences, Vol. 22, No. 9, 1980, pp. 583-594.

15. Hansen, N.E. and Jannerup, O.E., "Modelling of Elastic-Plastic Bending of Beams Using a Roller Bending Machine", Trans. of ASME, Journal of Engineering for Industry, Vol. 101, No. 3, August 1979, pp.304-310.

16. Cook, G., Hansen, N.E., and Trostmann, E., "General Scheme for Automatic Control of Continuous Bending of Beams", Trans. of ASME, Journal of Dynamic Systems, Measurement and Control, Vol. 104, No. 2, June 1982, pp. 173-179.

17. Foster, G.B., "Springback Compensated Continuous Roll Forming Machines", U.S. Patent No. 3,955,389, May 11,1976.

18. Hardt, D.E., Roberts, M.A., and Stelson, K.A., "Closed-Loop Shape Control of a Roll-Bending Process", Trans. of ASME, Journal of Dynamic Systems, Measurement and Control, December 1982, Vol. 104, No. 4, pp. 317-322.

19. Gossard, D.C., and Stelson, K.A., "An Adaptive Pressbrake Control Using an Elastic-Plastic Material Model", Trans. of ASME, Journal of Engineering for Industry, Vol. 104, No. 4, November 1982 , pp. 389-393.

20. Hale, M.B., and Hardt, D.E., "Closed Loop Control of a Roll Straightening Process", Annals of the CIRP, Vol. 33, No. 1, August 1984, pp. 137-140.

21. Lee, M., and Stelson, K.A., "Adaptive Control for a Straightening Process", Sensors and Controls for Automated Manufacturing and Robotics, ASME, New York, 1984, pp. 153-166.

22. Roberts, M.A., "Experimental Investigation of Material Adaptive Springback Compensation in Roller Bending", MS Thesis, Massachusetts Institute of Technology, 1981.

23. Crandall, S.H., Dahl, N.C., and Lardner, T.J., editors, An Introduction to the Mechanics of Solids, 2ed, McGraw-Hill, New York, 1959, pp. 455-477.

24. Cook, N.H., Mechanics and Materials for Design, McGraw-Hill, New York, 1984, pp. 388-396.

25. Franklin, G.F., and Powell, J.D., Digital Control of Dynamic Systems, Addison-Wesley, Reading, Mass., 1980.

26. Ogata, K., Modern Control Engineering, Prentice-Hall, Englewood Cliffs, N.J., 1970.

Appendix 1

EXPERIMENTAL BENDING APPARATUS

The experimental three-roll bending apparatus shown in Figure 10 consists of three roll-pairs mounted on a Bridgeport milling machine. The roll-pairs contain instrumentation needed to implement the closed-loop control scheme outlined in Chapter 2. The instruments and the milling machine are connected to a digital computer that is used for data acquisition and servo control. Descriptions of the hardware and implementation details are given below. The equations for calculating moment and curvature are also developed.

The Bridgeport milling machine is used as a drive mechanism to feed the workpiece through the rolls and also as the forming mechanism. The feed is achieved by mounting the center roll in the milling spindle, which is driven by the milling machine spindle motor. The forming action in any three-roll pyramid bending machine is achieved by moving the center roll relative to the outer rolls. In this particular case, the center roll is fixed and the outer rolls move. The result is identical in either case. The outer-roll position is changed by moving the milling bed to which the outer rolls are attached. The milling bed is driven by a DC motor through a 5 to 1 ballscrew. The DC motor is fitted with a brushless resolver which is used to measure the position of the milling bed. The position measurement system has a

resolution of 0.00032 in. The DC motor is controlled by a General Electric servo-controller which in turn receives commands from a DEC LSI-11 computer. The DEC computer, equipped with A/D and D/A converters, reads and stores measurements from all transducers. These measurements are used to generate a control signal according to some algorithm (see Chapter 4). The control signal is passed to the GE controller which directs the DC motor to move the milling bed. This movement causes a change in unloaded curvature of the workpiece. Figure 62 shows the hardware relationships in the roll bending apparatus.

The three roll-pairs all consist of one fixed and one adjustable "pinch" roller. The pinch rollers are adjustable by means of bolts which clamp the rolls together. This pinch roll scheme allows bidirectional (positive and negative curvature) forming. The three roll-pairs are all free to swivel about the centerline of the fixed roll (Figure 63). This allows the roll pairs to seek a "neutral" position so that no moment is applied to the workpiece due to the workpiece cocking in the rolls. The rotation of the center roll pair is also used to find the location of the maximum moment and maximum curvature along the workpiece as shown in Figure 71.

The center-roll housing, shown in Figure 64, contains instrumentation for measuring the curvature of the workpiece and the rotation of the roll-pair. The shaft of the fixed

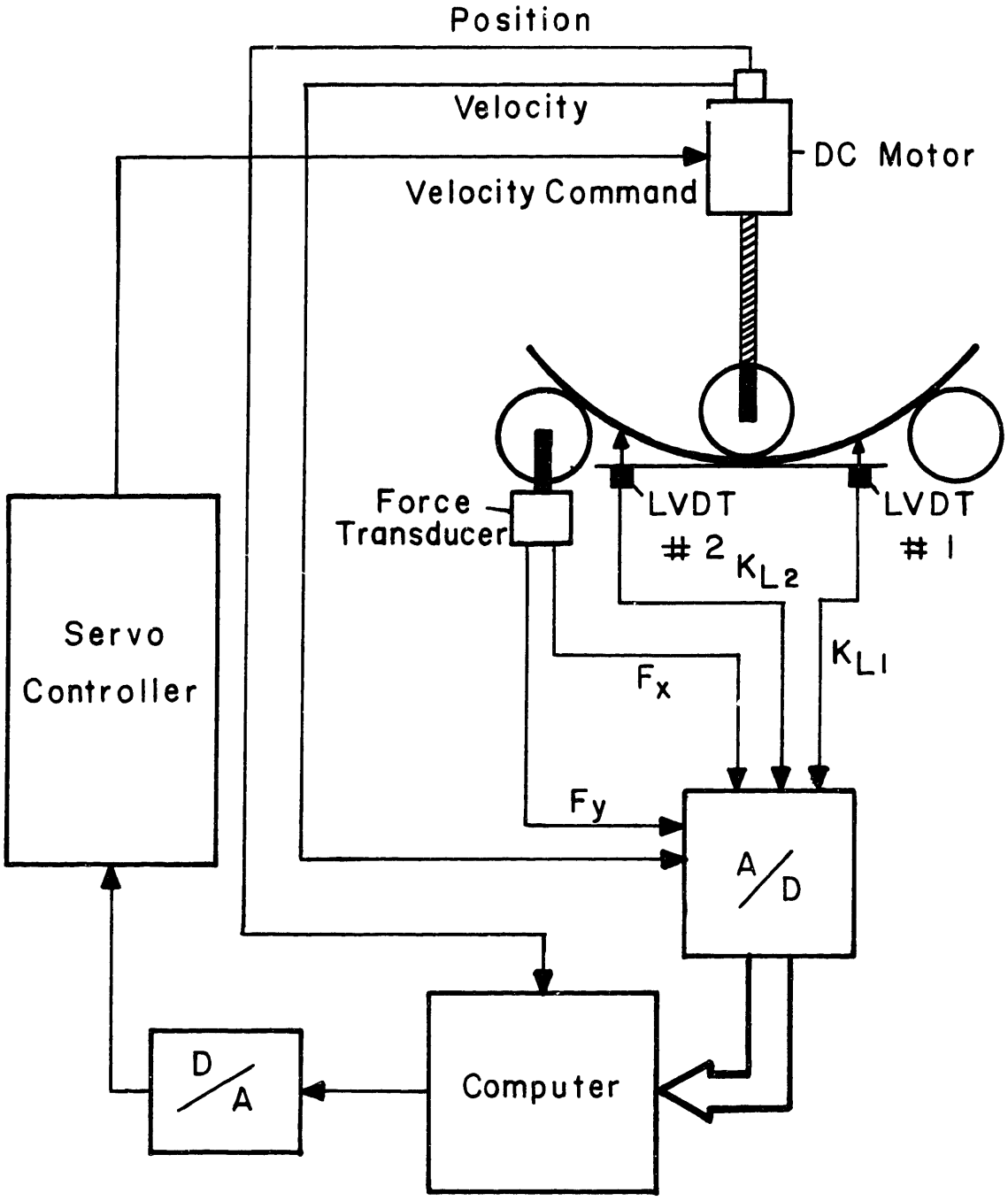

Figure 62. Roll Bender Hardware Relationships

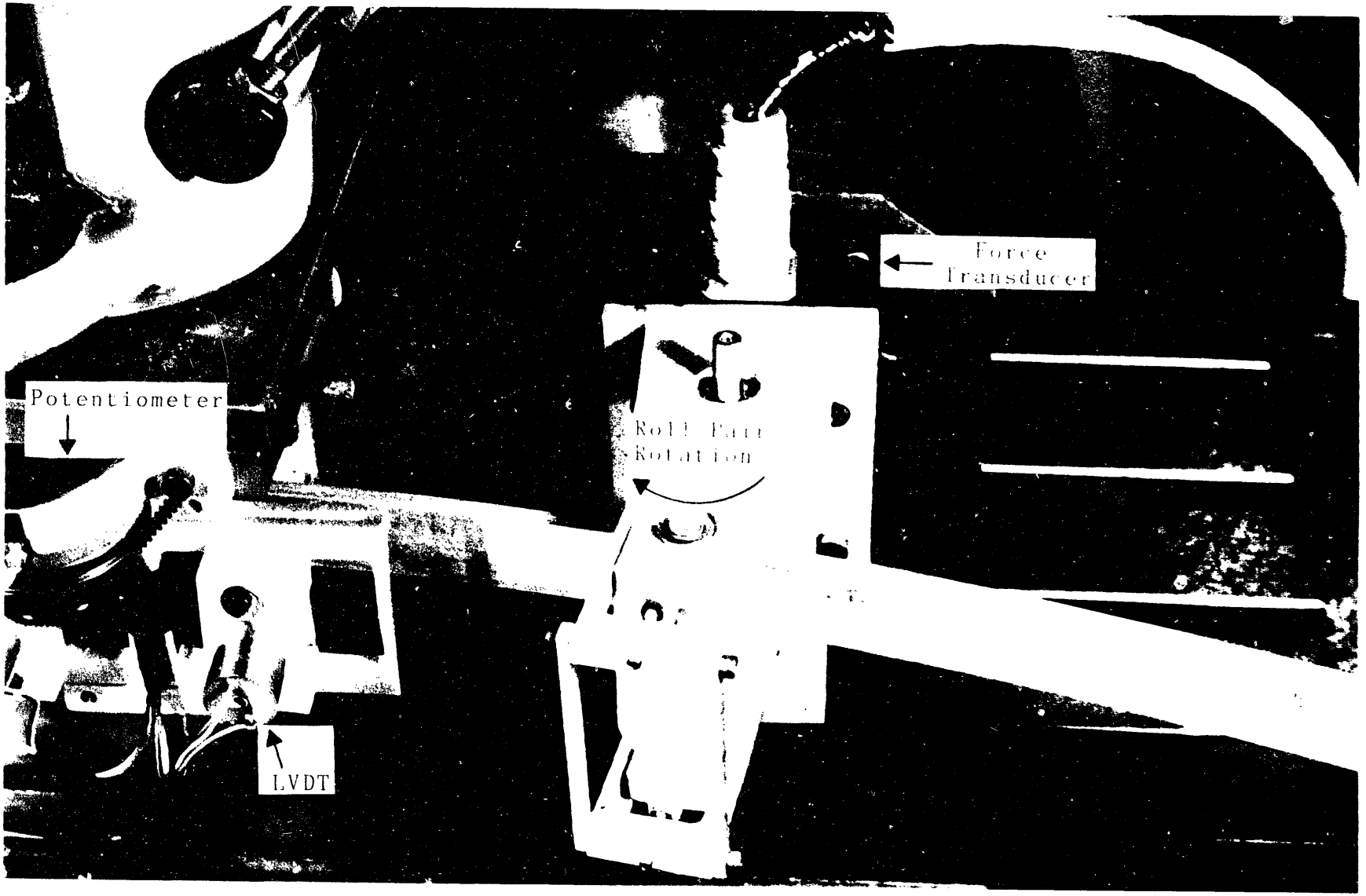

Figure 63. Outer Roll Pair Rotation

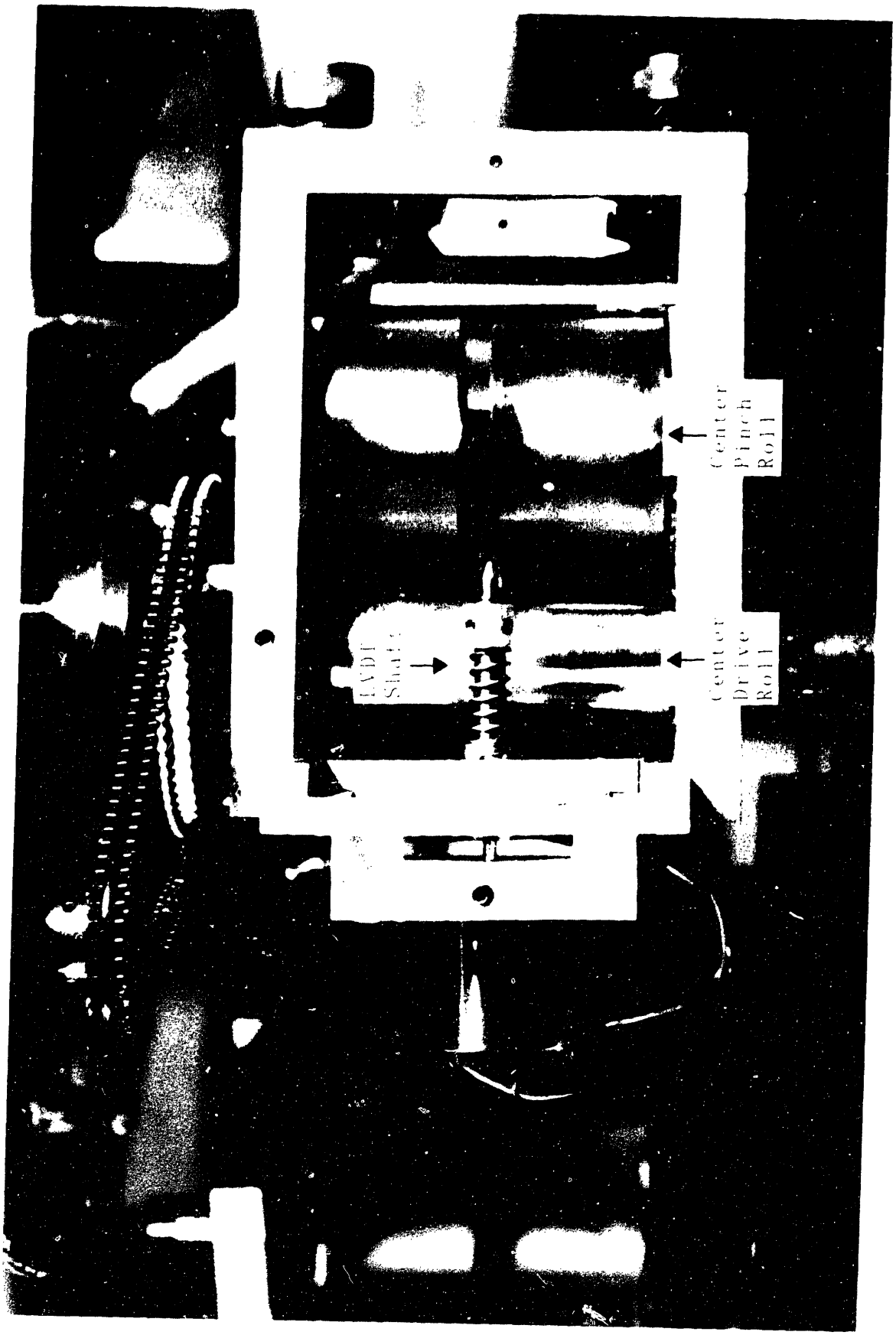

Figure 64. Center Roll Housing

center roll is mounted in the milling spindle. The spindle drive system is used to drive the center roll and feed the workpiece through the apparatus. The curvature is measured by two linear variable differential transformers (LVDT), each with a measurement range of ±0.1 in. The LVDT measurement resolution is infinite since LVDT's are analog transducers. Digitizing the signal in the computer introduces a finite resolution. For this particular application the LVDT's have a resolution of about 0.00005 in. On the experimental apparatus, one LVDT is placed on either side of the center roll. Appendix 2 contains a discussion of the merits of various LVDT positioning schemes. The position of the LVDT's is adjustable from 0.5 to 1.75 in from the centerline of the center roll. This allows the full measurement range of the transducers to be used with workpieces of different bending stiffnesses. The LVDT's do not measure curvature directly, but measure the linear displacement of the workpiece. The linear displacement can be used to estimate the curvature by any one of several methods. Specific curvature equations are derived below. The LVDT shafts are spring loaded to bear against the workpiece as shown in Figure 65. Rotation of the roll pair is measured with a potentiometer, shown in Figure 68. The LVDT and potentiometer signals are amplified and filtered before being sent to the computer. Figures 66 and 67 are plots of the static noise characteristics of the LVDT and potentiometer signals, respectively.

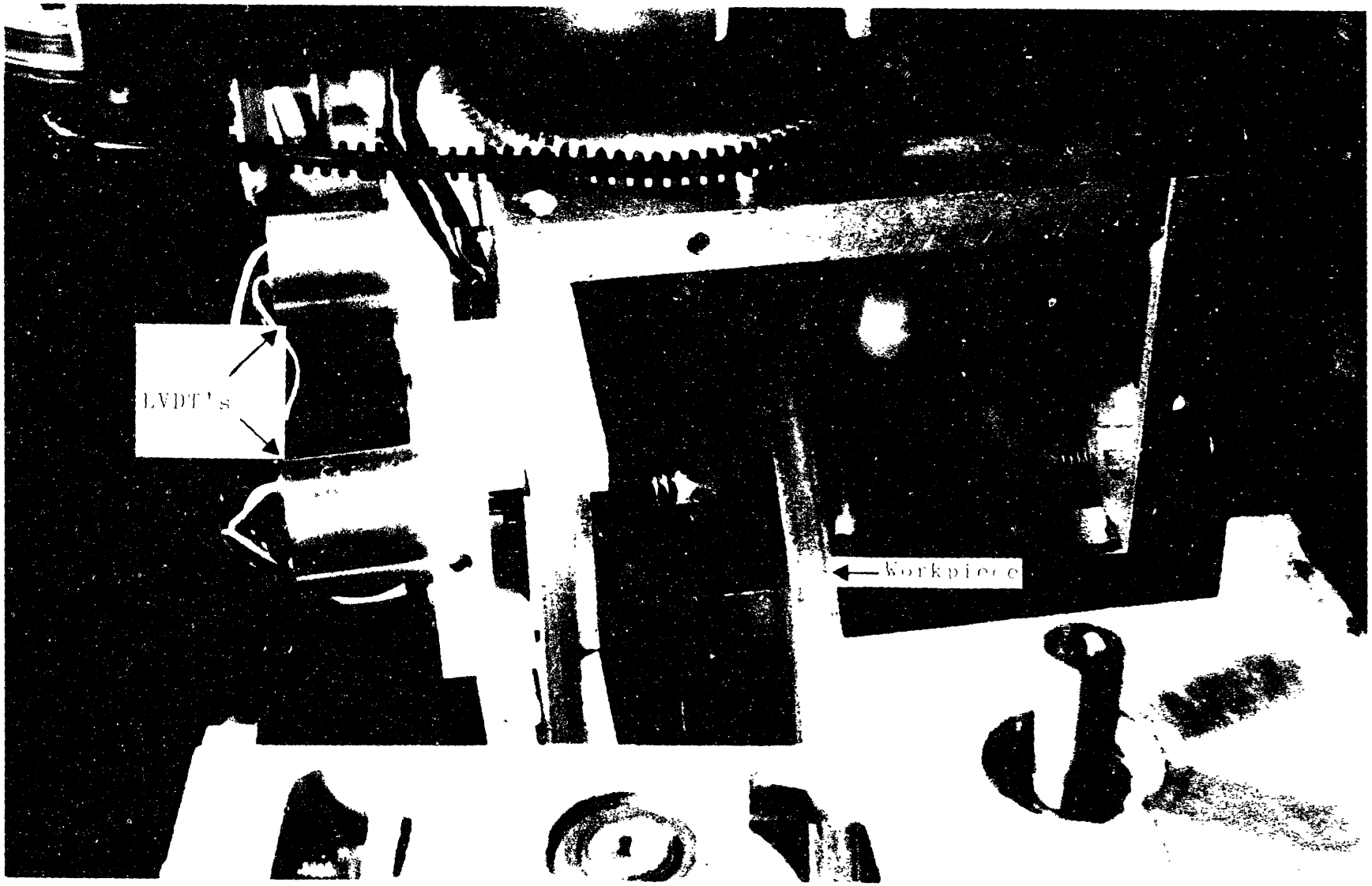

Figure 65. LVDT Curvature Measurement Device

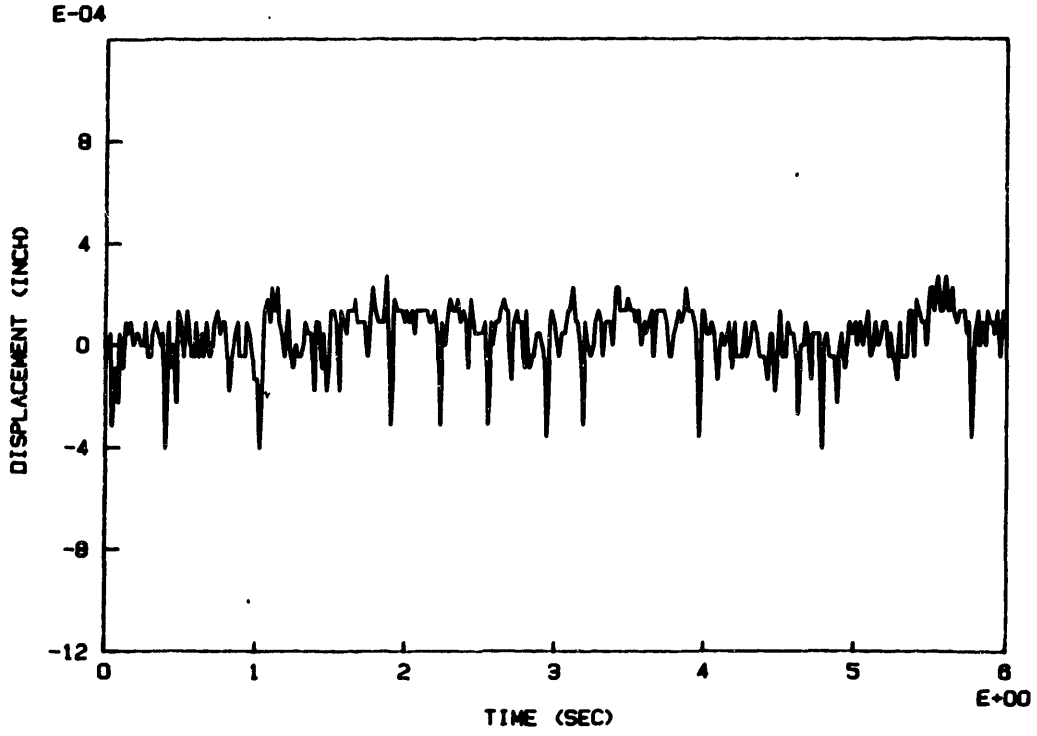

Figure 66. LVDT Noise

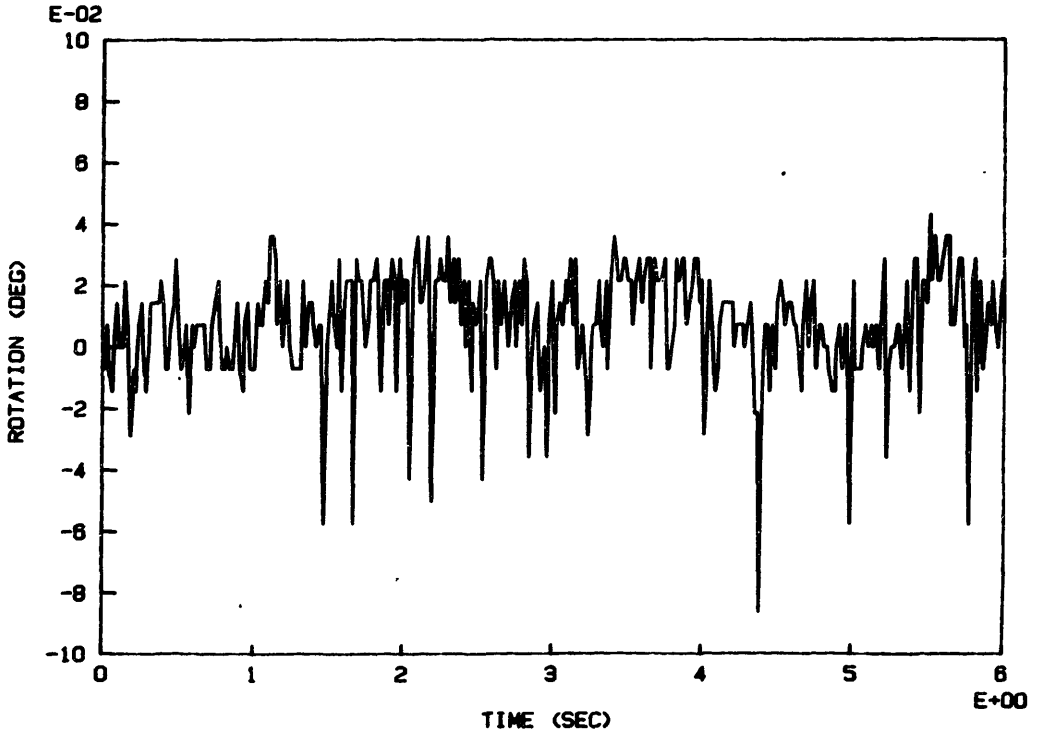

Figure 67. Potentiometer Noise

The infeed roll-pair, which has no instrumentation, is mounted directly on the milling bed. The outfeed roll-pair is attached to a strain-gage force transducer (Figure 68) which has a measurement range of ±250 lb on each axis. The force transducer is model SRMC3-2-250 manufactured by Advanced Mechanical Technology Inc. The resolution of the digitized force measurement is 0.087 lb in the x direction and 0.028 lb in the y direction. The force transducer is bolted to an L-bracket which is clamped to the milling bed. The force transducer measures the two orthogonal forces acting on the outfeed roll-pair. The relationship between the forces acting on the roll-pair and the maximum moment is developed below. The signals from the force transducer are amplified and filtered before being sent to the computer. Figures 69 and 70 are plots of the static noise characteristics of the force transducer.

Figure 71 is a schematic view of the experimental bending apparatus. The equations needed to calculate moment and curvature are developed below using the notation of Figures 71 and 72. Note that many of the terms in the moment equation are very small and can be neglected for certain bending conditions (see Appendix 2). The moment equation shown below assumes that the distance from the center roll contact point to the neutral axis of the workpiece is very small compared to radius of the rolls. If this is not true then an adjustment can be made to r_1 and r_2 to reflect this.

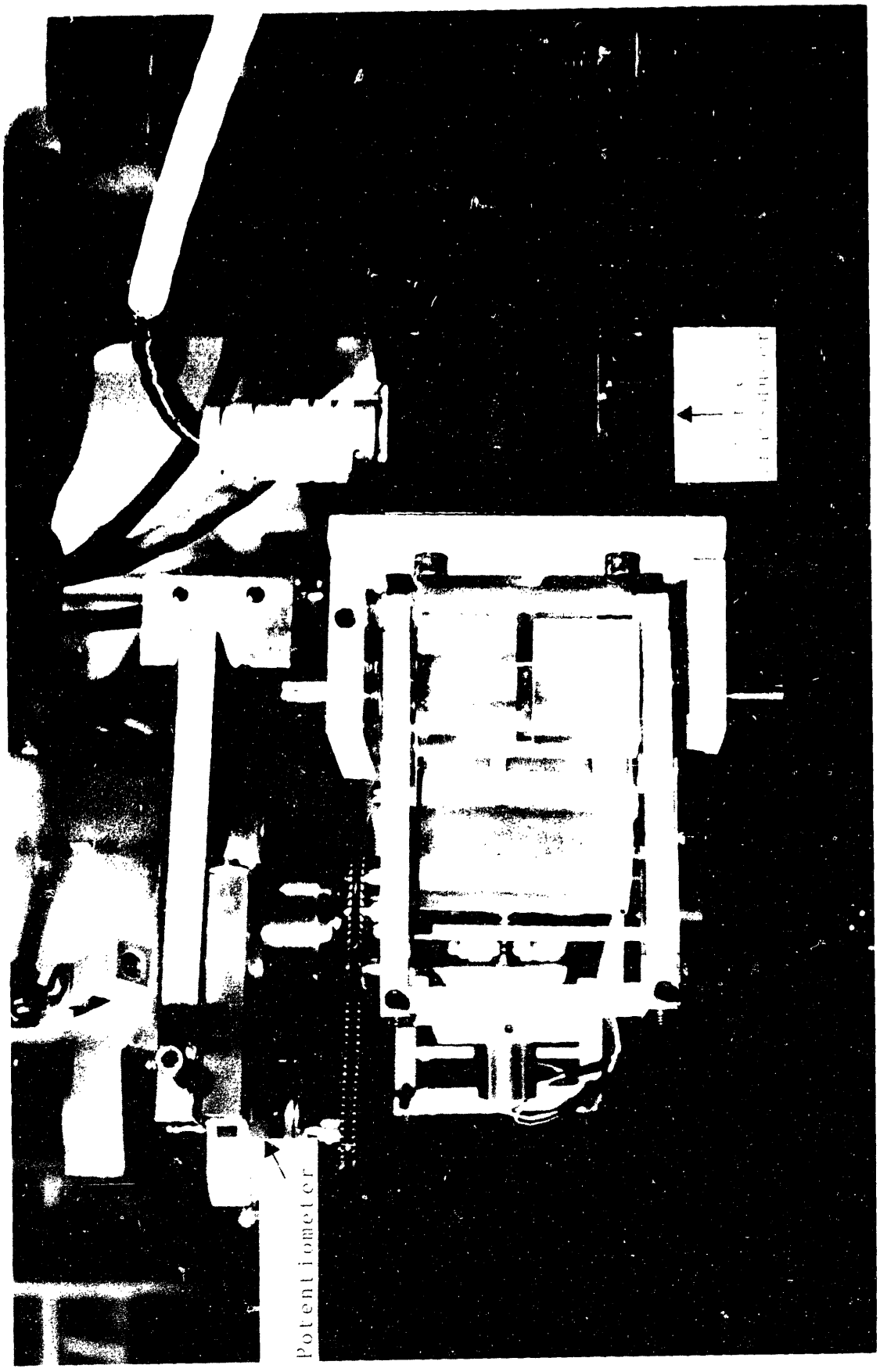

Figure 68. Force Transducer and Potentiometer

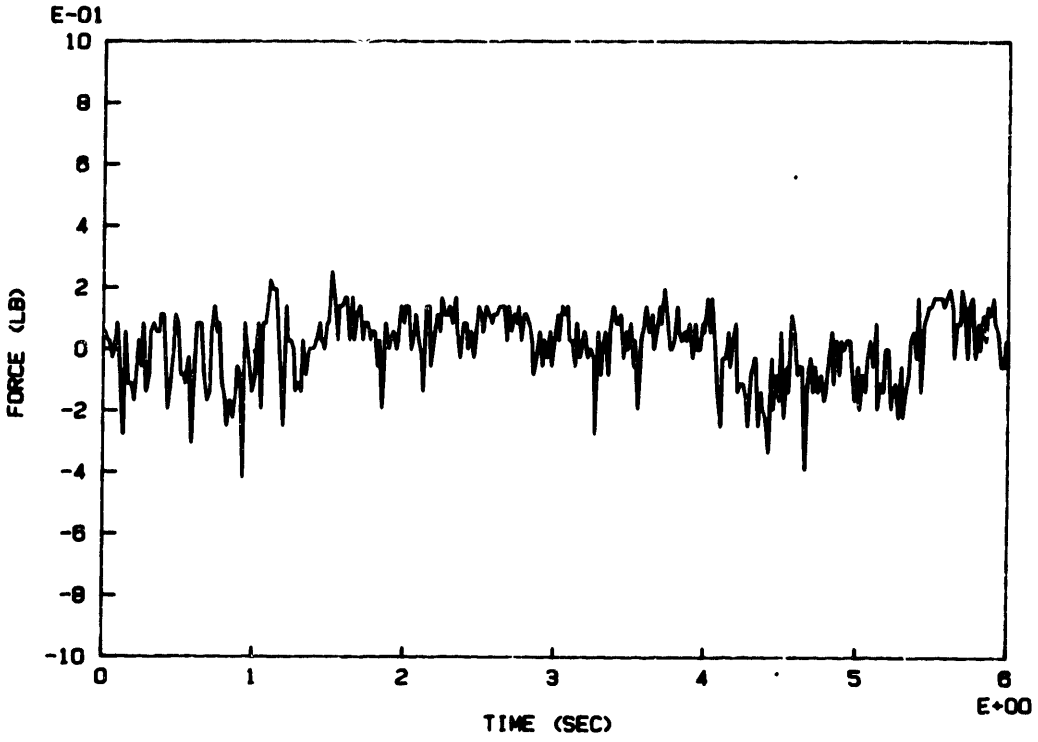

Figure 69. F_x Noise

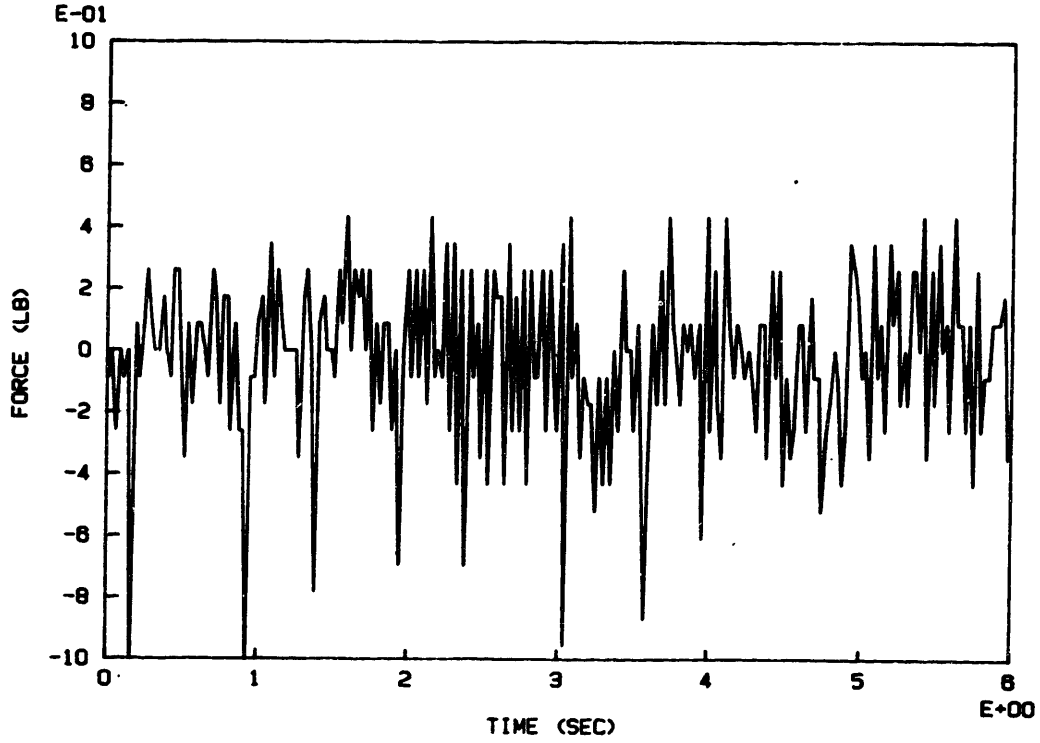

Figure 70. F_y Noise

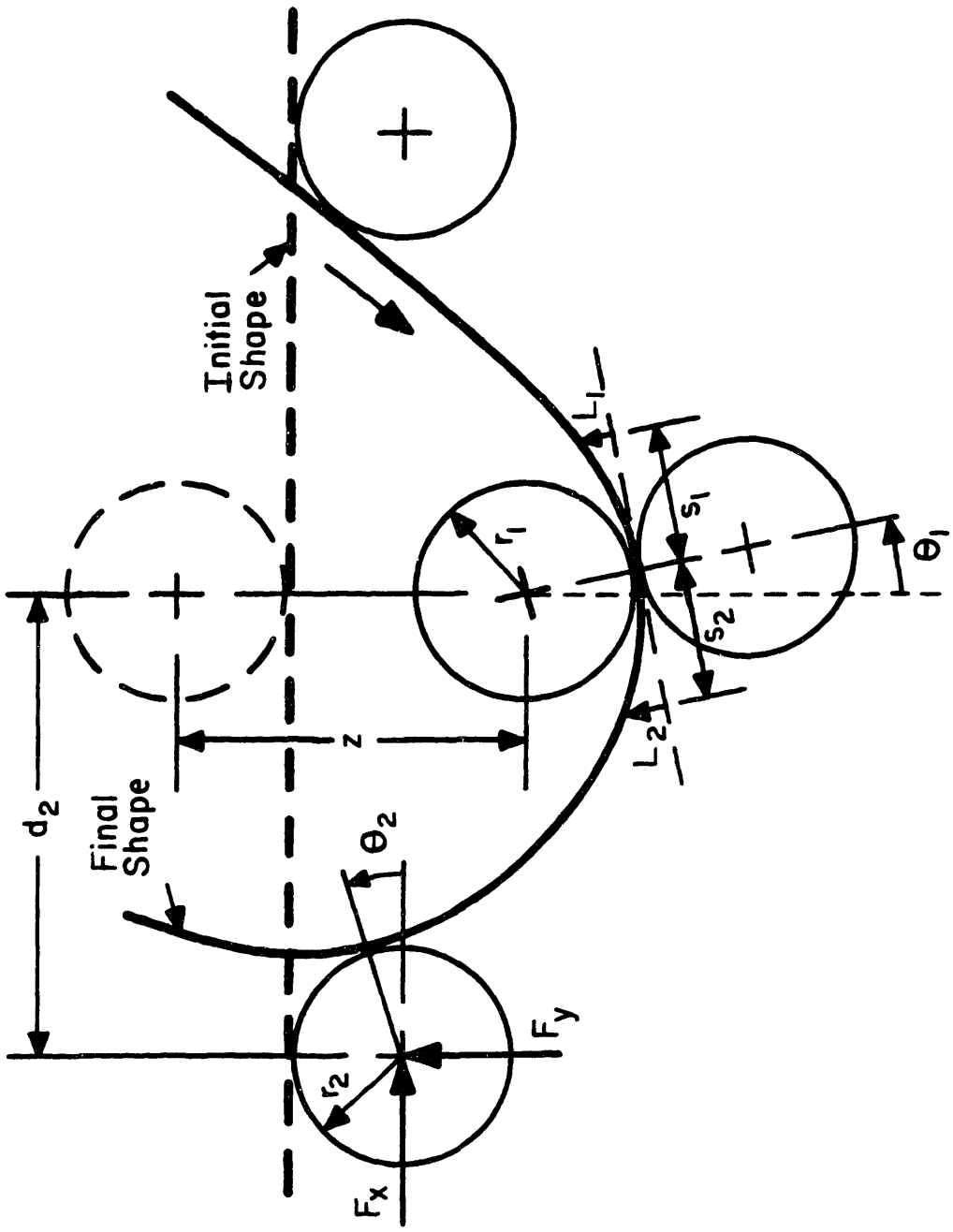

Figure 71. Roll Bender Geometry

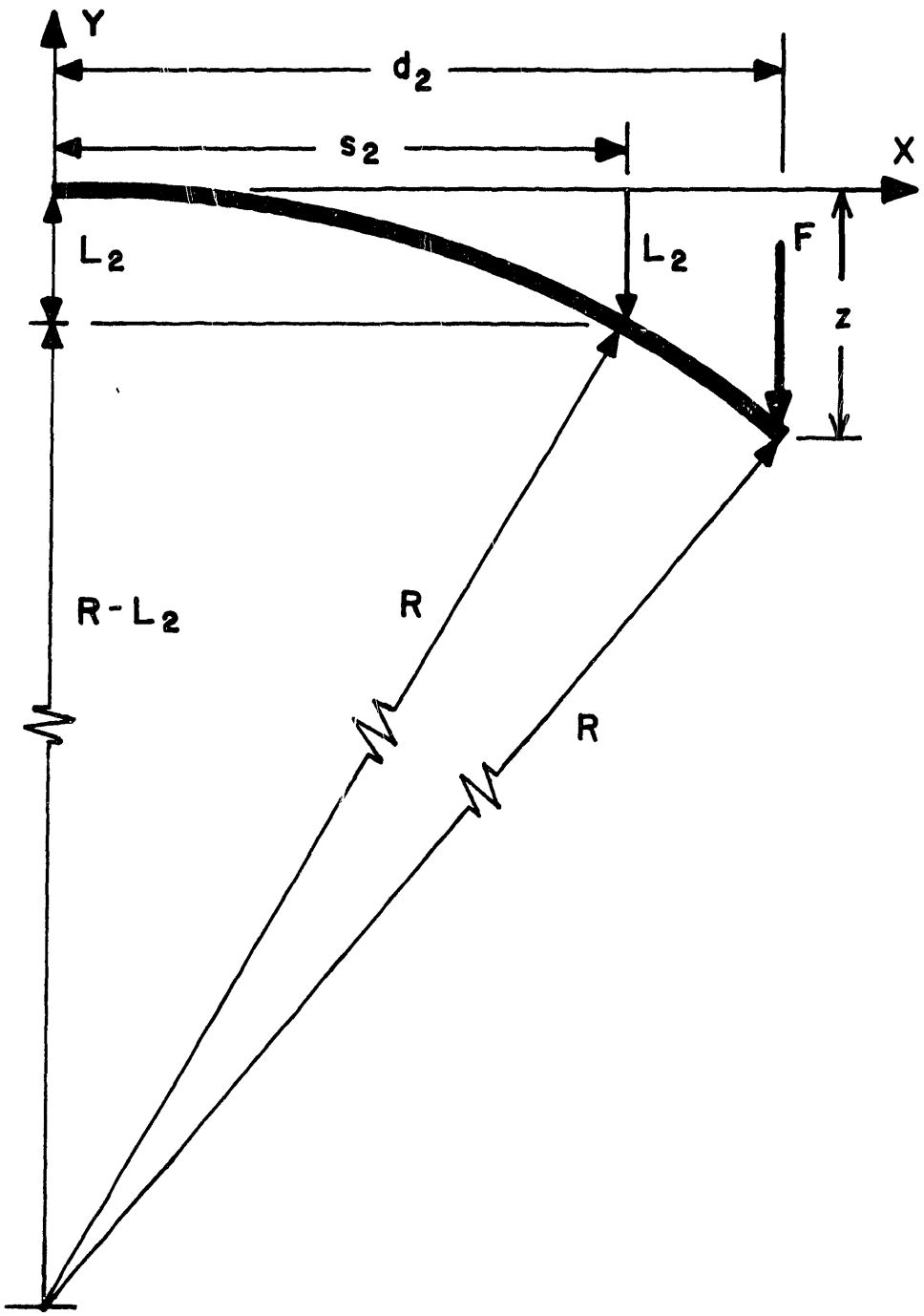

Figure 72. Curvature Measurement Scheme

The equation for calculating the maximum moment is:

$$M_{max} = F_x D_y + F_y D_x \tag{34}$$

where

$$D_y = z - r_1(1 - \cos\theta_1) - r_2(1 - \sin\theta_2)$$

$$D_x = d_2 + r_1\sin\theta_1 - r_2\cos\theta_2$$

There are several possible schemes for calculating loaded curvature, K_L. One option is to assume that the workpiece curvature in the region of the the maximum moment is constant. A curvature can then be calculated as follows (see Figure 72):

$$s_2^2 + (R - L_2)^2 = R^2$$

Rearranging this equation yields:

$$K_L = 1/R = 2L_2/(s_2^2 + L_2^2) \tag{35}$$

Equation 35 can be applied to each LVDT measurement and the results averaged as discussed in Appendix 2. An alternate method of calculating curvature can be found from linear beam

theory. Consider the cantilever beam shown in Figure 72 which represents the portion of the workpiece between the center and outer rolls. The relationship between the deflection of the beam at any point x along the beam and the maximum loaded curvature, assuming small deflections, is developed below.

$$\frac{\partial^2 y}{\partial x^2} = K_L = \frac{F(d_2 - x)}{EI} \tag{36}$$

where EI is the bending stiffness of the workpiece. The maximum curvature occurs at x = 0 which means that:

$$K_L = Fd_2/EI \tag{37}$$

Integrating Equation 36 twice with

$$\frac{\partial y}{\partial x}(0) = 0 \qquad \text{and} \qquad y(0) = 0$$

yields:

$$y_x = \frac{F}{EI}\left[\frac{d_2 x^2}{2} - \frac{x^3}{6}\right] \tag{38}$$

where y_x is the deflection of the workpiece at any point x

along the workpiece. Substituting Equation 38 into Equation 37 gives the relationship between the maximum loaded curvature and the deflection of the beam.

$$K_L = \frac{d_2 y_x}{\left(\frac{d_2 x^2}{2} - \frac{x^3}{6}\right)} \tag{39}$$

This equation shows that the loaded is a linear function of the displacement of the workpiece at any point x. In the limiting case, for $x = d_2$, the displacement of the workpiece is just the displacement of the center roll. The loaded curvature is then:

$$K_L = 3z/(d_2{}^2) \tag{40}$$

where z is the center-roll displacement.

Appendix 2

MEASUREMENT ALTERNATIVES

The closed-loop control of a roll bending process as developed in Chapter 2 depends entirely on the ability to measure the unloaded curvature, K_u, while the workpiece is still in the loaded state. As shown in Equation 4, K_u is actually a combination of three separate measurements. These are loaded curvature, K_L; moment, M; and bending stiffness, dM/dK. The bending stiffness is considered constant for a given workpiece and can be calculated rather than measured if enough information is known about the workpiece. In practice there are advantages to measuring the bending stiffness, so it will be considered a measurement for the general case.

The details of several measurement methods for K_L and M are given in Appendix 1. These are not the only available methods. This appendix contains a discussion of all the measurement methods used on the experimental roll bending apparatus. Because the choice of measurement method will depend on the type of bending to be performed and the required performance, an attempt is made to point out the advantages and disadvantages of each of the methods in regard to accuracy and type of bending.

It is important to notice that absolute measurements of loaded curvature and moment are not required. As shown in the control program listing in Appendix 4, the analog instru-

ments on the experimental apparatus must be initialized for each workpiece. But, even though the instruments must be initialized using a flat section of the workpiece, it is not necessary to initialize them at absolute zero moment and curvature. To see this consider Figure 73. The unloaded curvature measurement will be the same regardless of whether Point A or Point B is considered zero moment and loaded curvature. In fact any point along the linear elastic loading line may be considered the origin. Practically, this means that extreme care in setting up the roll bending apparatus for each workpiece is unnecessary. This is a nice feature of the unloaded curvature measurement scheme since less setup time results in higher productivity. Also high precision is sometimes difficult to obtain on a factory floor.

Loaded Curvature Measurement

According to the bending control algorithm developed in Chapter 2, it is necessary to know, or measure, the curvature at a specific point, namely the point of contact with the center roll. But measuring a point curvature is extremely difficult, if not impossible. The assumption behind the following measurement methods, then, is that the curvature is nearly constant in the region of interest and can be calculated by finding, or estimating, the shape of the workpiece in this region.

Figure 74 shows two of the methods used to measure

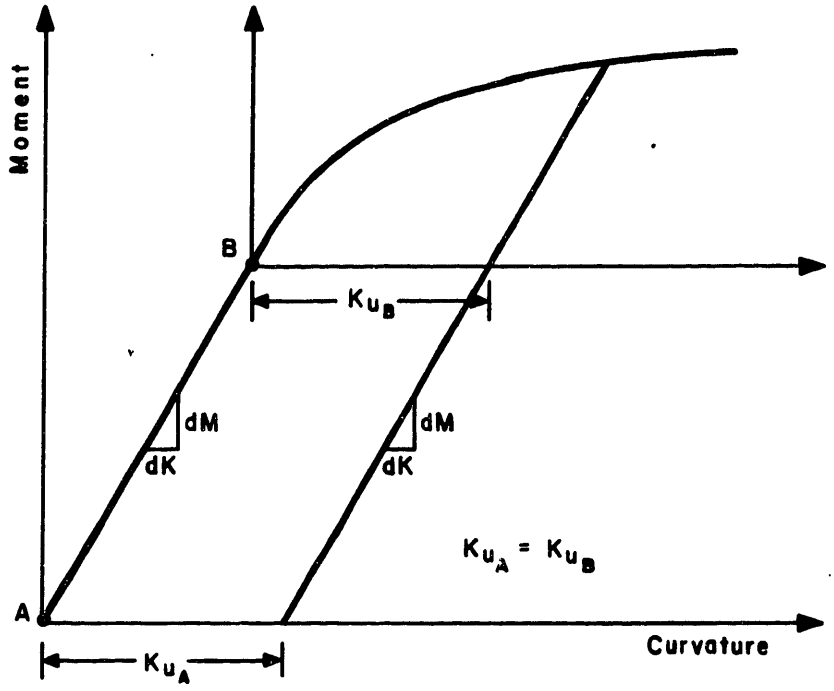

Figure 73. Translated Moment-Curvature Origin

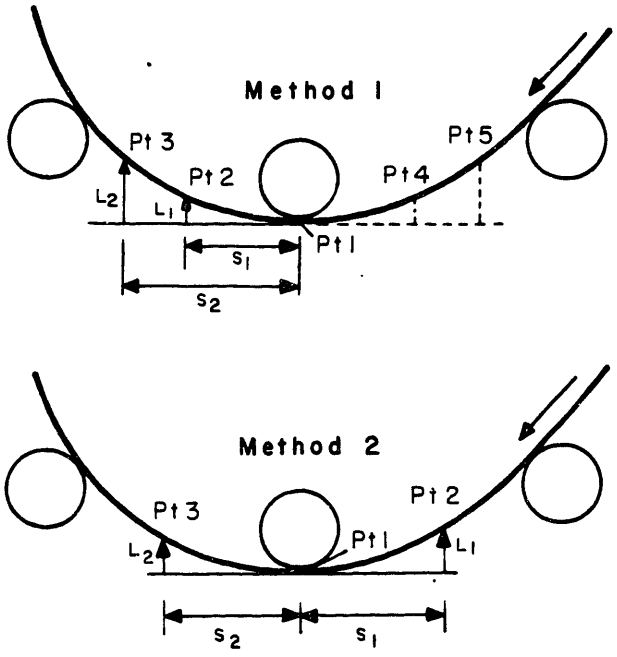

Figure 74. LVDT Configurations

loaded curvature. These methods employ a roller that contacts the sheet. A linear displacement transducer is used to measure the displacement of the workpiece as it deflects during the bending process. Contacting methods of curvature measurement are generally much simpler to implement than non-contacting methods such as optical measurements, but noise is more of a problem because of surface irregularities. In both methods shown, only two displacement measurements were used. Additional measurements might provide greater precision, but at the cost of greater complexity and decreased performance due to increased computation in the discrete controller. In the first method, both measurements are made on the unloading side of the center roll. This is because the relationship between moment and curvature is linear in the unloading region as is seen in Figure 3. Because the moment is nearly a linear function of sheet position (Figure 4), it is easy to see that the curvature should vary linearly with distance along the workpiece on the unloading side. Thus the loaded curvature is a much better behaved function on the unloading side than on the loading side, which includes the nonlinear plastic region. The two measurements of each method can be combined in many ways to estimate curvature. The three known points are enough to define a unique circle through the points. If the workpiece shape is actually circular, then the curvature can be estimated by the inverse of the radius of curvature for this

circle. Or if the curvature, and therefore displacements, are assumed to be symmetric about point 1, then the five known points can be used to define two circles. A weighted average of the curvatures found from these two circles can then be used as an estimate for the loaded curvature. This approach is the basis for Equation 35, which is the equation for a circle defined by one of the displacements. Another option is to use the two displacement measurements to define a curvature and a rate of change of curvature along the workpiece. With this information it is possible to extrapolate the curvature backward from the location of the first transducer to the point of maximum curvature. A variation on all the above options is to assume that the relationship between curvature and displacement is as defined for an elastic cantilever beam (see Equation 39) rather than assuming a circular shape. One problem with all these measurement options is that many of the assumptions made are only valid near the point of interest. Greater error is expected as the displacement measurements are made farther from the point of maximum curvature under the center roll.

A more practical consideration eliminated all of these options as useful measurement methods, at least for the experimental apparatus used. The center-roll apparatus, shown in Figure 64, has a tendency to vibrate as the workpiece is rolled through the rollers. In addition, because the center roll is the drive roll, a moment is generated

between the center roll and the workpiece which causes the center-roll apparatus to rotate slightly when the drive motor is turned on. Because the linear displacement transducers are attached to the center-roll apparatus, any rotation of the apparatus results in a false reading on the displacement transducers. The rotation of the center-roll apparatus causes an offset in the curvature reading while the vibration causes large amplitude noise at about the natural frequency of the center-roll apparatus. Another source of error is due to runout of the center roll. If the center roll has any runout, the workpiece will translate perpendicular to the longitudinal axis of the workpiece. This translation is detected by the displacement transducers and interpreted as a change in curvature.

To eliminate the errors due to center roll rotation, one of the displacement transducers was moved to the loading side of the center roll. As noted above, the curvature-displacement relationship is not as well behaved on the input side, so this method would not appear to be as accurate as the first method. However, the new configuration greatly reduces the errors mentioned above. Any rotation of the center roll will cause one of the transducer displacement measurements to increase, but at the same time the measurement on the opposite side will decrease. If the transducers are both located the same distance from the contact point, then the displacements will be the same magnitude. Otherwise, the displace-

ments will only be proportional, with the proportion depending on the relative distance from the contact point for each measurement. Taking the average of the curvature based on these displacements should eliminate the errors due to rotation. Figure 75 shows the curvature measurements for each transducer and the average curvature measured for a disturbance test with the transducers mounted on opposite sides of the center roll. Notice that the errors due to rotation can easily be several times as large as the actual curvature. This indicates that measuring the displacement on both the loading and unloading sides is necessary despite the shortcomings mentioned above. The errors due to runout of the center roll are not eliminated with this method, but careful

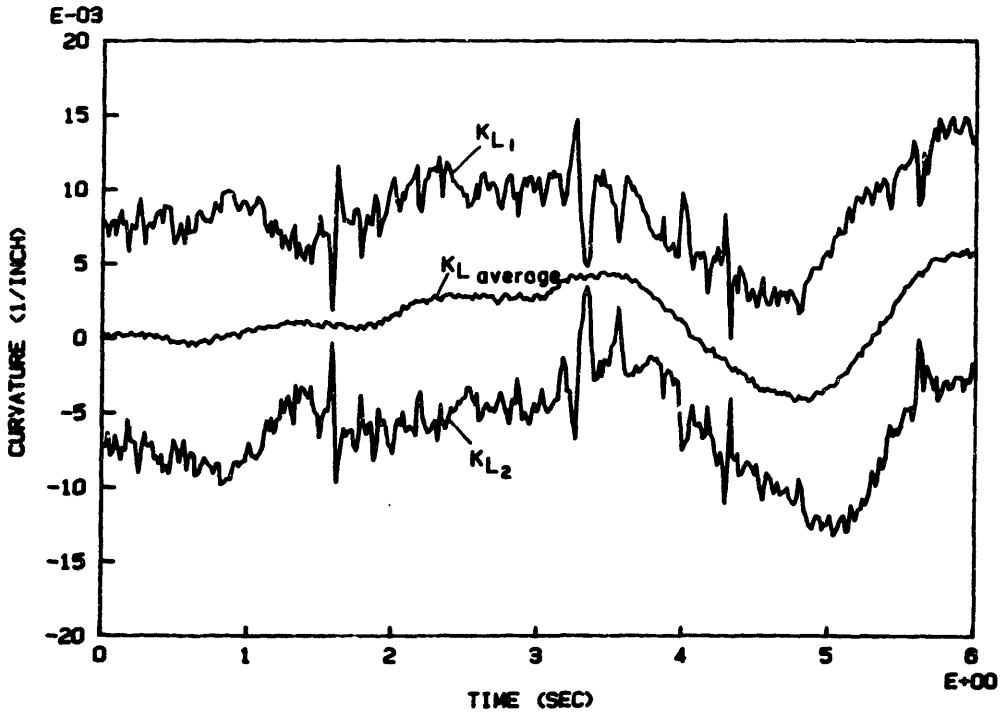

Figure 75. Opposing LVDT Curvature Measurement

machining of the center roll reduced runout to 0.001 in. This reduced error due to runout in the curvature measurement to below noise levels. This measurement method was used quite successfully in many of the bending experiments. This method was most successful for bending large curvatures, because the large curvatures result in large displacements. For straightening applications, the signal-to-noise ratio was low and good readings were difficult to obtain.

A final method of measuring curvature, which was also used successfully, is a specialized case of the method discussed above. For some bending operations, such as straightening, the curvature magnitudes are very small. This means that the displacements measured, if the transducers are very near the center roll, will be very small. To achieve the necessary resolution, the transducers can be moved farther from the center roll so that the displacements will be greater. In the limiting case the transducers can be moved outward as far as the outer rolls. Measurements from this limiting case result in exactly the same displacement as measuring the displacement of the center roll relative to the outer rolls. The loaded curvature, therefore, can be estimated using only a single measurement of the center-roll displacement. The advantage of this method is that fewer measurements and calculations are needed, which means increased speed in the discrete controller. In addition, this measurement is very easy to make. Most servo systems

incorporate the position measurement in the servo controller, so little additional hardware is needed. Another advantage is that this measurement is a non-contacting measurement in a sense and therefore does not have the noise problems associated with the contacting methods described above. The major disadvantage is that there is no simple, precise relationship between center-roll displacement and curvature. A linear approximation is given by Equation 40. But the errors due to the estimates and assumptions outlined above increase as the measurements are made farther from the point of maximum curvature and as the speed of response increases. Thus this method is less accurate than some other methods, but for certain bending applications, such as straightening stiff workpieces, the advantages might outweigh the disadvantages.

Moment Measurement

Figure 71 shows the measurements which are necessary to calculate the moment in the workpiece at the point of maximum curvature. In the most general case, it might also be necessary to include an applied moment at the outfeed roll, M_b, particularly if the outfeed roll-pair does not rotate. For this most general one-dimensional bending case there are two force measurements, each with a respective moment arm, and one moment measurement. Thus it is necessary to know five quantities to calculate the maximum moment. The relationship between each of these quantities and the maximum moment is

given by:

$$M_{max} = F_x D_y + F_y D_x + M_b \tag{41}$$

where

$$D_y = z - r_1(1 - \cos\theta_1) - r_2(1 - \sin\theta_2)$$

$$D_x = d_2 + r_1\sin\theta_1 - r_2\cos\theta_2$$

Careful study of this equation along with intuition should indicate that some of the quantities will be much more important than others, depending on the type of bending process under consideration. For instance, the angle θ_1 shown in Figure 71 is used to make adjustments to the moment arm D_x. The error that would be incurred by eliminating the adjustment and assuming D_x to be constant will be negligible for straightening very stiff workpieces, since θ_1 will be very small for this particular workpiece. For bending large curvatures θ_1 can be substantial, even for fairly stiff workpieces. Note, however, that if d_2 is very large compared to r_1, then even if θ_1 is very large, the effect on D_x will be small. This example indicates that it is not possible to design one moment measurement scheme that will be satisfactory for all bending machines and for all of the various bending processes. The following observations can be

used as general guidelines. More specific information can be obtained only if typical values of all variables in Equation 41 are available.

The moment M_b is almost always negligible if the outer roll-pair is free to rotate or if there is only a single outer roll, as there might be in unidirectional bending. It might also be negligible for the straightening process, even if the outer roll-pair is not free to rotate because the levels of curvature are low. If a small error can be tolerated, neglecting M_b certainly simplifies the hardware. For bending, where the levels of curvature are much higher, it is necessary to allow the outer roll-pair to rotate to eliminate the applied moment or to measure the applied moment.

The force F_y is generally the largest force and when combined with D_x, which is generally the largest moment arm, it is easy to see that F_y is the most dominant measurement in the calculation of the maximum moment. F_y cannot be ignored in any of the bending processes. F_x, however, will be small for most straightening operations. And since D_y is also very small for straightening, the combined effect of F_x and D_y is negligible for straightening. The component of the maximum moment due to F_x might also be negligible for many bending operations if high precision is not a concern.

The moment in the experiments described in Chapter 5 was measured using both the F_y and F_x measurements, but with no

adjustment to the moment arm D_y. A first-order approximation to the sine term in D_x was retained. The result of this moment measurement approximation was less precision but improved dynamic response because the decreased computation resulted in a much faster discrete controller. Nevertheless, the precision of this approximation was very good for the experiments in Chapter 5 because the geometry of the roll bending apparatus and the stiffness of the workpieces resulted in a very high signal-to-noise ratio from the force transducer.

Bending Stiffness Measurement

As mentioned earlier, the bending stiffness can usually be considered constant for a given workpiece. If this constant value is known for each workpiece that will be formed, then the value can simply be entered into the control program. Measuring the bending stiffness, though, is a more general procedure which allows workpieces with unknown properties to be formed. The procedure employed for measuring the bending stiffness with the experimental apparatus is as follows. The workpiece is first loaded in the bending apparatus and the instruments are initialized. Then the workpiece is loaded throughout the linear elastic range. At specific intervals in this loading cycle the computer calculates loaded curvature and maximum moment. After the loading cycle is completed, a least squares curve fitting routine is

used to fit a straight line to the moment-curvature data. This straight line is, by definition, the elastic loading line shown in Figure 3. The slope of this line is the bending stiffness. The loading line shown in Figure 3 is just the positive half of the elastic loading line which continues into the negative loading region. The full elastic region, both negative and positive, is used to measure the bending stiffness.

Measuring the bending stiffness in this manner increases the roll bending system flexibility because no prior knowledge of the workpiece properties is needed. But there is an even more compelling reason for measuring the bending stiffness of each workpiece. The curvature and moment measurements are both calibrated separately, but if there is an error in either calibration then the calibrated bending stiffness measurement will tend to reduce the errors in the unloaded curvature calculation. This is because the bending stiffness calibration uses the measured curvature and the measured moment to establish the relationship between the elastic moment and curvature. For instance, suppose the calibration for the loaded curvature is off by a factor of two. In other words, suppose the actual loaded curvature is half the measured value. Then the measured bending stiffness (slope of the elastic loading line) will also be half the actual value. The unloaded curvature based on the incorrect loaded curvature measurement, the correct moment measurement,

and the calibrated bending stiffness will be exactly correct in the linear elastic region, and more nearly correct in the plastic region than a measurement based on precalculated bending stiffness. In fact the error with the calibrated bending stiffness will, for this example, be equal to the actual unloaded curvature, while the error with a precalculated bending stiffness would be equal to the actual loaded curvature. The reduction in error is equal to the difference between the loaded and unloaded curvatures. For bending operations, this reduction may not be significant because for large curvatures and stiff workpieces, the difference between the loaded and unloaded curvatures will be small. For straightening operations, where the unloaded curvature is zero, measuring the bending stiffness can result in a substantial reduction of error. In this particular bending operation the bending stiffness measurement is essentially a "system" calibration which encompasses the complete roll bending system.

Appendix 3

ERROR ANALYSIS

The experiments described in Chapter 5 were performed strictly to evaluate the new control scheme proposed in Chapter 4. Because the purpose was to attain the fastest system response possible, the system precision was compromised to increase speed. For this reason, system precision was ignored and no attempt was made to measure the precision of the final workpiece shape. The assumption is that if the closed-loop control system has the required response, then the system precision is only limited by the measurement precision. It is instructive, though, to examine the unloaded curvature equation to see the effect of errors in the individual measurements on the final workpiece shape. The following analysis presents some typical values which illustrate the precision required for a straightening operation, which generally has the most stringent requirements of all the bending processes. The analysis can be generalized for other bending operations to determine what instrumentation and measurement methods are most appropriate.

The equation used to calculate unloaded curvature is:

$$K_u = K_L - M/S \tag{42}$$

where K_u is unloaded curvature, K_L is maximum loaded curvature, M is maximum moment and S is the slope of the

elastic loading line shown in Figure 3. If there is any error in the three measurements, K_L, M or S, then the unloaded curvature can be expressed by:

$$K_u + dK_u = K_L + dK_L - \frac{M + dM}{S + dS} \tag{43}$$

where dK_u, dK_L, dM, and dS are the error for the respective terms. Equation 43 can be combined with Equation 36 and rearranged to obtain the following error equation.

$$dK_u = dK_L + \frac{M\,dS}{S^2 + SdS} - \frac{dM}{S + dS} \tag{44}$$

Figure 76 shows how each of the measurement errors affects the unloaded curvature of the workpiece. If $dK_u(max)$ is the maximum acceptable error for the unloaded curvature, then examination of Equation 44 and Figure 76 reveals:

1. If M and S are known exactly (dM = dS = 0) then the maximum acceptable error for the loaded curvature measurement, $dK_L(max)$, is exactly $dK_u(max)$.
2. If K_L and S are known exactly (dK_L = S = 0) then $dM(max) = -dK_u(max)S$.
3. If K_L and M are known exactly (dK_L = dM = 0) then $dS(max) = dK_u(max)S^2/(M-dK_u(max)S)$.

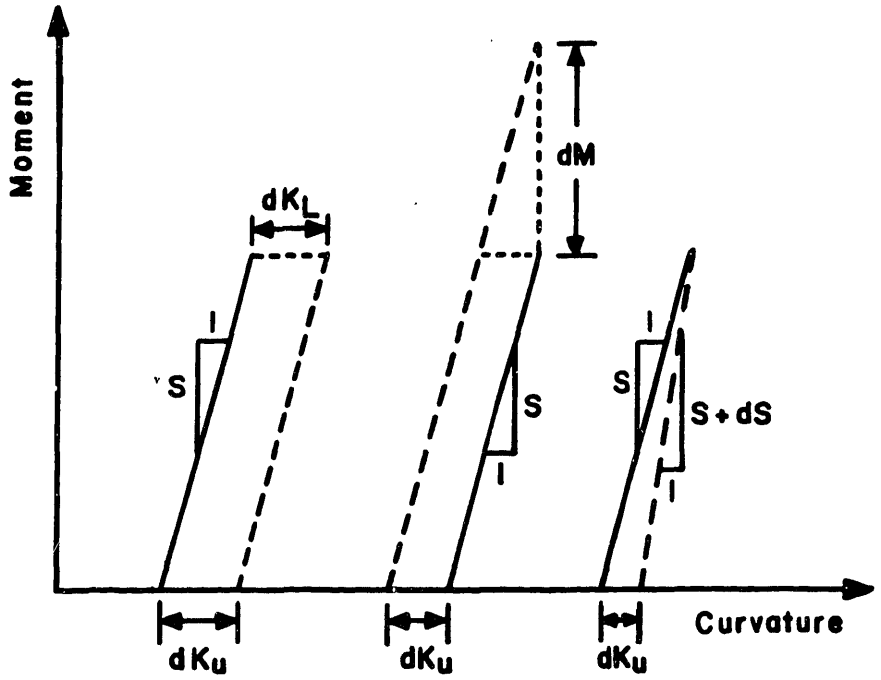

Figure 76. Measurement Errors

This analysis can be used to find the minimum required precision of a given measurement. Consider two specific examples:

1) 1/8" X 1" Aluminum Strip
   $S = 1880$ lb-in^2
   $M = 180$ in-lb
   $K_L = 0.1$ in^{-1}

2) 1/4" X 1" Aluminum Strip
   $S = 29000$ lb-in^2
   $M = 1400$ in-lb
   $K_L = 0.05$ in^{-1}

For the straightening operation, specifications for maximum acceptable curvature error are generally provided in terms of deviation from a flat surface. A typical maximum acceptable

deviation for the the two cases above is 0.0125 in/ft. Assuming a constant curvature over a 5 ft span, the straightness specification can be changed to curvature by applying Equation 35. The maximum acceptable unloaded curvature error is found to be 0.0007 in^{-1}. Using these numbers it is possible to establish typical values for the maximum acceptable error for each of the measurements.

Case 1:

$$dK_L(max) = \pm 0.0007\ in^{-1} \text{ or } \pm 0.7\%$$
$$dM(max) = \pm 1.3\ in\text{-}lb \text{ or } \pm 0.7\%$$
$$dS(max) = \pm 14\ lb\text{-}in^2 \text{ or } \pm 0.7\%$$

Case 2:

$$dK_L(max) = \pm 0.0007\ in^{-1} \text{ or } \pm 1.4\%$$
$$dM(max) = \pm 20\ in\text{-}lb \text{ or } \pm 1.4\%$$
$$dS(max) = \pm 420\ lb\text{-}in^2 \text{ or } \pm 1.4\%$$

These numbers show that required precision drops rapidly for the moment and bending stiffness measurements as the bending stiffness of the workpiece increases. The required loaded curvature measurement precision is independent of any of the workpiece properties. Of course the maximum allowable errors given above only define the minimum required precision since the errors may all occur at once. The errors can combine to increase the total error or to cancel one another.

Appendix 4

COMPUTER PROGRAMS

This appendix contains a listing of all the programs used in modeling, analysis, and control of the experimental bending apparatus. Many variations of these programs are used, depending on the instrumentation and control algorithm being employed for a particular experiment, but the various programs all contain the same structure and differ only in minor areas not important to the essential logic.

Bending Control Program

The program BEND is used to control the experimental bending apparatus during the closed-loop forming operation. A flow chart of the program is presented in Figure 77 and the program listing is given on the following pages. A description of the program and its operation is provided below along with a definition of the major variables and subroutines.

Variables:

K1 - Reading from the x direction of the force transducer.

K2 - Reading from the y direction of the force transducer.

K3 - Reading from the center-roll rotation potentiometer.

K4 - Reading from the servo tachometer.

K5 - Reading from the servo resolver.

C1 - Calibration factor to convert K1 to an equivalent curvature.

C2 - Calibration factor to convert K2 to an equivalent curvature.

C3 - Calibration factor to convert K3 to an equivalent curvature.

C4 - Calibration factor to convert K4 into center-roll velocity.

C5 - Calibration factor to convert K5 into center-roll position.

SLOPE - Bending stiffness of the workpiece.

GAIN1,GAIN2 - Controller gains.

RKD - Desired curvature.

RKU - Measured unloaded curvature.

ICOM - Controller command to the velocity servo.

Subroutines:

OUTPOS - sends a position command to the servo.

INPOS - reads the servo position.

OUTVEL - sends a velocity command to the servo.

SCAL - measures the workpiece bending stiffness.

SZERO - returns the initial value of all analog transducers.

ATOD - reads the analog transducers into the computer.

Lines 1-10 of the program initialize all variables. The calibration factors C1-C5 are all fixed for a given machine geometry, but they are scaled by the bending stiffness which varies with the particular workpiece. The subroutine SCAL (lines 36-91) is used to measure the bending stiffness (see

Appendix 2 for a discussion of various ways to find the bending stiffness). SCAL calculates the bending stiffness by loading the workpiece and taking measurements of loaded curvature and moment at various points in the elastic loading region. These measurements are then used to calculate a slope by means of a simple linear regression. The slope is, by definition, the bending stiffness. The variables M, N, and J, defined for several different workpieces in lines 44-62, are scale factors which are used to ensure that the workpiece is loaded throughout the full elastic region. This provides the best estimate of the bending stiffness for each particular workpiece. Notice that this technique does require some knowledge of the workpiece, but M, N, and J are fixed for a particular workpiece and must be found only once. The controller gains and the desired curvature are entered in lines 11-19. The listing shows the desired curvature as a constant, but it could easily be read in as an array if the desired curvature is variable. When the workpiece is set, the subroutine SZERO (lines 92-120) is called to read the initial values of the analog transducers. SZERO takes the average of 20 measurements for each transducer as the initial value. This minimizes any variance due to noise. The subroutine as written actually averages four sets of five average measurements. This is to eliminate the possibility of overflow because the computer has limited capacity in representing integer numbers.

The real-time bending control algorithm is contained in lines 21-27. The algorithm is placed within a DO-loop because the computer has limited memory to store the experimental data. For production runs, where data acquisition is ignored, the algorithm could be placed in an infinite loop with a statement to check for the end of the workpiece. In lines 22 and 23 the computer reads all measurements. The subroutine ATOD is a machine language procedure which reads the analog transducers and takes the difference between the measurements and the initial values. The result is returned in the variables K1-K4. INPOS returns the servo position, which is in digital form for this particular servo. Next, the unloaded curvature is calculated using the transducer measurements (line 24). The equation is of the form:

$$K_u = K_L - (F_x D_y + F_y D_x)/\text{SLOPE}$$

This is easily verified by making the appropriate substitutions from the variable definitions given above. The equation in line 24 uses scaled center-roll position as the loaded curvature measurement (see Appendix 1). This increases computation speed at the expense of precision. Appendix 2 contains a complete discussion of the effect of such compromises. Line 25 is the implementation of the digital controller design (see Chapter 4). In this particu-

lar case the controller is just a gain operating on the difference between the desired curvature and the feedback measurement. The feedback measurement is a weighted sum of the unloaded curvature and the center-roll velocity, which is related to the rate of change of unloaded curvature as shown in Chapter 4. Thus the velocity command to the servo shown in line 25 is of the form:

$$\text{COMMAND} = \text{GAIN1}(K_u\text{desired} - (K_u\text{measured} + \text{GAIN2}(\dot{K}_u)))$$

The velocity command is then sent to the servo through the subroutine OUTVEL. This completes one control cycle. The computer then reads a new set of measurements and begins a new control cycle. At the completion of the control DO-loop, the program writes all data to disk storage.

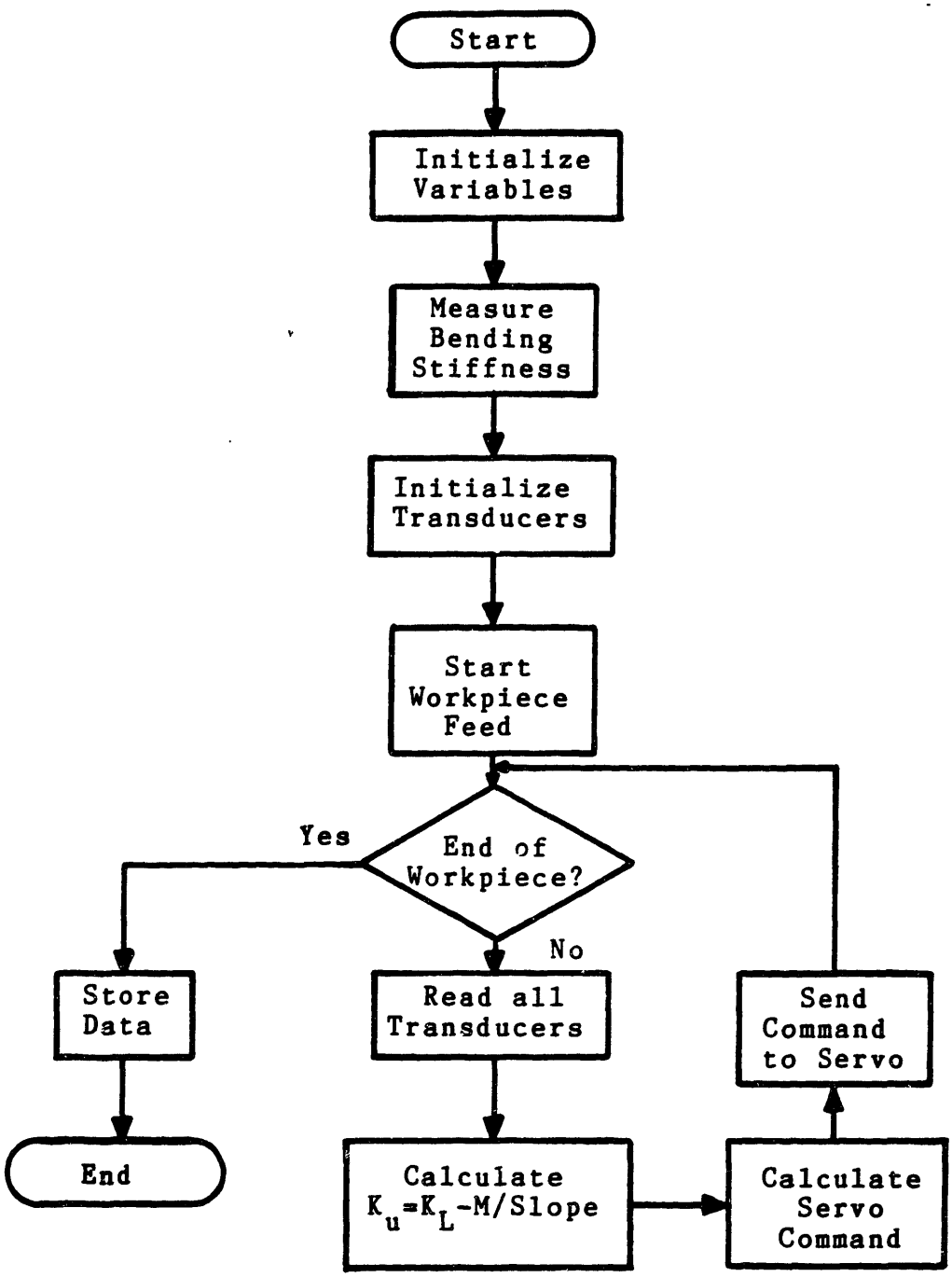

Figure 77. Bending Program Flow Chart

```
C
C                BEND
C
C      BENDING CONTROL PROGRAM
C              4/04/85
C
C
0001        DIMENSION K1(1000),K2(1000),K3(1000),K4(1000),K5(1000)
0002        COMMON C1,C2,C3,C4,C5
0003        DATA K1,K2,K3,K4,K5,/1000*0,1000*0,1000*0,1000*0
           &  1000*0/
C
C      MOVE THE SERVO TO ALLOW WORKPIECE INSERTION
C
0004        CALL OUTPOS(0)
C
C      MEASURE THE BENDING STIFFNESS
C
0005        CALL SCAL(SLOPE)
C
C      INITIALIZE ALL CONSTANTS
C
0006        C1 = 0.00032/(35.86*SLOPE)
0007        C2 = 6.0/(11.5*SLOPE)
0008        C3 = (0.875/2.0*0.000126)/(11.5*SLOPE)
0009        C4 = 0.00272
0010        C5 = 3.0*0.000032/36.
C
C      ENTER THE NECESSARY CONTROL VARIABLES AND INPUTS
C
0011        WRITE(5,10)
0012 10     FORMAT(/2X,'   ENTER CONTROL GAINS (GAIN1,GAIN2):')
0013        READ(5,20) GAIN1,GAIN2
0014 20     FORMAT(2F13.0)
0015        WRITE(5,30)
0016 30     FORMAT(/2X,'   ENTER THE DESIRED CURVATURE: ')
0017        READ(5,40) RKD
0018 40     FORMAT(F10.0)
C
C      INITIALIZE ALL TRANSDUCERS
C
0019        CALL SZERO(I1,I2,I3,I4)
0020        PAUSE ' PRESS RETURN TO BEGIN'
C
C     *******   REAL TIME CONTROL BEGINS HERE *******
C
C            K1 - FX      K2 - FY      K3 - ROTATION
C
C              K4 - VELOCITY      K5 - POSITION
C     ***********************************************
C
```

```
0021       DO 50 J=1,1000
C
C      READ ALL TRANSDUCERS
C
0022       CALL ATOD(I1,K1(J),I2,K2(J),I3,K3(J),I4,K4(J))
0023       CALL INPOS(K5(J))
C
C      CALCULATE THE UNLOADED CURVATURE
C
0024       RKU = C5*K5(J)-K1(J)*C1*K5(J)-K2(J)*(C2+C3*K3(J))
C
C      CALCULATE THE CONTROLLER COMMAND
C
0025       ICOM = INT(GAIN1*(RKD-RKU-K4(J)*C4*GAIN2))
C
C      SEND COMMAND TO THE SERVO
C
0026       CALL OUTVEL(ICOM)
C
C      REPEAT THE CONTROL LOOP
C
0027 50    CONTINUE
C
C
C
C
C
C
C      WRITE DATA TO DISK
C
0028       CALL NAMEIN(NAME1)
0029       OPEN (UNIT=1,NAME=NAME1,FORM='UNFORMATTED')
0030       WRITE(1) SLOPE,C1,C2,C3,C4,C5,RKD
0031       DO 60 J = 1,1000
0032       WRITE(1) K1(J),K2(J),K3(J),K4(J),K5(J)
0033 60    CONTINUE
0034       CLOSE (UNIT=1)
0035       END
C
C
C
C
C
0036       SUBROUTINE SCAL(SLOPE)
0037       DIMENSION RK(100),RM(100)
0038       COMMON C1,C2,C3,C4,C5
C
C      SET SCALE FACTORS ACCORDING TO THE DESIRED WORKPIECE
C
0039       WRITE(5,10)
0040 10    FORMAT(/2X,' ENTER OPTION '/'  1) 1/8 X 1 ALUMINUM '/
          & '  2) 1/4 X 1 ALUMINUM '/'  3) 1/8 X 1 STAINLESS ' /
```

```
     &   '  4) 1/4 X 1 STAINLESS'/'  5) 1/2 X 3/4 TEE '/)
0041       READ(5,20) IMAT
0042 20    FORMAT(I3)
0043       GOTO(30,40,50,60,70),IMAT
C 1/8 X 1 ALUMINUM
0044 30    M = 2000
0045       N = 100
0046       J = 40
0047       GO TO 80
C 1/4 X 1 ALUMINUM
0048 40    M = 600
0049       N = 100
0050       J = 10
0051       GO TO 80
C 1/8 X 1 STAINLESS
0052 50    M = 200
0053       N = 100
0054       J = 4
0055       GO TO 80
C 1/4 X 1 STAINLESS
0056 60    M = 100
0057       N = 100
0058       J = 2
0059       GO TO 80
C 1/2 X 3/4 TEE
0060 70    M = 100
0061       N = 100
0062       J = 2
0063 80    CALL OUTPOS(0)
0064       CALL SZERO(I1,I2,I3,I4)
0065       CALL INPOS(I5)
0066       CALL OUTPOS(M+10)
0067       PAUSE 'PRESS RETURN TO CALIBRATE'
C
C     LOAD THE WORKPIECE THROUGHOUT THE ELASTIC REGION
C
0068       CALL OUTPOS(M)
0069       DO 90 I=1,N
0070       CALL OUTPOS(M-J*I)
0071       CALL INPOS(N5)
0072       CALL ATOD(I1,N1,I2,N2,I3,N3,I4,N4)
0073       N5 = N5-I5
C
C     CALCULATE MOMENT AND CURVATURE AT VARIOUS POINTS
C
0074       RK(I) = C5*N5
0075       RM(I) = N1*C1*N5+N2*(C2+C3*N3)
0076 90    CONTINUE
0077       CALL OUTPOS(0)
C
C     PERFORM LINEAR REGRESSION TO CALCULATE THE BENDING
C     STIFFNESS
```

```
C
0078        A1 = 0.
0079        A2 = 0.
0080        A3 = 0.
0081        A4 = 0.
0082        DO 100 I=1,N
0083        A1 = A1+RK(I)/FLOAT(N)
0084        A2 = A2+RM(I)
0085        A3 = A3+RK(I)*RK(I)
0086        A4 = A4+RK(I)*RM(I)
0087 100   CONTINUE
0088        SLOPE = (A4-A1*A2)/(A3-A1*A1*N)
0089        ROFF = A2/N-SLOPE*A1
0090        RETURN
0091        END
C
C
C
C
C
0092        SUBROUTINE SZERO(I1,I2,I3,I4)
0093        PAUSE 'PRESS RETURN TO ZERO TRANSDUCERS'
C
C           SEQUENCING START, ZERO ALL INPUTS
C
0094        I1 = 0
0095        I2 = 0
0096        I3 = 0
0097        I4 = 0
0098           DO 20 J=1,4
0099           N1 = 0
0100           N2 = 0
0101           N3 = 0
0102           N4 = 0
0103        DO 10 I=1,5
0104        CALL ATOD2(0,L1,0,L2,0,L3,0,L4)
0105        N1 = N1 + L1
0106        N2 = N2 + L2
0107        N3 = N3 + L3
0108        N4 = N4 + L4
0109 10    CONTINUE
0110        I1 = I1 + N1/5
0111        I2 = I2 + N2/5
0112        I3 = I3 + N3/5
0113        I4 = I4 + N4/5
0114 20    CONTINUE
0115        I1 = I1/4
0116        I2 = I2/4
0117        I3 = I3/4
0118        I4 = I4/4
0119        RETURN
0120        END
```

Modeling Program

The roll bending system modeling program, MODEL, consists of a main program and two subroutines. The subroutine RK4 is a general fourth-order Runge-Kutta integration routine. The subroutine SYSTEM is used to define the continuous system in standard state variable form. The modeling program is used to model the nonlinear effects of the workpiece and also to implement the discrete controller. A listing of the program is given on the following pages. A brief description of program logic is presented below.

All variables are initialized in lines 1-12. The system definition is stored in a file which is read into the program in line 7. The error and command equations in lines 10, 11, 34, and 35 are used to simulate the digital controller derived in Chapter 4 and implemented in the control program in line 25. Line 12 is a calculation of the shift in the moment-curvature relationship due to a disturbance. The loop starting at line 13 is completed once per time step. First the differential equations representing the continuous system are defined in the subroutine SYSTEM. The equations are integrated at the current time step in the subroutine RK4 using a standard Runge-Kutta integration routine. Lines 20-24 represent a velocity saturation nonlinearity. Lines 25-31 are used to model the nonlinear workpiece (see Chapter 3). The equations shown represent a unidirectional bending, moving workpiece model. The equations can be expanded to

include bidirectional bending and a stationary workpiece, but this introduces considerable complexity without a compensating increase in information. The equations in lines 32-35 are the implementation of the discrete controller. Notice that the controller command is not computed every time step, but at time steps which correspond to the discrete controller cycle time. The remainder of the program stores the data on disk.

```
C
C
C       ROLL BENDING MODELING PROGRAM
C
C
0001        DIMENSION X(7,750)
0002        COMMON /XYDATA/F(4),Y(4),SAVEY(4),PHI(4),M,RKU,COM,DT
           &          /CONST/C1,C2,C3,C4,C5,C6,C7
0003        DATA COM,ICOUNT,RKU,YO/0.,0,0.,0./
0004        DATA Y,X/4*0.0,5250*0.0/
0005        CALL NAMEIN(NAME1)
0006        OPEN(UNIT=1,NAME=NAME1,TYPE='OLD')
0007        READ(1,*) RKIN,DT,NT,ITC,YB,VMAX,SLOPE,RL,GAIN,
           &  C1,C2,C3,C4,C5,C6,C7,RKD
0008        CLOSE (UNIT=1)
C
C       INITIALIZE THE DISCRETE CONTROLLER
C
0009        ERROR = RKIN-RKU-C7*Y(2)
0010        COM = ERROR*GAIN
0011        YO = (RKD*(RL**2))/3.0
C
C       CALCULATE THE SYSTEM PARAMETERS FOR EACH TIME STEP
C
0012        DO 110 IT=1,NT
0013        ICOUNT = ICOUNT + 1
0014        K = 1
0015        N = 2
C
C       DEFINE SYSTEM
C
0016        DO 10 M=1,4
0017        CALL SYSTEM
C
C       INTEGRATE SYSTEM EQUATIONS
C
0018        CALL RK4(N,K)
0019 10     CONTINUE
C
C       CHECK FOR VELOCITY SATURATION
C
0020 20     IF(Y(2).LT.VMAX) GO TO 30
0021        Y(2) = VMAX
0022        Y(1) = X(1,IT-1)+VMAX*DT
0023 30     IF(Y(2).GT.(-VMAX)) GO TO 40
0024        Y(2) = -VMAX
0025        Y(1) = X(1,IT-1)-VMAX*DT
C
C       WORKPIECE MODEL
C
0026 40     RKL = 3.0*Y(1)/(RL**2)
```

```
0027        IF((Y(1)-YO).GT.YB) GO TO 60
0028 50     RM = 3.0*(Y(1)-YO)*SLOPE/(RL**2)
0029        GO TO 70
0030 60     RM = ((9.0*YB*SLOPE)/(2.0*(RL**2)))*
           & (1-(((YB/(Y(1)-YO))**2)/3.0))
0031 70     RKU = RKL-(RM/SLOPE)
C
C      CALCULATE DISCRETE CONTROLLER OUTPUT
C
0032        IF(ICOUNT.NE.ITC) GO TO 90
0033        ICOUNT = 0
0034        ERROR = RKIN-RKU-C7*Y(2)
0035        COM = ERROR*GAIN
C
C      STORE DATA
C
0036 90     DO 100 I=1,N
0037        X(I,IT)=Y(I)
0038 100    CONTINUE
0039        X(N+1,IT) = RKU
0040        X(N+2,IT) = RM
0041        X(N+3,IT) = ERROR
0042        X(N+4,IT) = COM
0043 110    CONTINUE
0044        CALL NAMEIN(NAME1)
0045        OPEN(UNIT=1,NAME=NAME1,TYPE='NEW',FORM='UNFORMATTED')
0046        WRITE(1) RKIN,DT,NT,ITC,YB,VMAX,SLOPE,RL,GAIN,
           &  C1,C2,C3,C4,C5,C6,C7
0047        DO 120 I=1,NT
0048        WRITE(1) X(1,I),X(2,I),X(3,I),X(4,I),X(5,I),X(6,I)
0049 120    CONTINUE
0050        CLOSE(UNIT=1)
0051        END
C
C
C
C
C
0052        SUBROUTINE SYSTEM
0053        COMMON /XYDATA/F(4),Y(4),SAVEY(4),PHI(4),M,RKU,COM,DT
           &          /CONST/C1,C2,C3,C4,C5,C6,C7
0054        F(1) = Y(2)
0055        F(2) = C1*Y(2)+C2*Y(1)+C3*COM
0056        RETURN
0057        END
C
C
C
C
C
0058        SUBROUTINE RK4(N,K)
0059        COMMON /XYDATA/F(4),Y(4),SAVEY(4),PHI(4),M,RKU,COM,DT
```

```
0060        GO TO (10,30,50,70),M
0061  10    DO 20 J=K,N
0062        SAVEY(J) = Y(J)
0063        PHI(J) = F(J)
0064        Y(J) = SAVEY(J)+0.5*DT*F(J)
0065  20    CONTINUE
0066        GO TO 90
0067  30    DO 40 J=K,N
0681        PHI(J) = PHI(J)+2.0*F(J)
0069        Y(J) = SAVEY(J)+0.5*DT*F(J)
0070  40    CONTINUE
0071        GO TO 90
0072  50    DO 60 J=K,N
0073        PHI(J) = PHI(J)+2.0*F(J)
0074        Y(J) = SAVEY(J)+DT*F(J)
0075  60    CONTINUE
0076        GO TO 90
0077  70    DO 80 J=K,N
0078        Y(J) = SAVEY(J)+(PHI(J)+F(J))*DT/6.0
0079  80    CONTINUE
0080  90    RETURN
0081        END
```

Step and Frequency Response Program

Program STEP is used to generate a step or frequency input to the servo system and store the output. The program shown is for a velocity servo, but can be used for a position servo by changing lines 12 and 13 as shown in the listing. A step input is generated by specifying zero frequency. The remainder of the program is self-explanatory.

```
C
C
C     STEP AND FREQUENCY RESPONSE PROGRAM
C
C
0001       DIMENSION K(3000),N(3000)
0002       CALL OUTPOS(0)
C
C     INITIALIZE SERVO INPUT
C
0003       WRITE(5,10)
0004 10    FORMAT(/2X,' ENTER  MAG. AND FREQ. ')
0005       READ(5,20) A,W
0006 20    FORMAT(2F10.0)
0007       DO 30 I=1,3000
0008       N(I) = INT(A*COS(W*I))
0009 30    CONTINUE
0010       PAUSE 'PRESS RETURN WHEN READY'
0011       DO 40 I=1,3000
C
C     SEND VELOCITY COMMAND
C
0012       CALL OUTVEL(N(I))
C
C     READ SERVO VELOCITY
C
0013       CALL ATOD(0,I1,0,I2,0,I3,0,K(I))
0014 40    CONTINUE
C  ***********************************************
C     THE PROGRAM CAN BE USED FOR A POSITION SERVO
C     BY CHANGING EQUATIONS 12 AND 13 TO
C
C             CALL OUTPOS(N(I))
C             CALL INPOS(K(I))
C  ***********************************************
C
C     STORE DATA
C
0015       CALL OUTPOS(0)
0016       CALL NAMEIN(NAME1)
0017       OPEN (UNIT=1,NAME=NAME1,FORM='UNFORMATTED')
0018       DO 50 I=1,3000
0019       WRITE(1) K(I),N(I)
0020 50    CONTINUE
0021       CLOSE (UNIT=1)
0022       END
```